LBNL-39719
UC-404

ERNEST ORLANDO LAWRENCE BERKELEY NATIONAL LABORATORY

Effects of Microstructural Control on the Failure Kinetics and the Reliability Improvement of Al and Al-Alloy Interconnects

Seung Hyuk Kang
Materials Sciences Division
Center for Advanced Materials

December 1996
Ph.D. Thesis

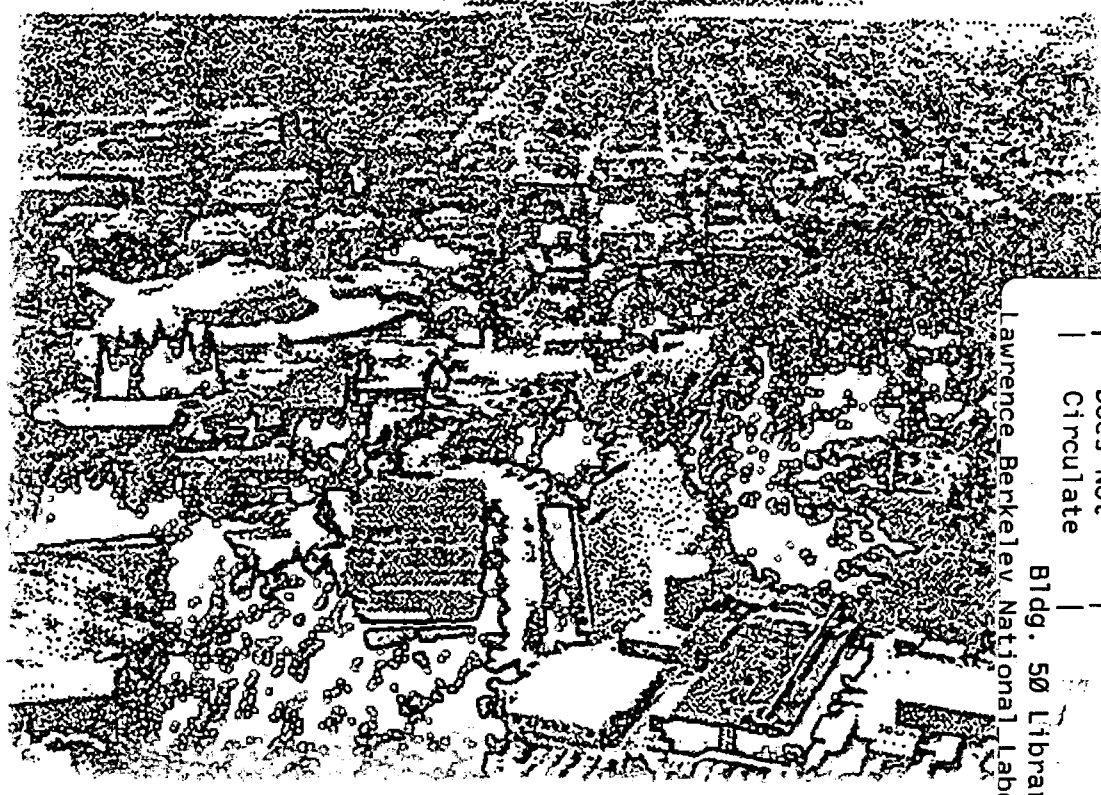

REFERENCE COPY
Does Not
Circulate
Bldg. 50 Library - Ref.
Lawrence Berkeley National Laboratory
LBNL-39719
Copy 1

DISCLAIMER

This document was prepared as an account of work sponsored by the United States Government. While this document is believed to contain correct information, neither the United States Government nor any agency thereof, nor the Regents of the University of California, nor any of their employees, makes any warranty, express or implied, or assumes any legal responsibility for the accuracy, completeness, or usefulness of any information, apparatus, product, or process disclosed, or represents that its use would not infringe privately owned rights. Reference herein to any specific commercial product, process, or service by its trade name, trademark, manufacturer, or otherwise, does not necessarily constitute or imply its endorsement, recommendation, or favoring by the United States Government or any agency thereof, or the Regents of the University of California. The views and opinions of authors expressed herein do not necessarily state or reflect those of the United States Government or any agency thereof or the Regents of the University of California.

LBNL-39719

Effects of Microstructural Control on the Failure Kinetics and the Reliability Improvement of Al and Al-Alloy Interconnects

Seung Hyuk Kang

Ph.D. Dissertation

Department of Materials Science and Mineral Engineering
University of California, Berkeley

and

Center for Advanced Materials
Materials Science Division
Lawrence Berkeley National Laboratory
1 Cyclotron Road
Berkeley, CA 94720

December 1996

This work was supported by the Director, Office of Energy Research, Office of Basic Energy Sciences, Materials Science Division, of the U.S. Department of Energy, under Contract No. DE-AC03-76SF00098.

Effects of Microstructural Control on the Failure Kinetics and the Reliability Improvement of Al and Al-Alloy Interconnects

Copyright © 1996

by

Seung Hyuk Kang

The U.S. Department of Energy has the right to use this document
for any purpose whatsoever including the right to reproduce
all or any part thereof

Abstract

Effects of Microstructural Control on the Failure Kinetics and the Reliability Improvement of Al and Al-Alloy Interconnects

by

Seung Hyuk Kang

Doctor of Philosophy

in

Materials Science and Mineral Engineering

University of California, Berkeley

Professor John W. Morris, Jr., Chair

The reliability of microelectronic systems is often limited by electromigration failure in Al-based thin-film conducting lines which interconnect devices to form an integrated circuit. Under an applied electric field Al atoms migrate with the electron flow, causing a counterflow of vacancies that accumulate into voids, eventually leading to an open circuit failure. The work reported here is concerned with clarifying the microstructural mechanism of electromigration failure, and with developing a metallurgical method to improve the electromigration resistance of Al-based interconnects. Pure Al, Al-2Cu, and Al-2Cu-1Si lines with quasi-bamboo microstructures are explored as a function of heat treatment conditions and current density. The "weakest" microstructural unit that causes failure is

identified by electron microscopy; with rare exceptions, failure occurs at the upstream end of the longest polygranular segment in a given line. This microstructural characteristic of electromigration failure is even observed in lines whose maximum segment lengths are less than a few microns. The time to failure appears to increase exponentially with decreasing longest polygranular segment length. A simple constitutive equation is reported to describe the failure kinetics as a function of the polygranular segment length that leads to failure. Given correct values of the kinetic constants included in the equation, this microstructure-based constitutive relation will provide a way to assess interconnect reliability. An effective metallurgical method that can eliminate relatively long polygranular segments is post-pattern annealing. This heat treatment particularly narrows the distribution of the longest polygranular segment lengths over a large set of lines. As a consequence, the time-to-failure distribution narrows as well, so that the time to first failure increases more substantially than the median time to failure.

DEDICATED TO

my parents

and

God, my Lord

TABLE OF CONTENTS

CHAPTER 1: INTRODUCTION 1

1.1 Background 3

1.2 Atomic Transport in Thin-Film Conducting Lines 3

1.2.1 Electromigration: Diffusion under Electronic Current 3

1.2.2 Thermomigration: Diffusion under Temperature Gradient 6

1.2.3 Electromigration-Induced Back Diffusion 7

1.2.4 Stress-Induced Voiding 9

1.3 Electromigration and Reliability 11

1.3.1 Vacancy Flux Divergence 11

1.3.2 Damage Formation and Microstructure 12

1.3.3 Lifetime Testing and Reliability Evaluation 16

1.4 Methods to Improve Electromigration Resistance 19

1.4.1 Reducing the Atomic Flux 19

1.4.2 Reducing the Flux Divergence 20

1.5 Objectives 22

1.6 References 23

CHAPTER 2: EXPERIMENTAL TECHNIQUES 30

2.1 Experiments using Conventional Test Structures of Al-based Interconnects 30

2.1.1 Composition 30

2.1.2 Film Deposition and Patterning 30

2.1.3 Post-Pattern Annealing 31

2.1.4 Electromigration Testing and Microstructure Analysis 32

2.2 Microfabrication of Thin-Film Conducting Lines onto Silicon Nitride Windows 33

2.3 References 39

CHAPTER 3: INTERCONNECT MICROSTRUCTURAL CONTROL 40

3.1 Introduction 40

3.2 Microstructural Characteristics prior to Patterning 42

3.2.1 As-deposited Films 42

3.2.2 Pre-Pattern Annealing 43

3.3 Microstructural Control by Post-Pattern Annealing 48

3.3.1 Post-Pattern Annealing 48

3.3.2 Evolution of Quasi-Bamboo Microstructures 50

3.4 TEM Analysis of Polygranular Segments 53

3.4.1 Metallography 53

3.4.2 Statistical Analysis of Polygranular Segment Lengths 55

3.5 Conclusion 64

3.6 References 64

CHAPTER 4: EFFECT OF POST-PATTERN ANNEALING ON THE RELIABILITY OF Al-BASED INTERCONNECTS 68

4.1 Introduction 68

4.2 Post-Pattern Annealing of Al Alloy Lines 72

4.2.1 Effect of Annealing Time 72

4.2.2 Effect of Annealing Temperature 75

4.2.3 Failure Time as a Function of Polygranular Segment Length 77

4.3 Post-Pattern Annealing of Pure Al Lines 81

4.4 Effect of Grain Structure on the Kinetics and Mechanism of Electromigration Failure 85

4.4.1 Effect of Post-Pattern Annealing on Reliability 85

4.4.2 Failure Mechanism in "Near-Bamboo" Structures 86

4.4.3 Current Density Dependence 87

4.5 Investigation of Failure Mechanism and Kinetics using Silicon Nitride Windows 90

4.5.1 Identification of the Weakest Polygranular Segment 90

4.5.2 Reliability Improvement by Microstructural Modification 93

4.6 Conclusion 96

4.7 References 97

CHAPTER 5: FAILURE KINETICS: THE KINETIC EQUATION 100

5.1 Introduction 100

5.2 Review of the Diffusion Model 101

5.3 Experimental Analysis of the Kinetic Equation 105

5.3.1 Characteristic Time 106

5.3.2 Characteristic Length 106

5.3.3 Effect of Current Density 108

5.4 Implications 111

5.5 Conclusion 113

5.6 References 114

APPENDIX: BLECH LENGTH vs. CRITICAL POLYGRANULAR SEGMENT LENGTH 116

A.1 Blech Length: Effect of Line Length on Electromigration 116

A.2 Blech Length and Quasi-Bamboo Microstructures 119

A.3 References 123

LIST OF TABLES

Table 1.1 IC technology roadmap from Semiconductor Industry Association (SIA). 2

Table 1.2 Theoretical values of activation energy (E_a) for different diffusion mechanisms. 18

Table 3.1 The changes in polygranular segment lengths with the changes in annealing condition. Also, see Figs. 3.11 and 3.12. 59

Table 3.2 The changes in the longest polygranular segment lengths from the set of twenty Al-2Cu lines with the changes in annealing condition. Also, see Fig. 3.13. 61

Table 4.1 The kinetic constants t_0 and l_0 values calculated from the curves in Figs. 4.10 and 4.11. 80

Table 5.1 The kinetic constants t_0 and l_0 values with the change in current density. These values were calculated from the curves in Fig. 5.5. 110

Table A.1 The threshold product, $(jl)_c$, values reported from prior work. 120

LIST OF FIGURES

Fig. 1.1 Schematic illustration of the electromigration flux at a grain-boundary triple junction. 13

Fig. 1.2 Schematic illustration of non-uniform grain size distribution. Significant mass depletion occurs at the boundary from large to small grains. 14

Fig. 1.3 Schematic illustration of quasi-bamboo microstructures. The vacancy accumulation at the upstream end of a polygranular segment creates a void. 15

Fig. 1.4 A log-normal distribution of failure times. This distribution was obtained from a set of fifty Al-2Cu lines. 17

Fig. 1.5 Schematic plot showing the variations in median time to failure (MTF) and deviation of the time to failure (DTF) as a function of effective line width, w/G (w: line width, G: mean grain size). ... 21

Fig. 2.1 Schematic illustration of thin-film conducting lines that are designed for electromigration lifetime testing using a four-point probe station. 33

Fig. 2.2 Schematic representations of silicon nitride (SiN_x) windows that are fabricated on a silicon wafer. 34

Fig. 2.3 Cross-sectional view of the major steps in a basic process that fabricates Al-2Cu thin-film conducting lines on silicon nitride windows. 36

Fig. 2.4 Schematic illustration of Al-2Cu conducting lines fabricated on silicon nitride windows: (a) multiline structure and (b) single line structure. 38

Fig. 3.1 TEM micrographs showing the quasi-bamboo microstructure of Al-2Cu lines used in this work. The width of the lines is 1 μm. 41

Fig. 3.2 A TEM micrograph showing a typical microstructure of a pure Al film deposited at room temperature. 44

Fig. 3.3 A TEM micrograph showing a typical microstructure of an Al-2Cu-1Si film deposited at 450 °C. 44

Fig. 3.4 A TEM micrograph showing a typical microstructure of an Al-2Cu-1Si film after a heat treatment of 500 °C for 5 min. 45

Fig. 3.5 A TEM image showing an abnormally large and irregularly shaped grain (a), and selected area diffraction patterns obtained from the boundaries A (b) and B (c). 46

Fig. 3.6 A TEM image showing two boundaries (a), and selected area diffraction patterns obtained from the boundaries C (b) and D (c). 47

Fig. 3.7 Relevant portion of the Al-Cu phase diagram showing the post-pattern-annealing temperatures used for this study. The broken lines indicate the metastable GP zone, θ″and θ′ solvuses. 49

Fig. 3.8 TEM micrographs showing the grain structures of pure Al lines during post-pattern annealing: (a) as-patterned, (b) annealed for 5 min. and (c) annealed for 60 min. at 480 °C. 51

Fig. 3.9 TEM micrographs showing the grain structures of Al-2Cu-1Si lines: (a) as-patterned and (b) annealed at 480 °C for 2 hrs. 51

Fig. 3.10 TEM images of an Al-2Cu line (50 μm in length) that was fabricated on a silicon nitride window. These show the microstructure along the whole line from the cathode to the anode. The thickness of the window was 0.1 μm. 54

Fig. 3.11 Histograms of polygranular segment length for three annealing conditions: (a) 520 °C, 30 min. (b) 520 °C, 1 hr. (c) 540 °C, 1hr. Three Al-2Cu lines were randomly chosen for each condition. 56

Fig. 3.12 The distributions of the polygranular segment lengths from three randomly chosen Al-2Cu lines with the change in annealing parameters. 58

Fig. 3.13 The distributions of the longest polygranular segment lengths for three sets of Al-2Cu lines for three different annealing conditions. 62

Fig. 4.1 Schematic illustration of the mechanism of electromigration failure in an Al-2Cu line with a quasi-bamboo structure. The spacing between the void and the Al_2Cu precipitate is approximately equal to the length of the polygranular segment (Ref. 4.1). 69

Fig. 4.2 SEM micrographs showing the typical morphology of the failure site. The void-precipitate separation is a reasonable measure of the polygranular segment length. 70

Fig. 4.3 Schematic illustration of patterning from a polygranular film. The microstructure of the line is derived from that of the film. Line (a) has a much longer polygranular segment length that line (b). ... 71

Fig. 4.4 Time-to-failure distribution with annealing times for Al-2Cu-1Si lines, annealed at T = 480 °C. The lines were tested at j = $3x10^6$ A/cm^2 and T = 225 °C. 73

Fig. 4.5 Variations in MTF and DTF as a function of annealing time for Al-2Cu-1Si lines, annealed at T = 480 °C. 73

Fig. 4.6 Variations in MTF and DTF as a function of annealing time for Al-2Cu lines, annealed at 480 °C. 74

Fig. 4.7 TEM micrographs showing the grain-structures of Al-2Cu-1Si lines: (a) as-patterned and (b) annealed at 480 °C for 2 hrs. Note the reduction in polygranular segment length after annealing. 74

Fig. 4.8 Time-to-failure distributions as a function of annealing temperature for Al-2Cu lines, annealed for one hour at each T. The lines were tested at j = $3x10^6$ A/cm^2 and T = 225 °C. 76

Fig. 4.9 The distributions of void-precipitate spacings at the failure sites of each group of the lines annealed at 520 °C and 540 °C for one hour. 76

Fig. 4.10 Semi-log curves showing the relation between polygranular segment length and failure time for 1.3 and 2 μm line. The open squares indicate data that were obtained by interrupting tests. Also see Ref. 4.1. 79

Fig. 4.11 A semi-log curve showing failure time as a function of polygranular segment length. The data for 520 °C and 540 °C anneals coalesce onto a single straight line. 79

Fig. 4.12 Time-to-failure distributions with annealing times for pure Al lines, annealed at T = 480 °C. The lines were tested at j = 1.2×10^6 A/cm^2 and T = 225 °C. 82

Fig. 4.13 Variations in MTF and DTF as a function of annealing time for pure Al lines, annealed at T = 480 °C. 82

Fig. 4.14 TEM micrographs of Al lines showing the microstructure evolution into a nearly bamboo structure by post-pattern annealing: (a) as-patterned, (b) annealed for 5 min., and (c) annealed for 60 min. at 480 °C. The dramatic reduction in the polygranular segment length is apparent in (c) which shows the longest polygranular segment in the line with the void at its upstream end. 83

Fig. 4.15 Variations in MTF and DTF for Al-2Cu lines as a function of current density. 89

Fig. 4.16 Void-precipitate spacing distributions at the failure sites with the change in current density. 89

Fig. 4.17 TEM micrographs of an Al-2Cu line (100 μm in length) that was tested at j = 0.8×10^6 A/cm^2 and T = 225 °C. (a) Image along the whole line; the void is located at the upstream end (with respect to electron flow) of the longest polygranular segment in the line. (b) Magnified image of the failure site. 91

Fig. 4.18 Time-to-failure distributions for three annealing conditions. The three sets of Al-2Cu lines were tested at 225 °C under j = $3x10^6$ A/cm^2. 94

Fig. 4.19 Variations in (a) MTF and (b) DTF as a function of annealing conditions. These values were calculated from the distributions plotted in Fig. 4.18. 95

Fig. 5.1 A straight grain boundary segment of length l which represents a sequence of grain boundary segment that terminates at blocking grains (Ref. 5.2). 101

Fig. 5.2 Schematic curves that follow Eq. (4.1) based on the argument that l_0 is determined by Eq. (5.7). Suppose that the three sets of lines have identical geometry and microstructural configuration. 104

Fig. 5.3 Schematic curves following Eq. (4.1) while having different l_0 values. It is assumed that the two curves are obtained from the two sets of geometrically identical lines that are tested at the same condition. 107

Fig. 5.4 Time-to-failure distribution for three different current densities. For the tests three sets of Al-2Cu lines were annealed at 520 °C for 30 min. 109

Fig. 5.5 Semi-log curves showing the relation between failure time and polygranular segment length with changing current density. 109

Fig. 5.6. SEM micrographs showing the reference lines (A and C) which were not stressed by current and the tested line (B) after the failure under j = $3x10^6$ A/cm^2. Line B shows the depletion of Cu from the

polygranular segment and the upstream bamboo grain. 112

Fig. A.1 TEM micrographs showing the typical failure and damage sites in near-bamboo Al lines that are annealed for one hour at 480 °C. The polygranular segment lengths are indicated. 122

ACKNOWLEDGMENTS

In the beginning God created the heavens and the earth (Genesis 1:1)

By the grace of God, I have been blessed to study some of His handiwork at the University of California, Berkeley. He has guided me to meet a number of people who have inspired and challenged me, not only scientifically but also spiritually.

For the completion of this thesis, I would like to thank Professor Bill Morris. He has my respect as a research supervisor, a distinguished instructor, and an amiable person of humor and wit. I also want to thank my other thesis-committee members, Professor E. R. Weber and Professor C. Hu, for their precious time and valuable discussions. Special thanks are extended to Dr. Choongun Kim who first introduced me to the field of *electromigration,* and gave me a foundation to build from. Thanks are also extended to Dr. F. Y. Génin who deposited Al and Al-2Cu thin films for this research.

I cannot thank enough the people in the Morris Group who have been supportive, approachable, generous, and patient throughout our time together. Especially, I thank Pamela Kramer, Chris Krenn, Heidi Reynolds, and Peter Skarpelos for their constructive and careful review of this thesis. Special thanks to Koji Sato for being such a kind and cheerful officemate, and to Jane Fortado who has helped me navigate the bureaucratic web of tedious paper work on numerous occasions.

I would like to acknowledge the Ministry of Education, Korea, for the fellowship ~~by which~~ I could search for an opportunity to study abroad. Primary support for this work was provided by the Director, Office of Energy Research, Office of Basic Energy Sciences, Division of Materials Science, of the U.S. Department of Energy, under Contract No. DE-AC03-76SF00098.

Most of all, I have been blessed with the consistent support and encouragement from my parents, brothers, and long-time friends. Without my parents' endless prayer, this thesis could never have been completed. I dedicate this thesis to my parents, and to God who answered their prayers.

Finally, it is my delight to mention my fiancée, Eunjee. I must confess that the year 1996 will be remembered, not as the year when I obtained my Ph. D. degree, but as the year when I proposed marriage to her. I love you, Eunjee.

Seung Hyuk Kang

CHAPTER 1

INTRODUCTION

1.1 BACKGROUND

A modern microelectronic chip can contain millions of devices in an area of ~1 cm^2. As shown in Table 1.1, feature sizes as small as 0.35 μm are currently used in commercial chips and, in the next decade, it is expected that feature sizes will approach 0.12 μm. The devices are connected to form an integrated circuit (IC) utilizing Al or Al-alloy thin films that are patterned into narrow lines which function as conducting wires. These lines are fabricated through a variety of complicated processes, and carry extremely high current densities (~5×10^5 A/cm^2) during operation of an IC. The limiting factor in the reliability of microelectronic systems is frequently the integrity of the interconnects.

A common source of interconnect failure is a phenomenon known as electromigration. Starting from the late sixties, an enormous amount of data have been produced to characterize electromigration in metallic thin films, both theoretically and experimentally. Nonetheless, the complete comprehension of the fundamental mechanisms of electromigration is still unsatisfactory. From a physical perspective, electromigration is an atomic transport which is driven by momentum transfer from the highly accelerated electrons to the atoms of the conductors under an electric field. [1.1-1.3] Electromigration is then one of the major concerns in thin-film conducting

lines for the development of advanced devices. In the case of Al-based IC interconnects, Al atoms migrate with the electron flow causing a counter-flow of vacancies that accumulate into voids, which eventually leads to an open circuit failure. The driving force for electromigration increases with the current density. Hence, IC miniaturization ordinarily increases the possibility of electromigration failure.

Table 1.1 IC technology road map from Semiconductor Industry Association (SIA).

		1995	1998	2001	2004	2007
Feature Size (μm)		0.35	0.25	0.18	0.12	0.10
Gates/chip		800K	2M	5M	10M	20M
Bits/chip	•DRAM	64M	256M	1G	4G	16G
	•SRAM	16M	64M	256M	1G	4G
Chip Size (mm^2)	•Logic/microprocessor	400	600	800	1000	1250
	•DRAM	200	320	500	700	1000
Wafer Diameter (mm)		200	200-400	200-400	200-400	200-400
Number of Interconnect Levels (logic)		4-5	5	5-6	6	6-7
Max. Power (W/Die)	•High-performance	15	30	40	40-120	40-200
Power Supply (V)	•Portable	2.2	2.2	1.5	1.5	1.5
Number of I/Os		750	1500	2000	3500	5000
Performance	•Off-chip	100	175	250	350	500
	•On-chip	200	350	500	700	1000

Electromigration creates voids at the atomic flux divergence sites where vacancies are continuously accumulated. [1.4] Since electromigration flux is dominated by grain boundary diffusion, the flux divergence sites are

usually associated with inhomogeneity in grain structure. For this reason, modification of grain structure in order to minimize flux divergence is a subject of technological interest. [1.5-1.10] This work is primarily concerned with investigating the influences of grain structure on the mechanisms and kinetics of the electromigration failure in Al and Al-alloy interconnects, and then proposing a metallurgical method which can effectively improve the reliability.

1.2 ATOMIC TRANSPORT IN THIN-FILM CONDUCTING LINES

When atomic transport occurs in thin-film conducting lines under the application of an electric field, the dominant transport mechanism is electromigration. The detailed nature of the transport process is very complex, since electromigration is often coupled with atomic transport by the mechanical stress and temperature distributions along the lines. In this section, while particular emphasis is placed on electromigration itself, the mechanisms that can also contribute to the transport process are briefly reviewed.

1.2.1 Electromigration: Diffusion under Electronic Current

The driving force for electromigration is composed of two forces: an electrostatic force and an "electron-wind" force. [1.11-1.15] The electrostatic force is due to the interaction between the electric field and the ionic core of the atoms stripped of their valence electrons. The electron-wind force

arises from collisions of the flowing charge carriers with the ions. These two forces act in opposite direction. In metals, which are good electrical conductors, the electron-wind force is usually dominant.

In a one-component system, the net driving force due to an applied electric field is expressed in the following form:

$$F = Z^{*}eE = Z^{*}e\rho j \tag{1.1}$$

where Z^{*} is an effective charge number E is the electric field, e is the electronic charge, ρ is the resistivity of the conductor, and j is the current density. The effective charge number Z^{*} in Eq. (1.1) includes two contributions that are mentioned above, and can be given by

$$Z^{*} = Z^{*}_{el} + Z^{*}_{wd} \tag{1.2}$$

where Z^{*}_{el} represents the effect of the electrostatic field, and Z^{*}_{wd} reflects the effect of the electron-wind force. The nature of the electrostatic force is still under investigation. On the other hand, the electron-wind force has been estimated theoretically, and the Z^{*}_{wd} in Eq. (1.2) is written as

$$Z^{*}_{wd} = -\gamma z \frac{\rho_d}{N_d} \frac{N}{\rho} \frac{|m^{*}|}{m^{*}} \tag{1.3}$$

where $\gamma$is a numerical constant of the order of one-half, z is the electron-to-atom ratio of the lattice, ρ_d/N_d is the specific resistivity of the moving atom defect, ρ/N is the specific resistivity of the lattice atom, and m^{*} is the effective mass of the electron.

In Eq. (1.1) the sign of Z^{*} determines the direction of electromigra-

tion. In the case of $Z^* < 0$, the atomic transport occurs in the same direction as the electron motion (i.e. toward the anode). For $Z^* > 0$, the atoms diffuse toward the cathode. The value of Z^* for Al is around -10. Scorzoni et al. estimated the order of magnitude of the electromigration driving force in Al conductors, [1.16] Eq. (1.1) yields $|F| \approx 3000$ eV/m, at room temperature for $Z^* = -10$ and $j = 10^6$ A/cm^2.

From Eq. (1.1), in a lattice, the atomic flux J_l due to electromigration can be expressed as

$$J_l = N_l (D_l / kT) Z^* eE \tag{1.4}$$

where N_l is the atomic density, D_l is the uncorrelated diffusion coefficient at the absolute temperature T, and k is the Boltzman constant. In polycrystalline films, it is necessary to consider the transport along grain boundaries. It is convenient to write a new flux equation which is similar to Eq. (1.4). For a film with an ideally textured grain structure, the flux can be expressed as

$$J_{gb} = N_{gb} (\delta / d) (D_{gb} / kT) Z^*_{gb} eE \tag{1.5}$$

where the subscript gb refers to grain boundary parameters, δ is the effective width of the boundary (~10 Å), and d is the average grain size. It is difficult to calculate the magnitude of the flux given by Eq. (1.5) due to the limited knowledge of grain boundary parameters. A rough calculation of J_{gb} and J_l for Al electromigration in polycrystalline Al films shows that the ratio J_{gb}/J_l is about 10^6 at 175 °C. [1.17] In the case of Cu electromigration in Al films, the ratio is about 10^4 at 225 °C. [1.15] Thus, at moderate temperatures, the atomic flux from lattice diffusion is vanishingly small compared

with that from grain-boundary diffusion; grain-boundary electromigration is the dominating mode of atomic transport.

1.2.2 Thermomigration: Diffusion under Temperature Gradient

During device operation, temperature gradients exist both globally and locally in thin-film interconnects since heat can be generated by Joule heating. The global temperature gradient across the conductor is usually small except near the electrodes or the contact pads. On the other hand, large local temperature gradients can be caused by poor adhesion or contamination at the interface between metal film and substrate, or by the thickness variation of the metal film.

The driving force produced by a temperature gradient is often described by the following equation: [1.19]

$$F = - Q^* (\nabla T) / T \tag{1.6}$$

where Q^* is the heat of transport, defined to be the quantity of heat flow needed to maintain steady-state conditions with unit mass transport. Specific values of Q^* have been found, particularly, in the case of aluminum, gold, and indium. [1.20] Using data in the literature, Scorzoni et al. calculated the thermomigration driving force at a typical electromigration condition. [1.16] In the case of Al, Q^* is approximately 0.03 eV, while a maximum estimate for the temperature gradient is 2×10^3 °C/cm. These values lead to the result that $|F|$ is about 13 eV/m. This value is two orders of magnitude smaller than the electromigration driving force (~3000 eV/m) indi-

cated in the previous section. Hence, thermomigration effects on interconnect failure are usually neglected with respect to electromigration effects.

1.2.3 Electromigration-Induced Back Diffusion

Electromigration results in the depletion of atoms at the one end of the conductor and the accumulation of atoms at the other end, and, hence, creates concentration or stress gradients along the conductor. It has been suggested that either gradient can lead to a chemical-potential gradient which, in turn, leads to a back diffusion that opposes electromigration. Blech and Herring first formulated the back-diffusion effect by proposing the following flux equation: [1.21]

$$J = ND / kT (Z^{*}eE - \nabla\mu) \tag{1.7}$$

where N is the atomic density, D is a diffusion coefficient, and μ is a chemical potential. The chemical potential μ is the difference between the atomic and vacancy chemical potentials, that is, $\mu = \mu_a - \mu_v$, where μ_a and μ_v are the chemical potentials of the atoms and vacancies, respectively.

Diffusion Equation in the presence of Concentration Gradient

If there is no internally generated stress gradient, the chemical potential gradient in Eq. (1.7) can be expressed in terms of the concentration gradient. The one-dimensional flux equation is given in the following form:

$$J = (ND / kT)\, Z^{*}eE - D\left(\frac{\partial N}{\partial x}\right) \tag{1.8}$$

It follows that the diffusion equation is derived as

$$\frac{\partial N}{\partial t} = \frac{\partial}{\partial x}\left(D\frac{\partial N}{\partial x} - vN\right) = D\frac{\partial^2 N}{\partial x^2} - v\frac{\partial N}{\partial x} \tag{1.9}$$

where v is the drift velocity of atoms which is given by

$$v = (D / kT)\, Z^{*}eE \tag{1.10}$$

Eq. (1.9) is commonly referred as the "electromigration equation" which has been extensively used by many researchers. [1.22-1.24]

Diffusion Equation in the presence of Stress Gradient

Electromigration builds up stresses in the case that there is a vacancy equilibrium with the stress. The assumption for the stress generation is that there is no vacancy supersaturation in the presence of grain boundaries or dislocations. Blech and Herring proposed that, if a local equilibrium is maintained with respect to adding atoms or vacancies at the grain boundaries, the chemical potential in Eq. (1.7) is solely expressed in terms of the stress:

$$\mu = \mu_a - \mu_v = \mu_0 + \Omega\sigma_{nn} \tag{1.11}$$

where Ω is the atomic volume, σ_{nn} is the stress normal to the grain boundary, and μ_0 is a constant. By substituting Eq. (1.11) into Eq. (1.7), the one-dimensional flux equation is written as

$$J = ND / kT \ (Z^{*}eE - \Omega \frac{\partial \sigma_{nn}}{\partial x}) \tag{1.12}$$

From the same theoretical background, Korhonen et. al developed a diffusion equation concerning the stress build-up by electromigration. [1.25] They proposed that the main role of excess vacancies at a given temperature is to generate mechanical stress. The stress evolution under electromigration is described by

$$\frac{\partial \sigma}{\partial t} = \frac{\partial}{\partial x}\left[\kappa\left(\frac{\partial \sigma}{\partial x} + G\right)\right] \tag{1.13}$$

where σ is a uniform stress across a cross section, κ is $DB\Omega / kT$ (B: appropriate modules), and G is $Z^{*}eE / \Omega$. Eq. (1.13) has been solved, with the use of several simplifying assumptions, to explain various phenomena in thin-film conductors [1.26-1.28]. Interestingly, Lloyd pointed out that the equation is not formally correct, since it states that stress evolution is independent of the current density. [1.29]

1.2.4 Stress-Induced Voiding

Modern interconnects are relatively complicated, constructed of different materials, frequently fabricated with non-equilibrium processes, subjected to widely varying temperatures during fabrication. It is well known that voids can form from high residual stresses in metal films, which are usually the consequence of the thermal expansion mismatch between Al and Si or dielectric layers. These voids look similar to electromigration-induced voids, but they are definitely not caused by electromigra-

tion. The mechanism of stress-induced voiding is the condensation of supersaturated vacancies produced by hydrostatic tension. The presence of hydrostatic triaxial tensile stress increases the local equilibrium concentration of vacancies present at any given temperature. [1.30] Some of these vacancies coalesce to form a void. A void must reach a certain critical size before it is stable. Considering the residual stress only, which is on the order of 500 MPa in Al thin films, [1.31] the hydrostatic stress is not enough to overcome the activation energy to obtain a critical void size. Voids will then be formed preferably as a result of heterogeneous nucleation, especially on the grain boundaries where the surface energy is relatively high. [1.31, 1.32]

In general, mechanical stress induced voiding occurs only in metal lines encapsulated in passivation layers. In the absence of a passivation layer, the stress normal to the free surface of the metal is zero. [1.31] Hence there is no hydrostatic tension, and no driving force for void formation. When the metal is encapsulated in a passivation layer and bounded to a dielectric layer, however, a decrease in the metal volume relative to its surroundings will result in a triaxial tensile stress.

While both mechanical stress and electromigration lead to the formation of voids, it is commonly accepted that interconnect failure is predominantly caused by electromigration. Stress-induced voiding can be considered as a phenomenon enhancing failure kinetics rather than as a direct failure mechanism. When electromigration is coupled with thermal stress effects, failure in interconnects may be accelerated by potential pre-existing voids.

1.3 ELECTROMIGRATION AND RELIABILITY

1.3.1 Vacancy Flux Divergence

In thin-film conducting lines, electromigration-induced damage usually appears in the form of voids that can grow to cause electrical discontinuity. Electromigration creates voids at the atomic flux divergence sites where vacancies are continuously accumulated. Since the electromigration flux is dominated by the vacancy diffusion along grain boundaries, it is convenient to consider the role of grain-boundary vacancy flux J_v in void formation. The vacancy flux is expressed as the sum of the flux due to electromigration and the flux induced by the vacancy-concentration gradient:

$$J_v = J_{gb} - D_v \nabla C_v \tag{1.14}$$

where J_{gb} is given by Eq. (1.5), D_v is the vacancy diffusivity in the grain boundary, and C_v is a local vacancy concentration. The local variation of the vacancy concentration C_v can be deduced using the continuity equation:

$$\frac{\partial C_v}{\partial t} = -\nabla \cdot J_v + \frac{C_v - C_0}{\tau} \tag{1.15}$$

where C_0 is the equilibrium vacancy concentration at given temperature and τ is the average lifetime of a vacancy. The second term on the right-hand side describes the local deviation of the vacancy concentration from thermal equilibrium. It follows that, under steady-state conditions, Eq. (1.15) yields

$$C_v - C_0 = \tau \nabla \cdot J_v \tag{1.16}$$

Hence the extent of variation of the local vacancy concentration is simply

proportional to the vacancy flux divergence ($\nabla \cdot J_v$). Consequently, void failure occurs at the site where the local vacancy flux divergence is the maximum.

1.3.2 Damage Formation and Microstructure

Electromigration causes different kinds of failures in thin-film conducting lines. The most familiar is void failure along the length of the line, which is often called an "internal" failure. Another common type of failure is diffusive displacement at the studs of the line in a multilayered structure, which destroy electrical contact. Flux divergence that can lead to these kinds of failures is caused by inhomogeneities in microstructure, temperature, and geometry. In the particular case of an internal failure, microstructural inhomogeneities along the line have been considered the most important factor causing serious flux divergences, as discussed by Attardo and Rosenberg in their landmark paper.

A well-known microstructural inhomogeneity is found at the junction of three grains (i.e. grain-boundary triple point). From Fig. 1.1, in order to avoid vacancy or atom accumulations at the triple point, the following flux-balance equation should hold:

$$J_1 = J_2 + J_3 \tag{1.17}$$

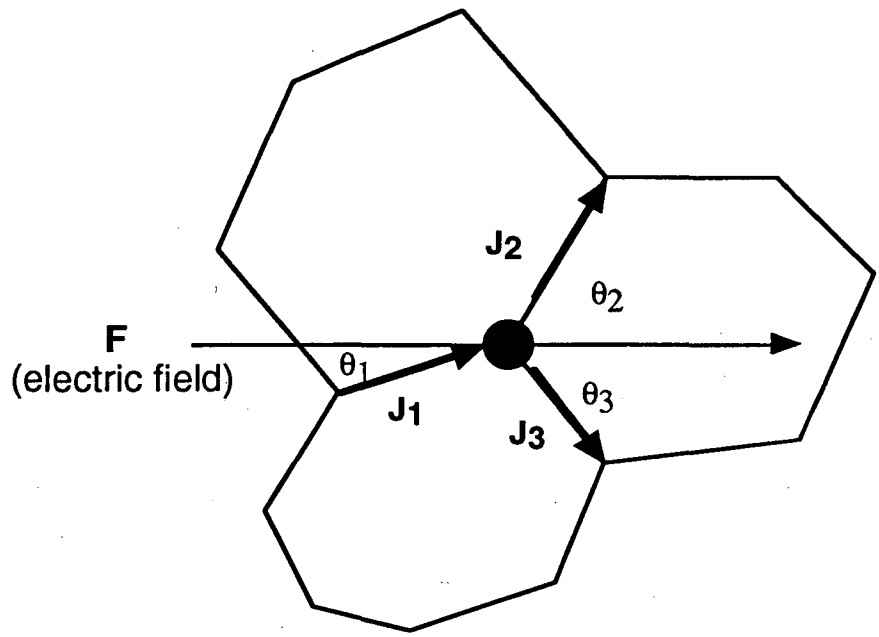

Fig. 1.1 Schematic illustration of the electromigration flux at a grain-boundary triple junction.

If electromigration is the only driving force for the atomic transport, from Eq. (1.5), Eq. (1.17) can be written as

$$N_1 D_1 Z^*_1 \cos\theta_1 = N_2 D_2 Z^*_2 \cos\theta_2 + N_3 D_3 Z^*_3 \cos\theta_1 \qquad (1.18)$$

where N_i, D_i, Z^*_i, and θ_i are the atomic density, the diffusivity, the effective charge number, and the angle between applied electric field and transport direction at the ith grain boundary, respectively. In the case where grain boundaries have reached an equilibrium configuration by means of a proper heat treatment, the flux divergence at the triple point is determined by the

differences in N_i, D_i, and Z_i^*. In general, the differences in N_i, D_i, and Z^*_i can arise from variations in the atomic structure or defect concentration at the grain boundary, such as that caused by the segregation of solute atoms or contaminants. This can affect the nature of the interaction between the migrating ion and the grain boundary atoms, consequently altering the diffusivity parameters and the activation energy.

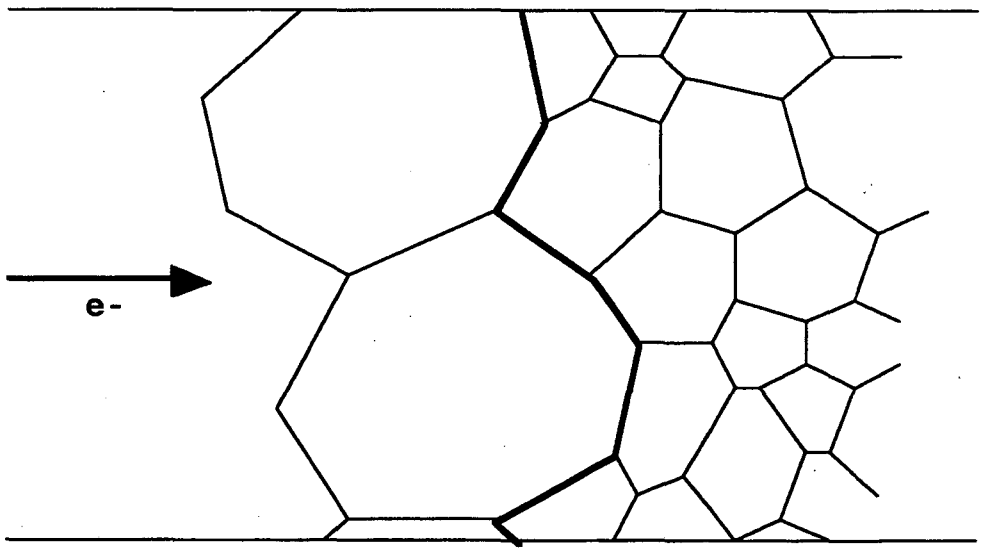

Fig. 1.2 Schematic illustration of non-uniform grain size distribution. Significant mass depletion occurs at the boundary from large to small grains.

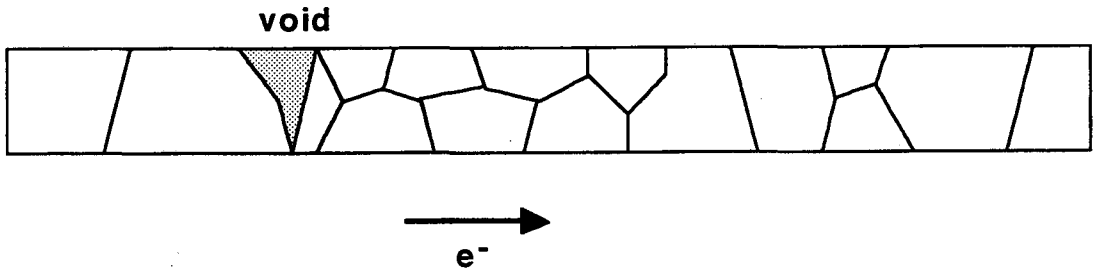

Fig. 1.3 Schematic illustration of quasi-bamboo microstructures. The vacancy accumulation at the upstream end of a polygranular segment creates a void.

A concurrent cause of non-zero flux divergence, and consequent sources of damage, is a localized grain-size variation. For example, vacancy build-up occurs when the number of atoms migrating out of the junction through the fine-grain side exceeds that migrating into the junction through the coarse-grain side. This situation is schematically described in Fig. 1.2. Thus, a uniform grain-size distribution is desirable to minimize electromigration-induced damage. This argument is particularly true in modern submicron interconnects that have "quasi-bamboo" microstructures like that schematically shown in Fig. 1.3. Since grain boundary diffusion is much more rapid than bulk diffusion at the relatively low temperatures at which microelectronic devices operate, the polygranular segments are regions of exceptionally high diffusivity. The rapid change in flux at the ter-

minal ends of polygranular segments causes these locations to be the preferred sites for electromigration damage; the vacancy accumulation at the upstream end of a polygranular segment induces a void formation. For this reason, a major percentage of recent research on electromigration has been concerned with understanding the voiding mechanism in the lines with quasi-bamboo microstructures, and proposing methods which can inhibit void failure.

1.3.3 Lifetime Testing and Reliability Evaluation

The most common method used to evaluate the resistance to electromigration failure is the lifetime measurement of interconnects. It is well known that failure times from a large set of macroscopically identical lines follow a log-normal distribution, [1.33-1.35] as shown in Fig. 1.4. The distribution of failure times are characterized by two statistical parameters: median time to failure (MTF) and deviation of the time to failure (DTF). MTF is the time at which 50 % of the tested lines fail. DTF reflects the scatter in failure time (i.e. standard deviation of a log-normal distribution).

The reliability of a chip against electromigration failure is determined by the time at which the first failure in a large set of lines occurs. The reliability margin is then usually set to 0.01 % or 0.1 % cumulative failures. For example, 0.01 % failure indicates the first failure in a set of 10^5 lines. Hence, an increase in MTF does not necessarily reflect a reliability improvement. To ensure a high value of the time to first failure, a method to improve the reliability must be one which not only increases MTF, but also decreases DTF or, at least, maintains low DTF values.

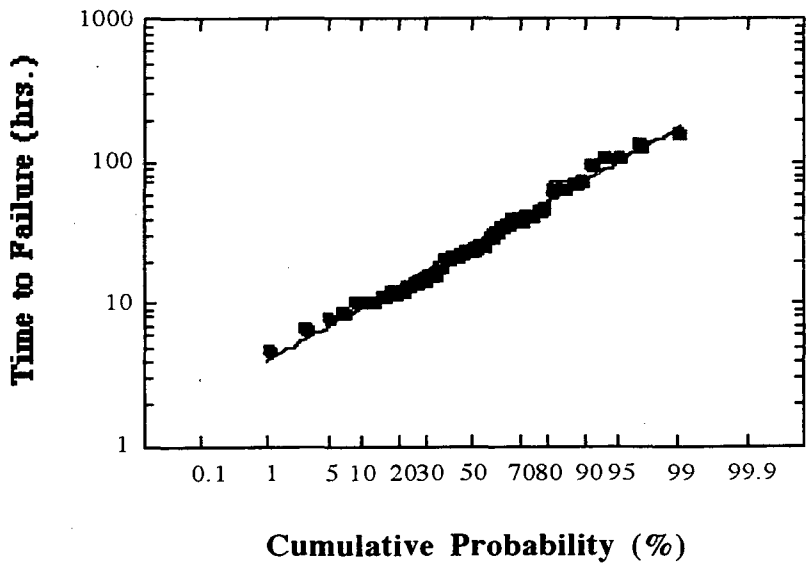

Fig. 1.4 A log-normal distribution of failure times. This distribution was obtained from a set of fifty Al-2Cu lines.

Lifetime testing needs to be finished in a reasonable time frame. The testing is conducted at a set of accelerated conditions under high current densities and at elevated temperatures. The data are extrapolated to the chip operating conditions, which are usually near room temperature and under current densities around 5×10^5 A/cm^2. For the extrapolation, an Arrhenius-like empirical equation, originally proposed by Black, [1.36] is used:

$$\mathrm{MTF} = A\, j^{-n} \exp\left(E_f / kT\right) \tag{1.19}$$

where A is a material constant relating to structural, electrical and diffusional properties of thin-film conductors, and E_f is the activation energy for electromigration-induced failure. The extrapolation assumes that the mechanisms leading to electromigration failures under the accelerated testing are the same as those under chip operating conditions. The temperatures in such accelerated tests should be lower than one-half of the melting point of the conductor below which the bulk contribution to the mass transport is not important. The activation energy E_f can depend on the microstructure, metallurgy, fabrication process, and geometry of the conducting line. For polycrystalline Al and Al alloy films, the experimental values of E_f lie in the range of 0.4 to 1.3 eV. [1.4, 1.36-1.39] Schreiber calculated the theoretical values of activation energy that depend on diffusion mechanisms. [1.40] Table 1.2 summarizes these values.

Table 1.2 Theoretical values of activation energy (E_a) for different diffusion mechanisms.

Diffusion Mechanism	E_a (eV)
lattice (bulk)	1.4
grain boundaries	0.4-0.5
grain boundaries to bulk	0.62
defects to bulk	> 0.62
surface	0.28

1.4 METHODS TO IMPROVE ELECTROMIGRATION RESISTANCE

The basic requirement for suppressing electromigration-induced damage is to minimize the local divergence of atomic flux. In principle, this can be accomplished in either of two ways.

1.4.1 Reducing the Atomic Flux

From Eq. (1.5), the magnitude of the atomic flux is determined by the grain size, the grain boundary diffusivity, and the current density. An increase in the grain size as well as decreases in the grain boundary diffusivity and the current density reduce the atomic flux. A reduction in the current density is not practical, since the current density is fixed by chip requirements. The remaining parameters are then the grain size and grain boundary diffusivity. Relatively large grain sizes can easily be achieved by proper film-deposition techniques and post-deposition heat treatments. Relatively small grain boundary diffusivity can be obtained by producing a texture or adding solutes. For example, a recent report by Hasunuma et al. has shown that very reliable Al lines can be developed by promoting a highly textured film with low angle grain boundaries. [1.6] Also, solute elements in the thin film can reduce the magnitude of the electromigration flux, which has been attributed to the segregation of these elements at the grain boundaries and their interaction with the migrating ions. The most commonly used solute in Al interconnects is Cu. While the exact role of Cu on Al electromigration is still under investigation, the original argument by

Rosenberg has been commonly accepted; excess Cu atoms segregate at the Al grain boundaries and reduce the grain boundary diffusivity of Al. [1.41] Excess Cu atoms above the solubility limit form Al_2Cu precipitates. The role of these precipitates has been emphasized, since these precipitates serve as sources of Cu atoms to Al grain boundaries. Dramatic improvements in electromigration resistance have been reported by modifying the distribution and stability of Al_2Cu [1.42] or Cu [1.43].

1.4.2 Reducing the Flux Divergence

Electromigration can only become a problem when there is source of a atomic flux divergence. In the ideal case, a conductor with a uniform microstructure and no temperature gradient creates no flux divergence so that electromigration-induced damage will not occur. The flux inhomogeneity that can cause an internal failure of the line is related to the grain size and its variation. In the case of the lines with quasi-bamboo microstructures (Fig. 1.3), it is clear that polygranular segments are "weak links" that are vulnerable to electromigration damage. The magnitude of flux divergence increases with the polygranular segment length, since the fast diffusion paths (grain boundaries) increase with the length. Hence, the failure time should be increased by modifying the microstructure to shorten the polygranular segment length.

A simple and common way to improve electromigration resistance is to decrease the effective line width, $w^* = w / G$, where w is the line width and G is the mean grain size. [1.44-1.46] For given line width, w^* can be decreased by changing the deposition conditions of the metal film to maximize

the grain size or by annealing the film to coarsen the grain size prior to patterning. Typical results from these methods are schematically illustrated in Fig. 1.5.

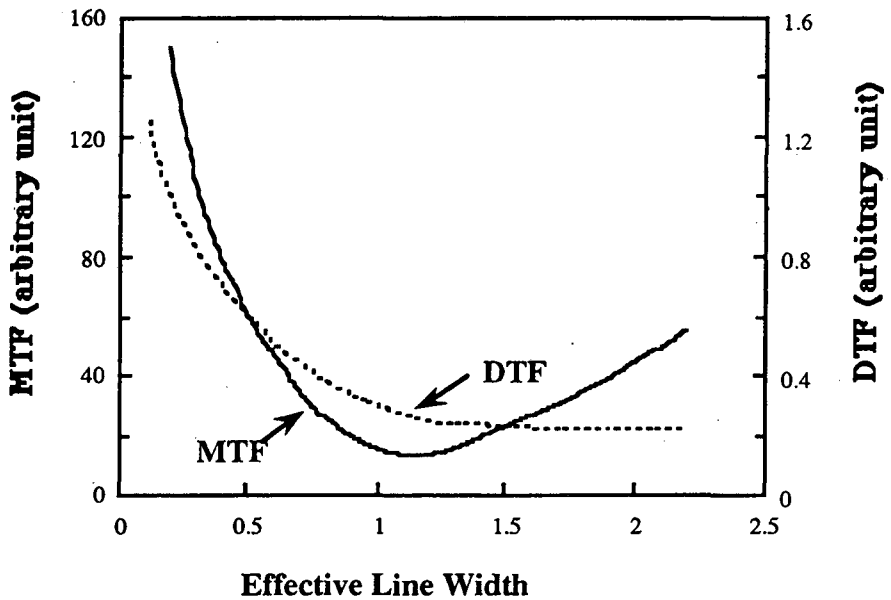

Fig. 1.5 Schematic plot showing the variations in median time to failure (MTF) and deviation of the time to failure (DTF) as a function of effective line width, w/G (w: line width, G: mean grain size).

The median time to failure (MTF) increases substantially as w^* is decreased below unity, that is, the microstructure evolves toward a bamboo structure. However, this increase in MTF does not ensure an improvement in reliability, since the standard deviation in the time to failure (DTF) increases as well. This increase in scatter of the failure time, coupled with

the fact that miniaturization ordinarily leads to an increase in the total number of lines and a rise in the current density, has the consequence that the expected time to first failure in a large set of lines may even decrease as the lines are narrowed. The likely reason for the increase in DTF lies in the fact that, even when w^* is very small, there remains a finite probability that a large population of lines will still include some lines with exceptionally long polygranular segment lengths. Therefore, a microstructural control method employed to improve the reliability must be one which breaks up exceptionally long polygranular segments, rather than decreases only the average length of polygranular segments.

1.5 OBJECTIVES

The objectives of this thesis are to identify the "weakest" microstructural units that cause electromigration failure in Al-based thin-film conductors, and to modify them metallurgically to develop microstructures that resist failure. For these purposes, pure Al, Al-2Cu, and Al-2Cu-1Si lines that have quasi-bamboo microstructures are explored to clarify the microstructural mechanism of electromigration failure. In order to characterize the failure unit, transmission (TEM) and scanning electron microscopy (SEM) are used for the specimens prepared by the techniques described in the following Chapter. As a beneficial metallurgical method that can control the nature of the failure unit, post-pattern annealing is proposed by presenting the results that show substantial improvement in electromigration resistance. Given the post-pattern annealing condition, statistical analyses of the failure unit are associated with statistical parameters (MTF

and DTF) of the results from lifetime testing.

A large amount of data have been documented to show that, in quasi-bamboo structures, polygranular segments are "weak" links that cause failure. However, prior results have often been contradictory, specifically with respect to the failure mechanism in lines which have predominantly bamboo structures with extremely short polygranular segments ("near-bamboo" structures). In this work, hence, lifetime testing and metallographic analyses are particularly concerned with studying the failure mechanism and kinetics for the "near-bamboo" lines.

Experimental techniques, which include a micromachining technique for the fabrication of "silicon nitride windows", are described in Chapter 2. Heat treatments that can modify the microstructures of Al-based interconnects are discussed in Chapter 3. Chapter 4 addresses the advantages of post-pattern annealing that can dramatically improve electromigration resistance. Chapter 5 discusses a simple equation, which describes the microstructural effects on electromigration lifetime, from the qualitative perspective based on the results in Chapters 3 and 4. In the Appendix the "Blech length" argument, which has been a subject of debate in relation to the failure mechanism in quasi-bamboo lines, is reviewed.

1.6 REFERENCES

[1.1] F. M. d'Heurle and R. Rosenberg, "Electromigration in thin films," Physics of Thin Films **7**, 257 (1973).

[1.2] H. B. Huntington, "Electromigration in metals," in *Diffusion in Solids: Recent Developments* (Academic Press, New York, 1974), edited by A. S. Nowick and J. J. Burton, p. 303.

[1.3] P. S. Ho and T. Kwok, "Electromigration in metals," Rep. Prog. Phys. **52**, 301 (1989).

[1.4] M. J. Attardo and R. Rosenberg, "Electromigration damage in aluminum film conductors," J. Appl. Phys. **41**, 2381 (1970).

[1.5] C. V. Thompson and H. Kahn, "Effects of microstructure on interconnect and via reliability: multimodal failure statistics," J. Electron. Mater. **22**, 581 (1993).

[1.6] M. Hasunuma, H. Toyoda, T. Kawanoue, S. Ito, H. Kaneko, and M. Miyauchi, "A highly reliable Al line with controlled texture and grain boundaries," MRS. Symp. Proc. **391**, 335 (1995).

[1.7] G. Rajagopalan, M. L. Dreyer, N. D. Theodore, and T. S. Cale, "Improving electromigration reliability in Al-alloy lines," Thin Solid Films **270**, 439 (1995).

[1.8] S. H. Kang, C. Kim, F. Y. Génin, and J. W. Morris, Jr., "The influence of grain structure on the reliability of narrow Al-based interconnects," MRS. Symp. Proc. **391**, 385 (1995).

[1.9] S. H. Kang, C. Kim, J. W. Morris , Jr., and F. Y. Génin, "Effect of post-pattern annealing on the grain structure and reliability of Al-based interconnects," J. Appl. Phys. **79**, 8330 (1996).

[1.10] S. H. Kang, F. Y. Génin, C. Kim, J. W. Morris, Jr., "Further investigations of the microstructural mechanism of electromigration failure in Al-Cu lines with quasi-bamboo microstructures," MRS. Symp. Proc. (in press).

[1.11] V. B. Fiks, "On the mechanism of the mobility of ions in metals," Sov. Phys. Solid State **1**, 14 (1959).

[1.12] H. B. Huntington and A. R. Grone, "Current-induced marker motion in gold wires," J. Phys. Chem. Solids **20**, 76 (1961).

[1.13] P. S. Ho and H. B. Huntington, "Electromigration and void observation in silver," J. Phys. Chem. Solids **27**, 1319 (1966).

[1.14] R. S. Sorbello, "A pseudopotential based theory of the driving forces for electromigration in metals," J. Phys. Chem. Solids **34**, 937 (1973).

[1.15] A. Lodder, J. Phys. Chem. Solids **51**, 19 (1990).

[1.16] A. Scorzoni, B. Neri, C. Caprile, and F. Fantini, "Electromigration in thin-film interconnection lines: models, methods and results," Mater. Sci. Rep. **7**, 143 (1991).

[1.17] F. M. d'Heurle and I. Ames, "Electromigration in single-crystal aluminum films," Appl. Phys. Lett. **16**, 80 (1970).

[1.18] P. S. Ho, F. M. d'Heurle, and A. Gangulee, "Implications of electromigration for device reliability," in *Electro- and Thermo-Transport in Metals and Alloys* (AIME, New York, 1977), edited by R. E. Hummel and H. B. Huntington, p. 108.

[1.19] A. Christou, "Electrothermomigration theory and experiments in aluminum thin film metallizations," in *Electromigration and Electronic Device Degradation* (John Wiley & Sons, New York, 1994) edited by A. Christou, Chap. 9.

[1.20] G. J. van Gurp and F. J. du Chatenier, Thin Solid Films **131**, 155 (1985).

[1.21] I. A. Blech and C. Herring, "Stress generation by electromigration," Appl. Phys. Lett. **29**, 131 (1976).

[1.22] R. Rosenberg and M. Ohring, "Void formation and growth during electromigration in thin films," J. Appl. Phys. **42**, 5671 (1971).

[1.23] M. Shatzkes and J. R. Lloyd, "A model for conductor failure considering diffusion concurrently with electromigration resulting in a current exponent of 2," J. Appl. Phys. **59**, 3890 (1986).

[1.24] J. J. Clement and J. R. Lloyd, J. Appl. Phys. **71**, 1729 (1991).

[1.25] M. A. Korhonen, P. Borgesen, K. N. Tu, and C.-Y. Li, "Stress evolution due to electromigration in confined metal lines," J. Appl. Phys. **73**, 3790 (1993).

[1.26] M. A. Borgesen, D. D. Brown, and C.-Y. Li, "Microstructure based statistical model of electromigration damage in confined line metallizations in the presence of thermally induced stresses," J. Appl. Phys. **74**, 4995 (1993).

[1.27] B. D. Knowlton, J. J. Clement, R. I. Frank, and C. V. Thompson, "Coupled stress evolution in polygranular clusters and bamboo seg-

ments in near-bamboo interconnects," MRS. Symp. Proc. **391**, 189 (1995).

[1.28] D. D. Brown, J. E. Sanchez. Jr., M. A. Korhonen, and C.-Y. Li, "Cluster interactions and stress evolution during electromigration in confined metal interconnects," Appl. Phys. Lett. **67**, 439 (1995).

[1.29] J. R. Lloyd, "Stress and electromigration," MRS Symp. Proc. **391**, 231 (1995).

[1.30] P. Flinn, "Understanding void phenomena in metal lines; effects of mechanical and electromigration stress," MRS Symp. Proc. **265**,15 (1992).

[1.31] P. Flinn, P. R. Besser, and T. N. Marieb, "Stress-induced void formation in metal lines," MRS Bulletin, December, 26 (1993).

[1.32] P. Flinn, "Mechanical stress in VLSI interconnects: origins, effects, measurements, and modeling," MRS Bulletin, November, 70 (1995).

[1.33] J. A. Schwarz, "Effect of temperature on the variance of the log-normal distribution of failure times due to electromigration damage," J. Appl. Phys. **61**, 801 (1987).

[1.34] L. P. Muray, L. C. Rarhbun, and E. D. Wolf, "New technique and analysis of accelerated electromigration life testing in multilevel metallizations," J. Appl. Phys. **61**, 798 (1987).

[1.35] J. M. Towner, "Are electromigration failures log-normally distributed?" IEEE Proceedings of the 28th International Reliability Physics Symposium, 100 (1990).

[1.36] J. R. Black, "Electromigration: a brief survey and some recent results," IEEE Trans. Electron Devices **ED-16**, 338 (1969).

[1.37] S. M. Spitzer and S. Schwarz, IEEE Trans. Electron Devices **ED-16**, 348 (1969).

[1.38] C.-K. Hu, M. B. Small, and P. S. Ho, "Electromigration in Al(Cu) two-level structures: effect of Cu and kinetics of damage formation," J. Appl. Phys. **74**, 969 (1993).

[1.39] A. S. Oates, "Electromigration transport mechanisms in Al thin-film conductors," J. Appl. Phys. **79**, 163 (1996).

[1.40] H .U. Schreiber, Solid State Electron **24**, 583 (1981).

[1.41] R. Rosenberg, A. F. Mayadas, and D. Gupta, "Grain boundary contributions to transport," Surface Sci. **31**, 566 (1972).

[1.42] C. Kim and J. W. Morris, Jr., "The mechanism of electromigration failure of narrow Al-2Cu-1Si thin-film interconnects," J. Appl. Phys. **73**, 4885 (1993).

[1.43] T. Nemoto and T. Nogami, "Segregation of Cu to grain boundaries by aging treatment and its effect on EM resistance for AlCu/TiN lines," IEEE Proceedings of the 32nd International Reliability Physics Symposium, 207 (1994).

[1.44] E. Kinsbron, "A model for the width dependence of electromigration lifetimes in aluminum thin-film stripes," Appl. Phys. Lett. **36**, 968 (1980).

[1.45] J. Cho and C. V. Thompson, "Grain size dependence of electromigration-induced failures in narrow interconnects," Appl. Phys. Lett. **54**, 2577 (1989).

[1.46] K. Y. Fu, "A model for linewidth-dependent electromigration lifetime and its application to design rule scaling for narrow interconnects," J. Appl. Phys. **69**, 2656 (1991).

CHAPTER 2

EXPERIMENTAL TECHNIQUES

2.1 EXPERIMENTS USING CONVENTIONAL TEST STRUCTURES OF Al-BASED INTERCONNECTS

2.1.1 Composition

Films with three nominal compositions were prepared: pure Al, Al-2Cu, Al-2Cu-1Si (compositions in weight percent). These compositions have commonly been used for Al-based metallizations of integrated circuits. The small amount of Cu solutes leads to a substantial increase of electromigration lifetime. [2.1] The addition of Si may also improve electromigration performance to some degree. [2.2] However, the main purpose of the Si addition is to prevent the formation of Al spikes which penetrate into the Si contact region. The spiking problem is caused by the interdiffusion through the contact between Al and Si. If the contact is to a shallow junction, the spike may cause a junction short. The intentional addition of Si over the solubility limit (~ 0.5 % in Al at 450 °C) suppresses the diffusion of Si into the interconnect, and, hence, can solve the problem. [2.3]

2.1.2 Film Deposition and Patterning

Films of 0.5 μm thickness were deposited by sputtering at room temperature onto p-type (001) Si wafers coated with a thermally grown oxide,

70 nm thick. All the films were patterned into test lines by standard photolithography and reactive-ion-etching (RIE) techniques using equipment in the Berkeley Microfabrication Laboratory. The Al and Al-2Cu films were patterned in the as-deposited condition; the Al-2Cu-1Si film was annealed for 5 min. at 500 °C prior to patterning. The patterned lines were 1 mm in length. The line widths were 1 μm for pure Al and Al-2Cu, and 1.3 μm for Al-2Cu-1Si. The lines were not passivated. A schematic illustration of a multiline test structure with 25 parallel lines is shown in Fig. 2.1. This structure was used for lifetime statistics and conventional electron microscopy. The short line segments (length: 100 μm) among the lines in Fig. 2.1 are reference lines that are not stressed by electrical current. These line segments were fabricated in order to compare the microstructure of tested lines with that of the lines without electromigration.

Some of Al-2Cu films (0.4 μm in thickness) were deposited onto a silicon nitride layer which was grown by LPCVD on p-type (001) Si wafers. The silicon nitride layer was 0.1 μm thick. Multiline (20 parallel lines) and single-line test structures of 100 μm in length were fabricated by the same fabrication techniques.

2.1.3 Post-Pattern Annealing

The grain structure of the lines was modified by post-pattern annealing at several different temperatures (480 °C ~ 540 °C) over a period from 5 min. to 2 hrs. The Al lines were annealed in an Ar atmosphere. The Al-2Cu and Al-2Cu-1Si lines were annealed in forming gas (5% H_2, 95%

N_2). Si diffusion from the substrate was negligible for these annealing conditions. Post-pattern annealing of Al-2Cu and Al-2Cu-1Si lines was conducted at temperatures for which the Cu content is soluble, and were quenched in air after annealing.

2.1.4 Electromigration Testing and Microstructure Analysis

The lines were stressed under electrical currents in an ordinary probe station with a hot plate, a power supply, a multi-channel voltage scanner, and a computer. The hot-plate temperature was maintained at 225 °C during the test. The applied current densities (j) were 1.2×10^6 A/cm^2 for pure Al lines, and over the range from 0.75×10^6 A/cm^2 to 3.0×10^6 A/cm^2 for Al-alloy lines. In these tests, the temperature increase due to Joule heating was less than 5 °C. The failure criterion was an open circuit. The failure times were measured by monitoring the total current of the set of parallel lines. Each failure causes a step-shaped decrease in the total. The failure times were fitted to log-normal distribution curves. The median time to failure (MTF) and the deviation in the time to failure (DTF) were then calculated from the distributions. At least two independent tests were conducted for each annealing condition in order to validate each set of results.

The grain structure and other microstructural characteristics were examined using transmission (TEM) and scanning electron microscopy (SEM). For TEM, planar samples of the lines were prepared by grinding, dimpling, and ion milling.

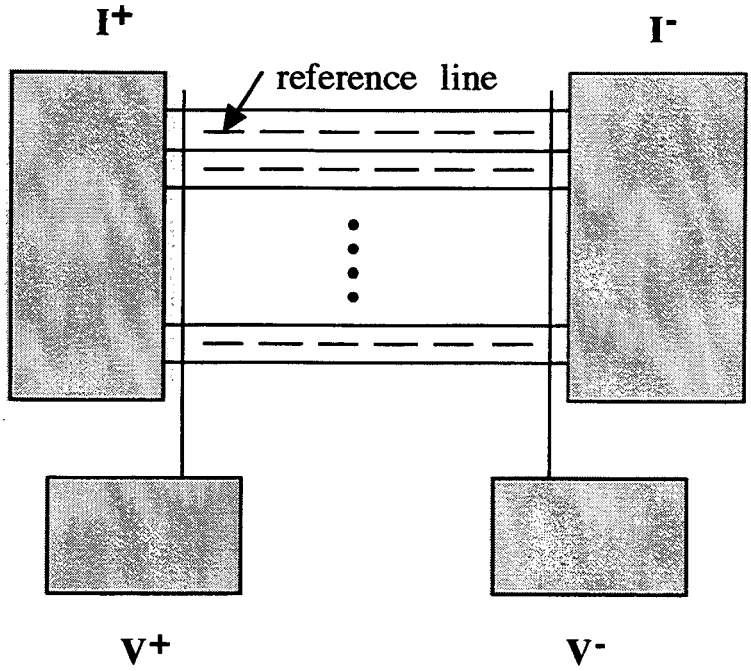

Fig. 2.1 Schematic illustration of thin-film conducting lines that are designed for electromigration lifetime testing using a four-point probe station.

2.2 MICROFABRICATION OF THIN FILM CONDUCTING LINES ON SILICON NITRIDE WINDOWS

A "silicon nitride window" is the local region, under which the substrate material is removed, of a blanket silicon nitride (SiN_x) film that usually sits on a Si wafer, as schematically illustrated in Fig. 2.2. The local area of the SiN_x film is transparent to TEM. Silicon nitride windows then provide great advantages in microstructural analysis of the films that are

deposited directly onto the windows. A recent investigation reports the use of this technique on the observation of precipitate evolution under electromigration. [2.4] In addition, the technique can be used for in-situ electromigration testing, [2.5] although interpreting the result is still subject to debate, due to the serious temperature effect on failure.

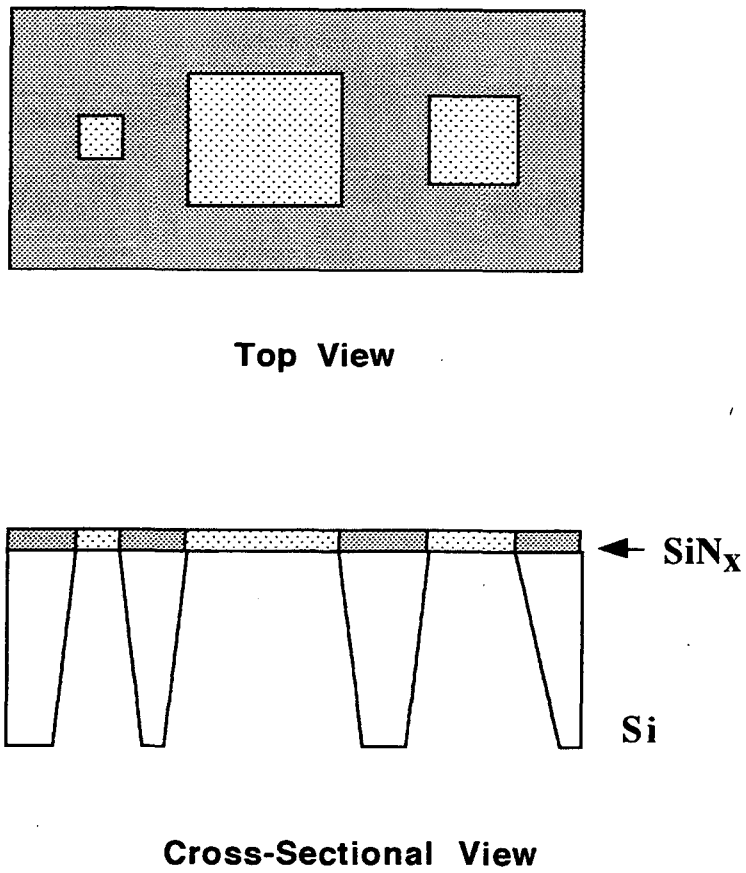

Fig. 2.2 Schematic representations of silicon nitride (SiN_x) windows that are fabricated on a silicon wafer.

The work reported here utilizes the silicon nitride window technique, particularly, to investigate the effect of post-pattern annealing and to clarify the microstructural mechanism of electromigration failure. The microfabrication techniques to produce the Al-2Cu lines on the windows are summarized in Fig. 2.3. The patterned lines on the windows are schematically shown in Fig. 2.4.

The shortcoming of the technique which limits its usefulness is that the thickness of silicon nitride windows should be as thin as possible, since a thin layer of amorphous material causes strong diffuse scattering of the electrons, and substantially reduces the transparency of a specimen.[2.6] In order to maximize resolution, thus, the thickness of the silicon nitride windows used in this study is less than 0.1 μm. The thickness of Al-2Cu lines on these windows is in the range, 0.35 μm to 0.50 μm.

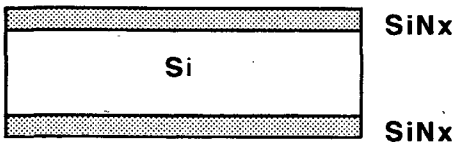

(a)

LPCVD : silicon-nitirde deposition

(b)

Photolithography I (back side)

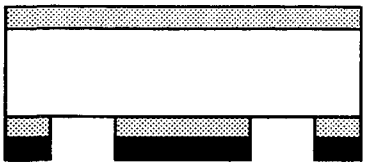

(c)

Plasma etching of silicon nitride

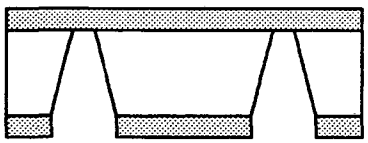

(d)

KOH wet-etching of silicon

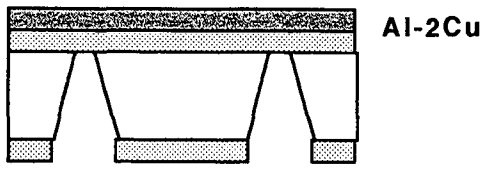

(e)

Sputtering : Al-2Cu deposition

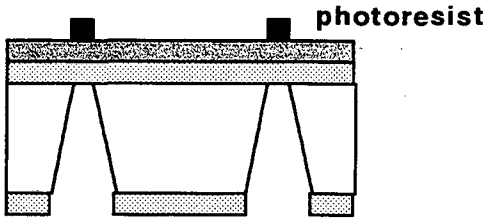

(f)

Photolithography II (line patterning)

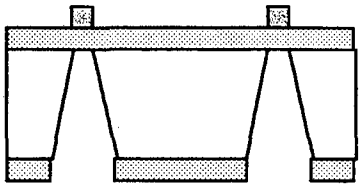

(g)

Reactive Ion Etching (Al-2Cu)

Fig. 2.3 Cross-sectional view of the major steps in a basic process that fabricates Al-2Cu thin-film conducting lines on silicon nitride windows.

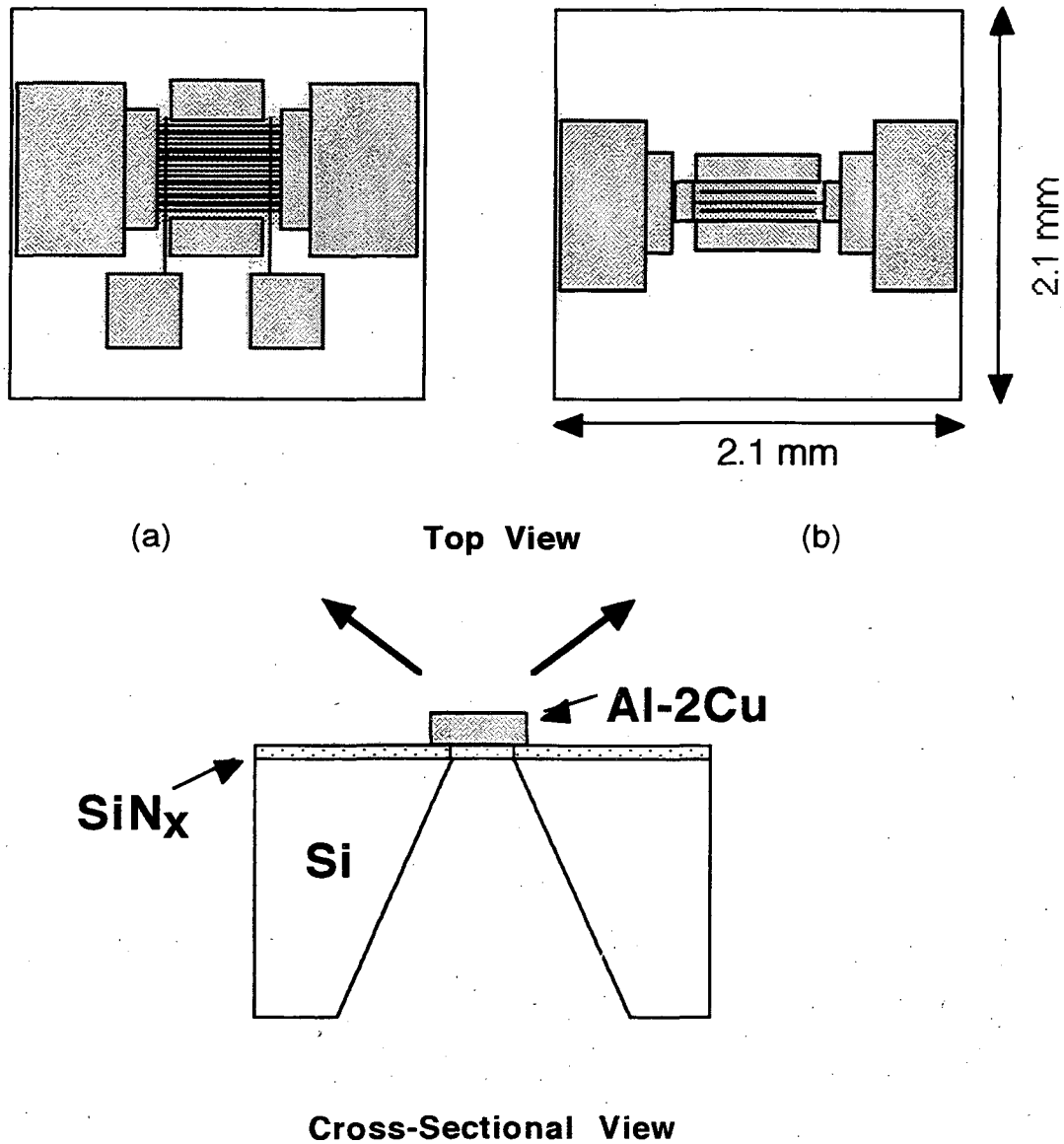

Fig. 2.4 Schematic illustration of Al-2Cu conducting lines fabricated on silicon nitride windows: (a) multiline structure and (b) single-line structure.

2.3 REFERENCES

[2.1] I. Ames, F. M. d'Heurle, and R. Horstmann, "Reduction of electromigration in aluminum films by copper doping," IBM J. Res. Develop. **14**, 461 (1970).

[2.2] G. J. van Gurp, "Electromigration in Al films containing Si," Appl. Phys. Lett. **19**, 476 (1971).

[2.3] R. S. Muller and T. I. Kamin, *Device Electronics for Integrated Circuits* (John Wiley & Sons, New York, 1977).

[2.4] T. M. Shaw, C.-K. Hu, K. Y. Lee, and R. Rosenberg, "The microstructural stability of Al(Cu) lines during electromigration," Appl. Phys. Lett. **67**, 2296 (1995).

[2.5] S. P. Riege, A. W. Hunt, and J. A. Prybyla, "Real-time TEM studies of electromigration in submicron aluminum runners," MRS Symp. Proc. **391**, 249 (1995).

[2.6] P. Hirsch, A. Howie, R. B. Nicholson, D. W. Pashley, and M. J. Whelan, *Electron Microscopy of Thin Crystals* (R. E. Krieger Publishing Company, Huntington, New York, 1977), Chap. 2.

CHAPTER 3

INTERCONNECT MICROSTRUCTURAL CONTROL

3.1 INTRODUCTION

The reliability of interconnects is strongly affected by their microstructure. A number of studies have been conducted to investigate the effect of microstructure on electromigration lifetime. Early studies have shown that, in polygranular lines, the grain size and film orientation influence electromigration lifetime. [3.1-3.3] These studies have proposed that reliable interconnects should have polygranular structures with uniformly large grain sizes and preferred crystallographic orientations. However, with the decrease in feature size, modern interconnects do not usually have polygranular structures. Instead, they have quasi-bamboo structures like those shown in Fig. 3.1. The lines contain both bamboo segments in which grains span the width, and polygranular segments in which grain boundaries lie along the length of the line. It is well established that these polygranular segments play an important role in electromigration failure; the characteristics of polygranular segments including their length and distribution are dominant microstructural parameters that govern electromigration lifetime.

In this Chapter, the effects of thermal history on the microstructural characteristics of narrow Al and Al-alloy lines will be discussed. The emphasis will be placed on the advantage of post-pattern annealing which modifies the length and distribution of polygranular segments. This heat

treatment is carried out at sufficiently high temperatures, after the line has been patterned. Thermodynamically, grain boundaries are high-energy defects. Hence thermally induced grain boundary migration naturally tends to eliminate internal grain boundary segments, and drive the microstructure toward a fully bamboo configuration. This method has been used for decades to achieve bamboo structures in thin metal wires. [3.4, 3.5] As demonstrated in this Chapter, it is also successful in eliminating long polygranular segments from thin-film conductors. Of course other heat treatments (e.g. pre-pattern annealing) can also be used to promote large grains and short polygranular segments. However the present work tests the hypothesis that post-pattern annealing is particularly useful, since it can achieve narrow distributions of polygranular segment lengths by specifically attacking exceptionally long segments.

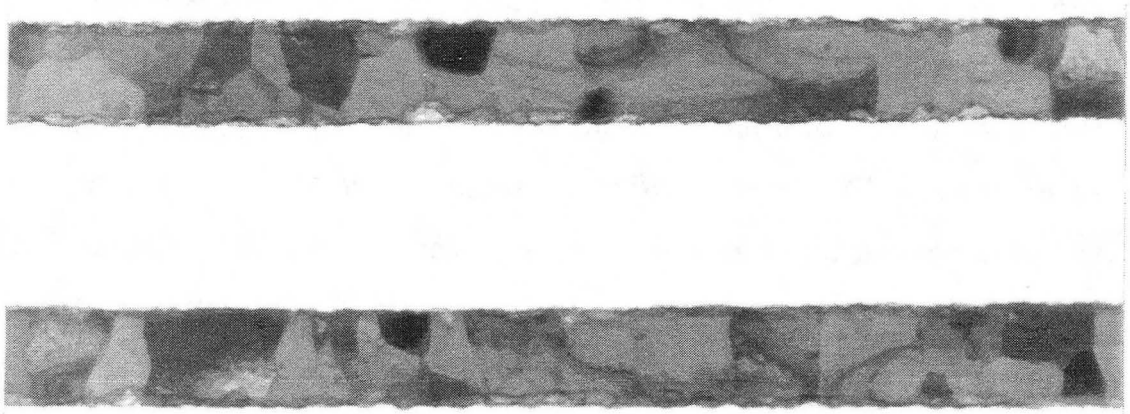

Fig. 3.1 TEM micrographs showing the quasi-bamboo microstructure of Al-2Cu lines used in this work. The width of the lines is 1 μm. (XBD 9511-05699)

This Chapter reports the statistical analysis of polygranular segment distributions for different post-pattern anneals. These results are compared with the predictions from computer simulations by other researchers. [3.6, 3.7] For the experiment, a "silicon nitride window" technique was utilized; the lines were made transparent to TEM by depositing them directly onto electron transparent silicon nitride membranes. This technique reveals the whole microstructure of the lines on the windows, and is useful in clarifying the microstructure evolution during post-pattern annealing.

3.2 MICROSTRUCTURAL CHARACTERISTICS PRIOR TO PATTERNING

3.2.1 As-Deposited Films

The microstructure of a patterned line is derived from that of the as-deposited film. A key parameter that determines the microstructure of the as-deposited film is the substrate temperature during deposition, since the formation of the film onto the substrate is governed by a thermally activated process. The effect of substrate temperature on the microstructure of the as-deposited film has often been explained by the "zone diagram" studied by several researchers. [3.8, 3.9] This diagram illustrates grain structure as a function of substrate temperature and inert gas pressure. Ordinarily, low substrate temperatures promote relatively fine and randomly oriented grains.

The films (Al, Al-2Cu, Al-2Cu-1Si) used for the investigation of this thesis were deposited at room temperature. A typical microstructure that

represents those films is shown in Fig. 3.2, which is a TEM micrograph of a pure Al film. The mean grain size of the film is 0.13 μm. Both Al-2Cu and Al-2Cu-1Si films had almost identical grain sizes as well. The small grain sizes of the as-deposited films have a consequence that the as-patterned lines (width ≈ 1 μm) are fine-grained polygranular. Thus, without any pre-pattern heat treatment, there is no possibility of bamboo grains in as-patterned lines. Since these polygranular structures are rarely observed in modern submicron lines, they are, practically, of little interest. On the other hand, they are useful for the purpose of this work, since a variety of quasi-bamboo microstructures can be generated from the polygranular lines by means of post-pattern annealing.

In manufacturing, films are usually deposited at about 200 °C, or even higher temperatures (in excess of 450 °C) to achieve good step coverage. For the comparison of microstructure, a TEM micrograph of an Al-2Cu-1Si film deposited at 450 °C is shown in Fig. 3.3. The mean grain size of the film is 2.4 μm, which is more than 10 times larger than those of the films deposited at room temperature (Fig. 3.2).

3.2.2 Pre-Pattern Annealing

It is known that grain growth in thin films can occur at relatively low temperatures, due to large driving forces for grain growth in thin films as well as the high purity of thin films.[3.10] Hence annealing the films deposited at room temperature, prior to patterning, promotes significant

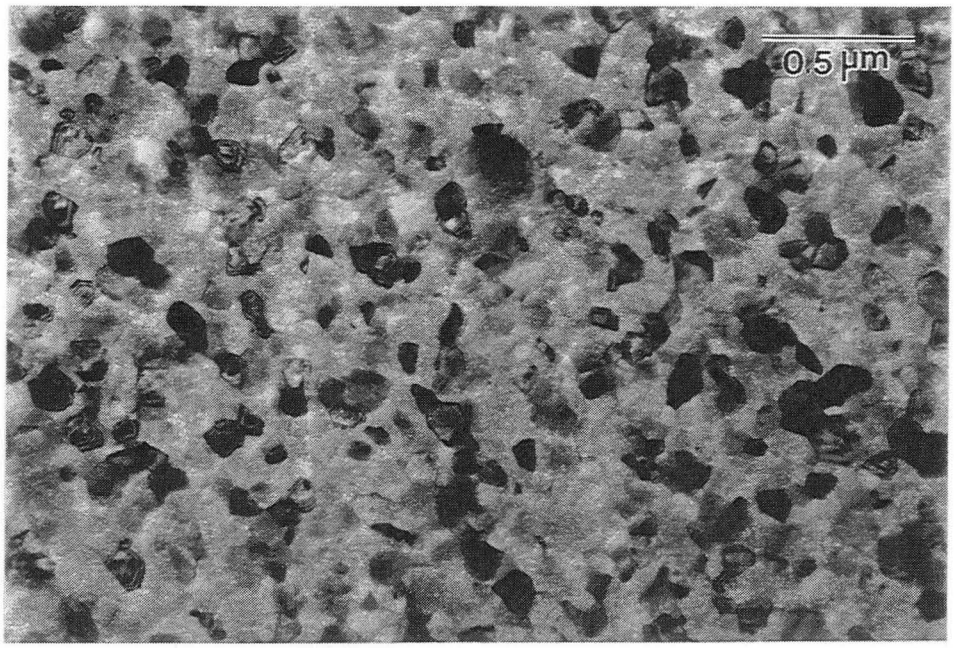

Fig. 3.2 A TEM micrograph showing a typical microstructure of a pure Al film deposited at room temperature. (XBD-9611-05466)

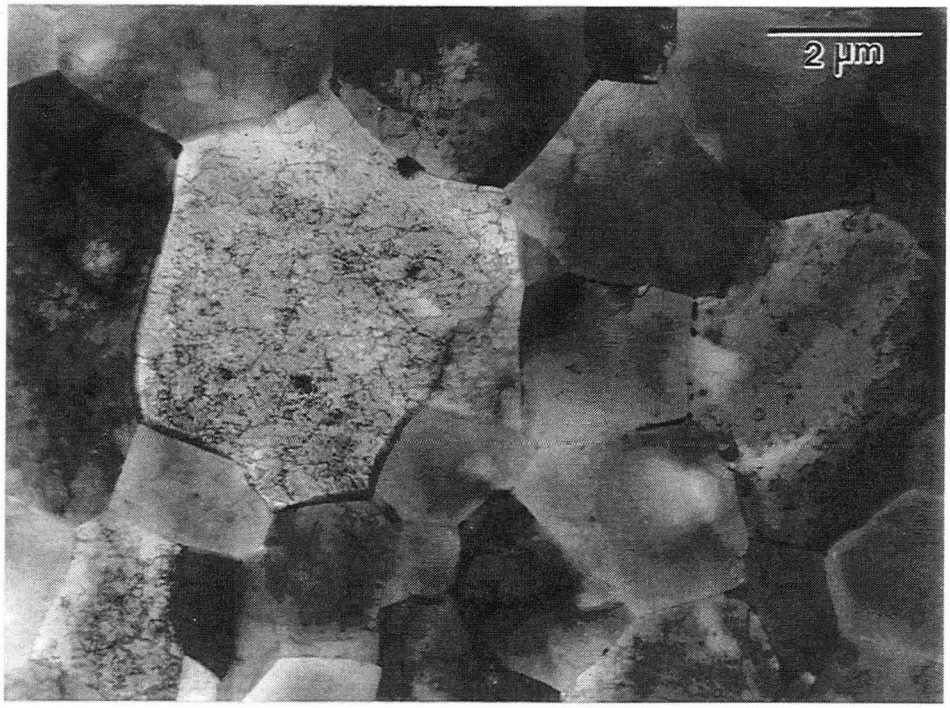

Fig. 3.3 A TEM micrograph showing a typical microstructure of an Al-2Cu-1Si film deposited at 450 °C. (XBD 9611-05466)

grain growth, depending on the annealing parameters such as temperature and time. In this work pre-pattern annealing was conducted in Al-2Cu-1Si films only; a RTA (rapid thermal annealing) treatment was conducted at 500 °C for 5 min. A typical microstructure after the heat treatment is shown in Fig. 3.4. The mean grain size is 0.9 μm. However, there exist exceptionally large grains, which result from abnormal grain growth during the heat treatment. [3.10] The large grains play an important role in deriving the microstructure of patterned lines. They create occasional bamboo grains bounded by exceptionally long polygranular segments that still contain fine grains. Under an electric field, these bamboo grains are the sites at which large flux divergences are created (Fig. 1.3).

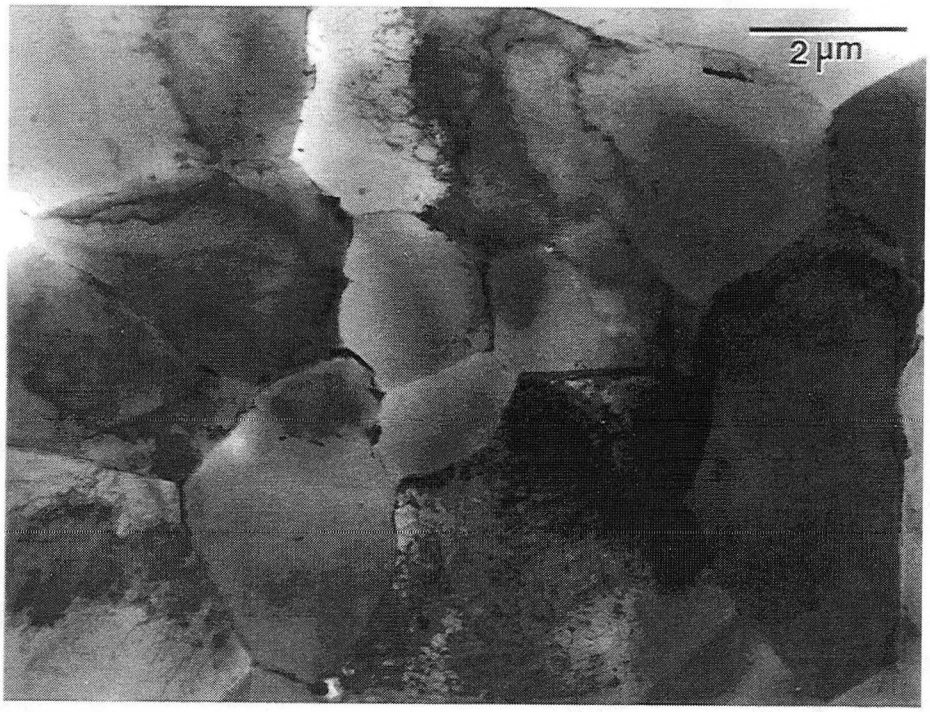

Fig. 3.4 A TEM micrograph showing a typical microstructure of an Al-2Cu-1Si film after a heat treatment of 500 °C for 5 min. (XBD 9611-05467)

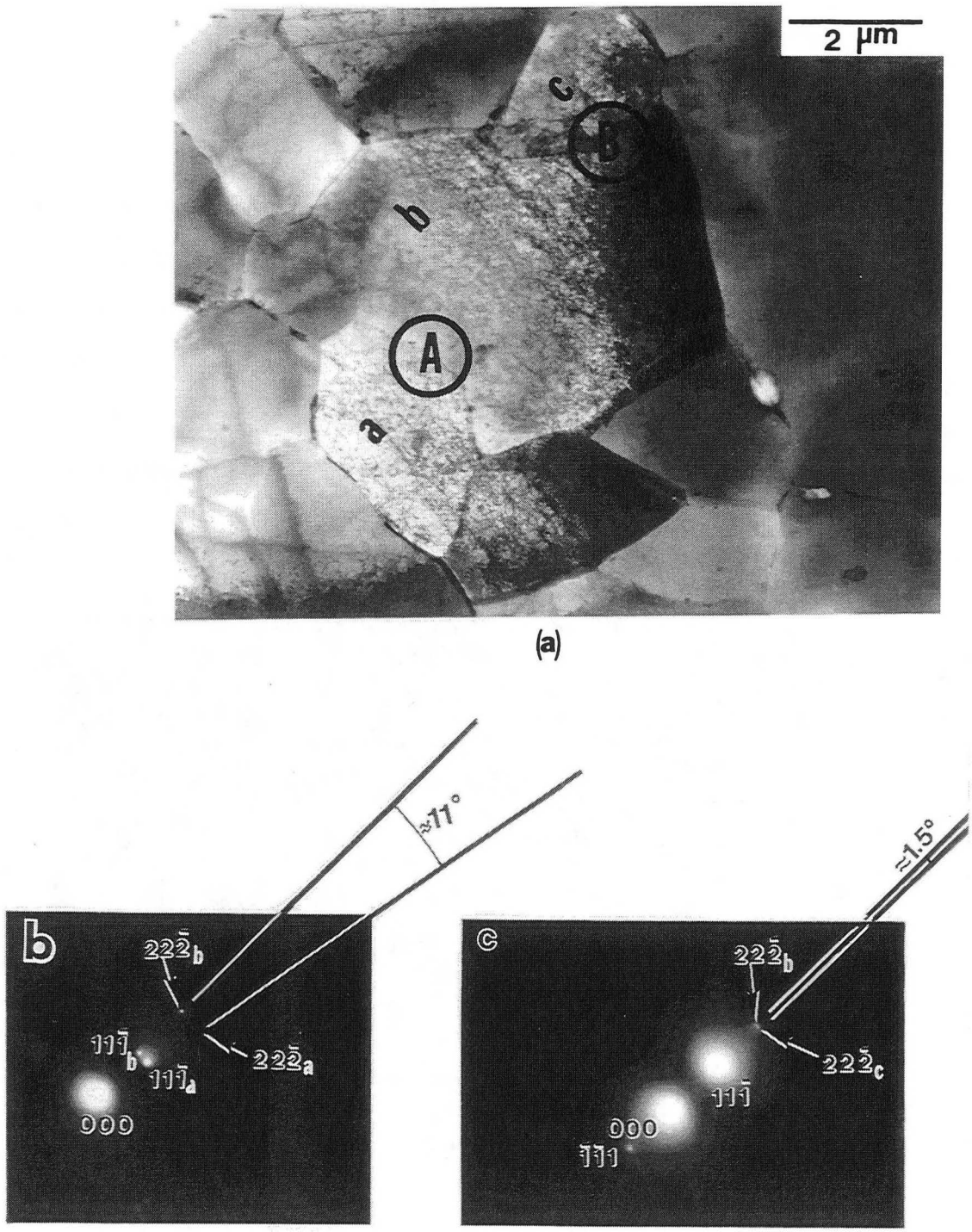

Fig. 3.5 A TEM image showing an abnormally large and irregularly shaped grain (a), and selected area diffraction patterns obtained from the boundaries A (b) and B (c). (XBD 9611-05465)

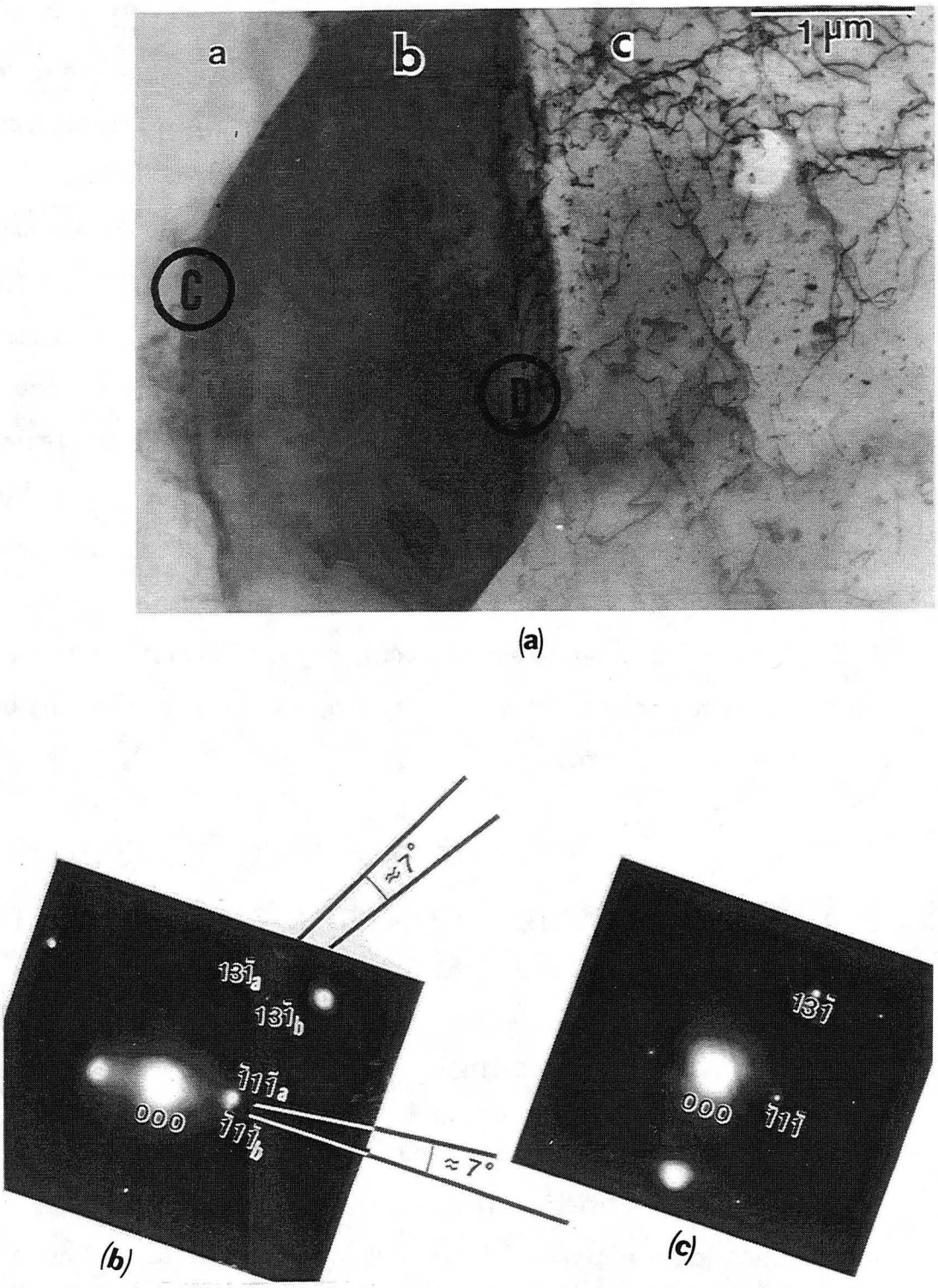

Fig. 3.6 A TEM image showing two boundaries (a), and selected area diffraction patterns obtained from the boundaries C (b) and D (c). (XBD 9611-05464)

In general, the large grains are irregularly shaped with high dislocation density and low angle grain boundaries. A typical example is demonstrated in Fig. 3.5. The high dislocation density seems to result from the residual thermal stress after the rapid cooling following the anneal at 500 °C. Because of the wide difference in thermal expansion coefficient between the metal film and the oxide layer (e.g. Al: 23×10^{-6} /K, CVD SiO_2: 1.5×10^{-6} /K), substantial tensile stress is induced in the metal film; the stress level in Al-based films is on the order of hundreds of MPa. [3.11] Fig. 3.5 shows the selected area diffraction patterns that were used to characterize the boundaries associated with the abnormally large grain. For example, the boundary B has a very small misfit angle 1.5 ° that is in the range of misfit angle of low angle grain boundaries. Another example is illustrated in Fig. 3.6. Since the misfit angle along the boundary D is so small that it cannot even be measured on the diffraction pattern, it is believed that the boundary is a dislocation network.

3.3 MICROSTRUCTURE CONTROL BY POST-PATTERN ANNEALING

3.3.1 Post-Pattern Annealing

The extent of microstructural modification in narrow lines is a function of deposition condition, patterning technique, and metallurgy. Post-pattern annealing is of particular interest in controlling as well as in stabilizing the grain structure of patterned lines at service conditions. This heat treatment can be an effective method to eliminate polygranular segments,

and eventually leads to fully bamboo microstructures. As discussed in the next Chapter, the result of the microstructural evolution will be a substantial improvement in reliability.

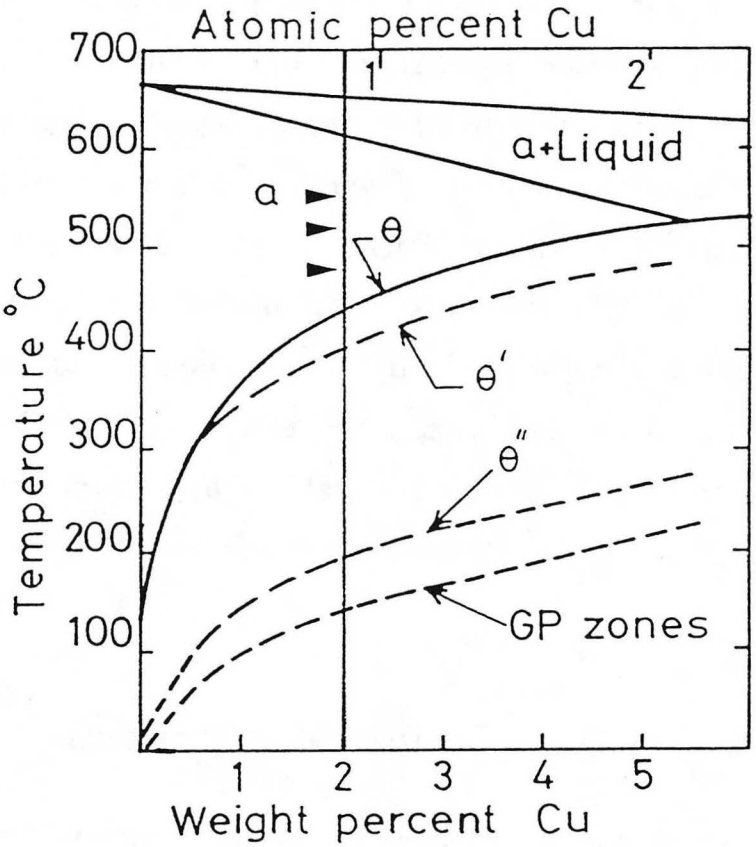

Fig. 3.7 Relevant portion of the Al-Cu phase diagram showing the post-pattern-annealing temperatures used for this study. [3.23] The broken lines indicate the metastable GP zone, θ″, and θ′ solvuses.

Fig. 3.7 is the relevant portion of the Al-Cu phase diagram showing

the annealing temperatures chosen for this study. Post-pattern annealing of Al-2Cu and Al-2Cu-1Si lines was conducted at temperatures above the solvus line for 2 % Cu content to ensure solution of the Cu. During annealing, hence, there was no Al_2Cu precipitates. In addition, prior work [3.12] reports that the precipitation of Si in Al-2Cu-1Si lines is insignificant, even at temperatures much lower than those for post-pattern anneals of this work. Therefore, the retarding effect due to precipitates which pin grain boundaries against grain growth during annealing is negligible. The lines were quenched in air after annealing. Quenching from above the Cu solvus line produces a microstructure in which Cu is in supersaturated solution or in GP-zone clusters. [3.13] Therefore, in the present work, post-pattern anneals at various conditions control only the grain structure of the lines, as a function of annealing time and temperature. The effects of low-temperature aging which controls the stability and distribution of the alloying element Cu has been well described by others. [3.14, 3.15]

3.3.2 Evolution of Quasi-Bamboo Microstructures

In the case of pure Al lines post-pattern annealing was conducted at 480 °C for 5 min., 15 min., 30 min., and 60 min. Fig. 3.8 shows typical TEM micrographs which demonstrate a dramatic microstructure evolution during the heat treatment. While the mean grain size of as-deposited films was 0.13 μm, the line width was 1 μm. Before annealing, then, the line is fine-grained and polygranular along the whole length (line length: 1000 μm). During the first 5 min. of annealing, however, bamboo grains quickly develop at isolated points along the line, dividing the line into very long

Fig. 3.8 TEM micrographs showing the grain structures of pure Al lines during post-pattern annealing: (a) as-patterned, (b) annealed for 5 min. and (c) annealed for 60 min. at 480 °C. (XBD 9611-05462)

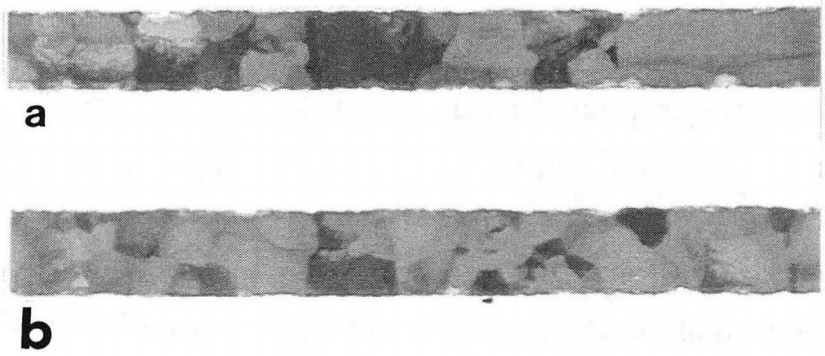

Fig. 3.9 TEM micrographs showing the grain structures of Al-2Cu-1Si lines: (a) as-patterned and (b) annealed at 480 °C for 2 hrs. (XBD 9611-05462)

polygranular segments (Fig. 3.8-(b)). At this point, the length of polygranular segments is often in excess of 100 μm. In addition, the polygranular segments still contain small grains. The abrupt microstructural discontinuities at their terminal points are expected to create large flux divergences under electromigration. When the annealing time is raised to 60 min., however, the microstructure evolves into a nearly bamboo structure with very short polygranular segments. For example, Fig. 3.8-(c) shows that the longest polygranular segment in the line at this annealing condition, which is about 2 μm. While the segment may still cause a flux divergence, its magnitude should be much smaller than those from long polygranular segments like that shown in Fig. 3.8-(b).

The sequence of microstructure evolution during post-pattern annealing for Al-2Cu and Al-2Cu-1Si lines was essentially identical to that for pure Al lines, except that Al-2Cu-1Si lines already contained occasional bamboo grains in the as-patterned condition. This difference results from the fact that, because of the RTA (rapid thermal annealing) before patterning, the mean grain size (0.9 μm) of Al-2Cu-1Si films is comparable with the line width (1.3 μm). In Al-2Cu-1Si lines, the microstructural effect of the annealing treatment is illustrated in Fig. 3.9, which compares TEM micrographs of the lines in the as-patterned condition, and after annealing at 480 °C for 2 hrs.

The rate of microstructure evolution toward a bamboo structure appears to be faster in pure Al lines than in the lines containing solutes. This is due to a slower grain-growth rate in the Al alloy lines. Prior work has shown that Cu atoms tend to accumulate in grain boundaries. [3.16] These grain boundary solutes produce a drag that decreases the rate of grain

boundary migration. It is well understood that grain-boundary solute atmospheres are broken up by thermal vibrations with the increase in heat-treatment temperature. [3.17] Increasing annealing temperatures will then be an effective way to facilitate the evolution to bamboo structures in the Al alloy lines. This argument is examined in the following section.

3.4 TEM ANALYSIS OF POLYGRANULAR SEGMENTS

3.4.1 Metallography

Many researchers have attempted to describe the evolution of quasi-bamboo microstructures during heat treatments in thin-film conducting lines. There have been a considerable number of results from computer simulations. It seems that, however, no systematic experimental observations have yet been reported. The lack of experimental data is presumably due to difficulties in carrying out proper metallographic characterizations for those lines. For example, SEM hardly reveals grain structures of the lines. In the case of TEM, it has been extremely difficult to make a specimen which allows a complete microstructure analysis of long and narrow lines (~ 1 μm x 1000 μm).

In order to resolve the problems mentioned above, new Al-2Cu test structures, which can also be directly used as TEM specimens were successfully developed. The details of sample fabrication are described in Chapter 2. These test structures allowed the whole microstructure along the entire line to be imaged. An example is shown in Fig. 3.10.

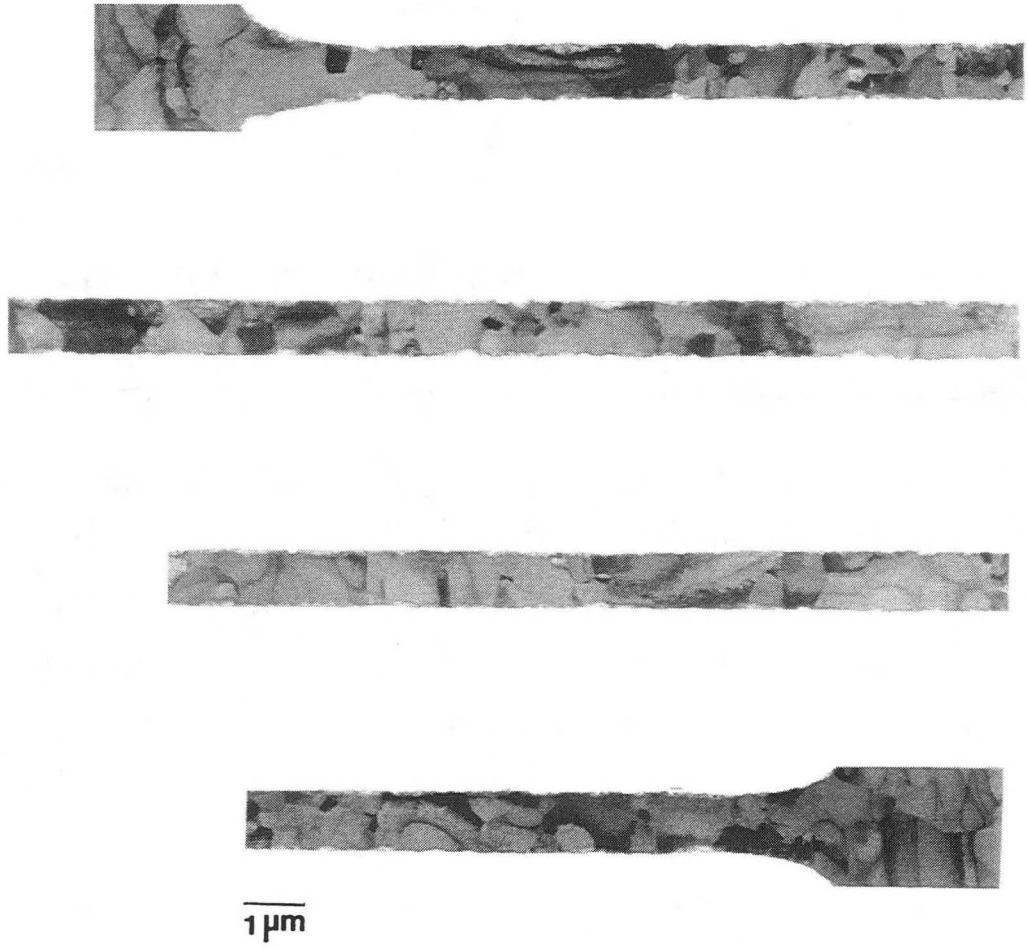

Fig. 3.10 TEM images of an Al-2Cu line (50 μm in length) that was fabricated on a silicon nitride window. These show the microstructure along the whole line from the cathode to the anode. The thickness of the window was 0.1 μm. (XBD 9611-05463)

3.4.2 Statistical Analysis of Polygranular Segment Lengths

Electron-transparent silicon nitride windows were particularly useful for the statistical analysis of polygranular segment lengths which were controlled by post-pattern annealing. Three groups of Al-2Cu lines that were annealed under different conditions were investigated by TEM; each group contained 20 macroscopically identical lines (width: 1 μm, length: 100 μm). The microstructural evolution during post-pattern annealing is studied by analyzing polygranular segment lengths measured from randomly chosen lines. In addition, the distributions of the longest polygranular segment lengths (a set of the longest one in each member of the groups of lines, i.e., 20 data points for each annealing condition) are discussed to demonstrate the metallurgical advantage of the heat treatment.

Effect of Post-Pattern Annealing

Three lines from each annealing condition were randomly chosen, and the lengths of all the polygranular segments that existed in those lines were measured using TEM. Fig. 3.11 shows histograms of the polygranular segment lengths for each annealing condition. These data can also be plotted as shown in Fig. 3.12, which is the cumulative probability plot of the polygranular segment lengths. In addition, Table 3.1 summarizes the changes in the mean length as well as the shortest and the longest lengths of the segments as a function of annealing parameters. The results shown in Figs. 3.11, 3.12 and Table 3.1 lead to the following conclusions on the microstructural modification by post-pattern annealing.

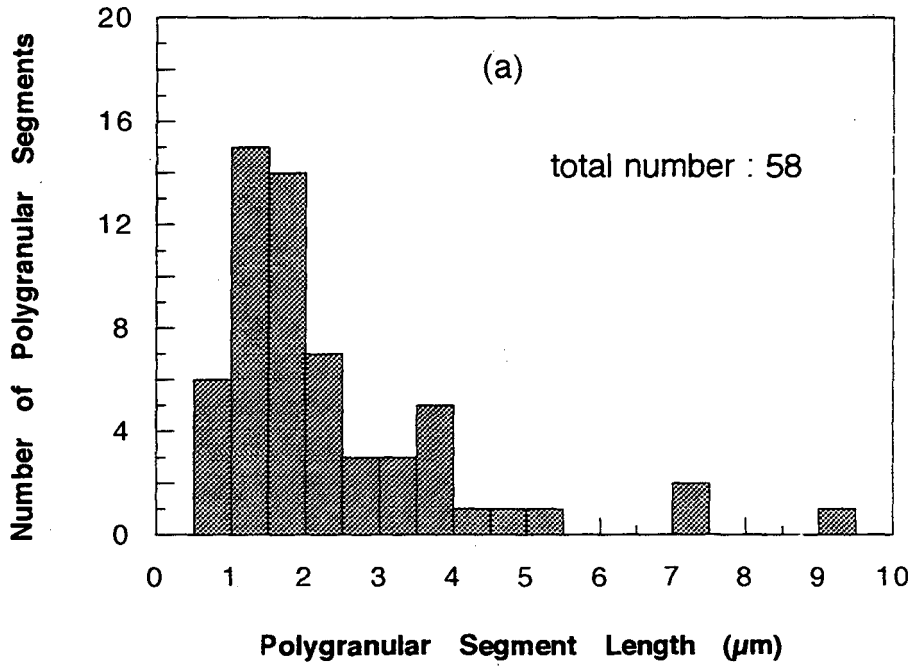
(a)
total number : 58
Number of Polygranular Segments
Polygranular Segment Length (μm)
0
4
8
12
16
20
0 1 2 3 4 5 6 7 8 9 10

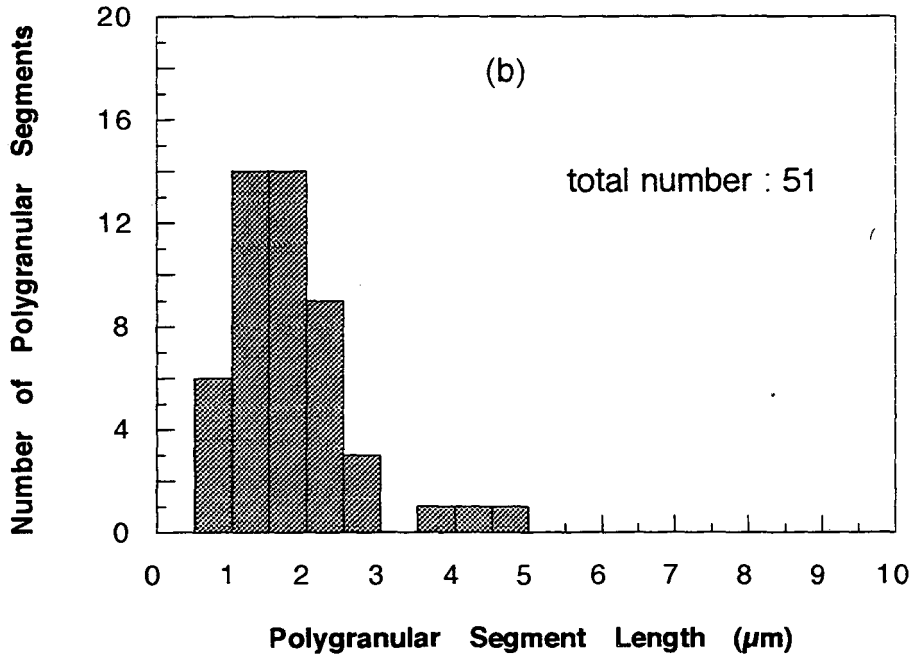
(b)
total number : 51
Number of Polygranular Segments
Polygranular Segment Length (μm)
0
4
8
12
16
20
0 1 2 3 4 5 6 7 8 9 10

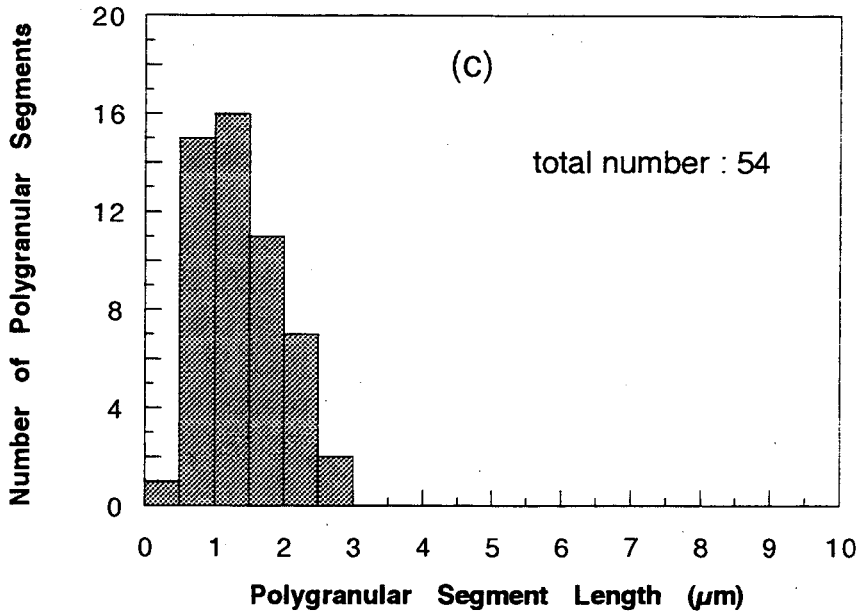

Fig. 3.11 Histograms of polygranular segment length for three annealing conditions: (a) 520 °C, 30 min. (b) 520 °C, 1 hr. (c) 540 °C, 1 hr. Three Al-2Cu lines were randomly chosen for each condition.

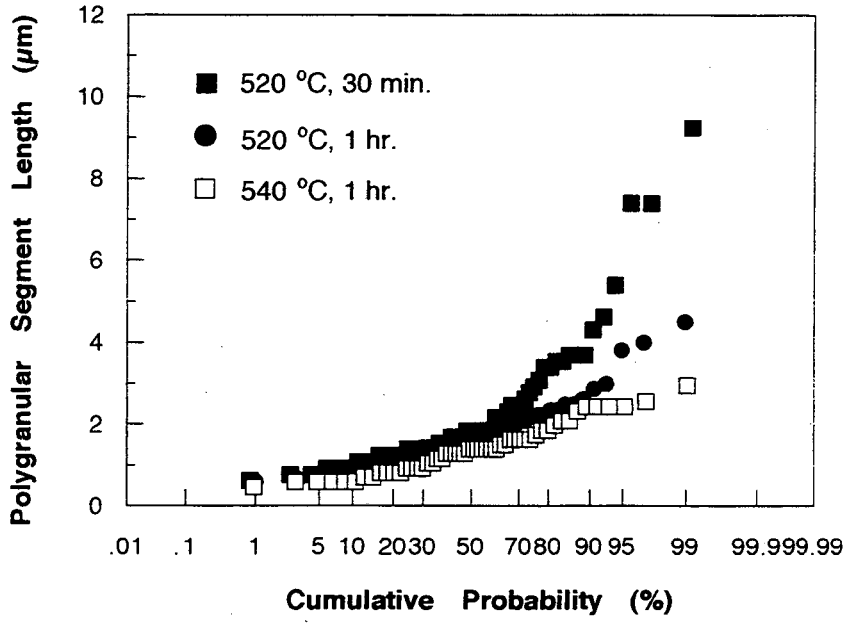

Fig. 3.12 The distributions of the polygranular segment lengths from three randomly chosen Al-2Cu lines with the change in in annealing parameters.

1) The most significant effect of post-pattern annealing is the substantial reduction in the length of exceptionally long polygranular segments.

2) The mean length of polygranular segments decreases with the increase in annealing kinetics. But, the reduction in the mean length is much less significant than the reduction in relatively long segments.

3) The total number of polygranular segments does not change significantly with post-pattern annealing.

Therefore, when the reliability of the lines is predicted based on the microstructural change induced by post-pattern annealing, the relevant parameter should be the length of long polygranular segments. This argument is of great importance in relation to the reliability improvement that can be achieved by the heat treatment, since it has been suggested that the longest segment within a line is the "weakest" failure unit. [3.18 - 3.20]

Table 3.1 The changes in polygranular segment lengths with the changes in annealing condition. Also, see Figs. 3.11 and 3.12.

annealing condition	shortest length	mean length	longest length
520 °C, 30 min.	0.61 μm	1.96 μm	9.24 μm
520 °C, 1 hr.	0.58 μm	1.62 μm	4.50 μm
540 °C, 1 hr.	0.46 μm	1.26 μm	2.95 μm

Walton et al. [3.6] have proposed from their computer simulation that the distribution of polygranular segments is given in the following form

$$C(l) = M^2 \exp(-Ml) \tag{3.1}$$

where $1/M$ is the average polygranular segment length. They have assumed that all polygranular segments shrink at a constant rate at a given post-pattern annealing temperature. It follows that the distribution of segment lengths as a function of annealing time is given by

$$C(l,t) = M^2 \exp\{-M(l + 2vt)\} \tag{3.2}$$

where $v = dl/dt$. Thus, as it evolves with time, the segment length distribution remains exponential with the same shape parameter M. This result is also based on other simplifying assumptions that segment shortening occurs only at the segment ends, and that new spanning bamboo grains do not form within a segment.

Although the distributions of polygranular segments in Fig. 3. 11 do not seem to be inconsistent with the exponential distributions predicted by Walton et al., the results of the present work suggest that their segment-shortening mechanism is not correct for the following reasons. First, segment shortening does not occur only at the segment ends. Second, the shortening rate is not same regardless of the segment length.

As pointed out by Miner et al.,[3.21] no simple rules describe grain boundary movement during post-pattern annealing. However, according to the results of the present work (Figs. 3.11 and 3.12), post-pattern annealing

is more effective in shortening relatively long polygranular segments. As a result, the segment length distribution narrows. The reason for this phenomenon is at least qualitatively simple. Longer polygranular segments have more grains, among which at least one grain quickly grows and spans the line width. Consequently, the longer the polygranular segment, the higher the probability that the segment is broken up by grain growth.

Table 3.2 The changes in the longest polygranular segment lengths from the set of twenty Al-2Cu lines with the changes in annealing condition. Also, see Fig. 3.13.

	longest polygranular segment lengths		
annealing condition	minimum	mean	maximum
520 °C, 30 min.	2.0 μm	4.29 μm	9.30 μm
520 °C, 1 hr.	1.3 μm	2.31 μm	4.40 μm
540 °C, 1 hr.	0.82 μm	1.76 μm	2.91 μm

Distributions of Longest Polygranular Segments

The longest polygranular segment in each member of the groups of lines was also measured using TEM. Fig. 3.13 shows the distributions of the longest segment lengths from those groups. In addition, Table 3.2 summarizes the minimum and the maximum segment lengths as well as a

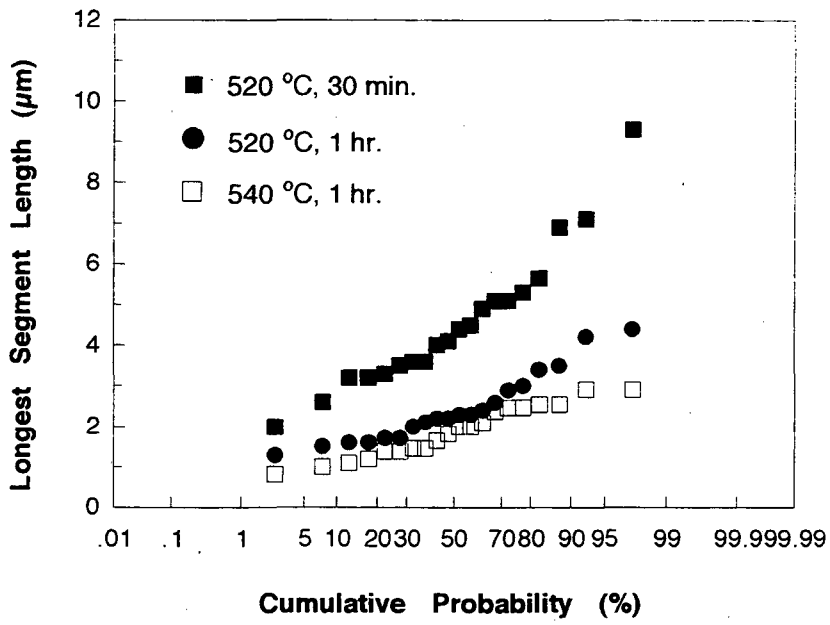

Fig. 3.13 The distributions of the longest polygranular segment lengths for three sets of Al-2Cu lines for three different annealing conditions.

mean length over the 20 longest segment lengths from each annealing condition. Increasing either the temperature or time of annealing dramatically decreases the lengths of the longest polygranular segments. As a result, after the lines were annealed at 540 °C for 1 hr., the longest segment lengths over 20 lines were only in the range, 0.8 μm to 2.9 μm. However, it was not easy to obtain a fully bamboo structure by the method; none of the lines had a fully bamboo structure in this study. This result is also in disagreement with the prediction from the computer simulation reported by Walton et al. [3.6]

The most interesting result to emerge from Fig. 3.13 is the fact that post-pattern annealing narrows the distribution of the longest segment lengths in a set of lines as well. This should influence the time-to-failure distribution of the lines under electromigration. As mentioned in Chapter 1, obtaining a narrow failure-time distribution (low DTF) is an important reliability issue. In light of the view that the "weakest" microstructural unit is the longest polygranular segment, it is promising for post-pattern annealing to achieve a fairly narrow distribution of the longest segment lengths, since it may promote a narrow failure-time distribution as well. In contrast to the result of post-pattern annealing, it has been reported that other methods such as increasing the substrate temperature during film deposition or pre-pattern annealing unfortunately broaden the segment length distribution. This results in a relatively high possibility of exceptionally long polygranular segments. The broadening in the distribution results from a concomitant increase in mean grain size and its standard deviation caused by those methods. [3.22] The impact of the segment-length distributions on the reliability of Al-based interconnects will be discussed in

the next Chapter.

3.5 CONCLUSION

The microstructure of interconnects is affected by substrate temperature during deposition, pre-pattern annealing, and post-pattern annealing. The microstructural modification by post-pattern annealing is of particular interest, since this heat treatment determines the microstructural configuration of quasi-bamboo lines at service conditions. The results show that post-pattern annealing modifies the length and distribution of polygranular segment lengths. The most beneficial result is the fact that post-pattern annealing narrows the distribution of polygranular segment lengths by preferentially breaking up relatively long segments. The success of this technique in improving line reliability is documented in the next Chapter.

3.6 REFERENCES

[3.1] M. J. Attardo and R. Rosenberg, "Electromigration damage in aluminum film conductors," J. Appl. Phys. **41**, 2381 (1970).

[3.2] S. Vaidya and A. K. Sinha, "Effect of texture and grain size structure on electromigration in Al-0.5%Cu thin films," Thin Solid Films **75**, 253 (1981).

[3.3] J. Cho and C. V. Thompson, "Grain size dependence of electromigration-induced failures in narrow interconnects," Appl. Phys. Lett. **54**,

2577 (1989).

[3.4] H. Udin, A. J. Shaler, and J. Wulff, Trans. AIME **185**, 186 (1949).

[3.5] L. E. Murr, *Interfacial Phenomena in Metals and Alloys* (Addison Wesley, Reading, MA, 1975), Chap. 3.

[3.6] D. T. Walton, H. J. Frost, and C. V. Thompson, "Computer simulation of grain growth in thin-film interconnect lines," MRS Symp. Proc. **225**, 219 (1991).

[3.7] H. J. Frost, Y. Hayashi, C. V. Thompson, and D. T. Walton, "The effect of variability among grain boundary energies on grain growth in thin film stripes," MRS Symp. Proc. **338**, 295 (1994).

[3.8] B. A. Movchan and A. V. Demchishin, Phys. Met. Metallogr. **28**, 83 (1969).

[3.9] J. A. Thornton, J. Vac. Sci. Technol. **11**, 666 (1974).

[3.10] C. V. Thompson, "The effect of thermal history on interconnect reliability," MRS Symp. Proc. **309**, 383 (1993).

[3.11] P. A. Flinn, A. S. Mack, P. R. Besser, and T. Marieb, "Stress-induced void formation in metal lines," MRS Bulletin, December, 26 (1993).

[3.12] C. Kim, *Ph. D. Thesis* (University of California at Berkeley, 1993), Chap. 3.

[3.13] R. E. Reed-Hill, *Physical Metallurgy Principle* (Van Nostrand, New York, 1973), 2nd ed., Chap. 9.

[3.14] C. Kim and J. W. Morris, Jr., "The influence of Cu precipitation on electromigration failure in Al-Cu-Si," J. Appl. Phys. **72**, 1837 (1992).

[3.15] T. Nemoto and T. Nogami, "Segregation of Cu to grain boundaries by aging treatment and its effect on EM resistance for AlCu/TiN lines," IEEE Proceedings of the 32nd International Reliability Physics Symposium, 207 (1994).

[3.16] D. R. Frear, J. E. Sanchez,Jr., A. D. Romig, Jr., and J. W. Morris, Jr., "The evolution of microstructure in Al-2%Cu thin films; precipitation, dissolution and reprecipitation," Metall. Trans. **21A**, 2449 (1990).

[3.17] R. E. Reed-Hill, *Physical Metallurgy Principle* (Van Nostrand, New York, 1973), 2nd ed., Chap. 7.

[3.18] E. Arzt and W. D. Nix, "A model for the effect of line width and mechanical strength on electromigration failure of interconnects with near-bamboo grain structures," J. Mater. Res. **6**, 731 (1991).

[3.19] C. Kim and J. W. Morris, Jr., "The mechanism of electromigration failure of narrow Al-2Cu-1Si thin-film interconnects," J. Appl. Phys. **73**, 4885 (1993).

[3.20] J. R. Lloyd, "Electromigration failure in thin film conductors possessing a near-bamboo structure," MRS Symp. Proc. **338**, 367 (1994).

[3.21] B. Miner, E. A. Atakov, A. Shepela, and S. Bill, "Microstructural evolution of aluminum interconnects during post-pattern anneals:

correlation to improved EM lifetime," MRS Symp. Proc. **338**, 333 (1994).

[3.22] G. Rajagopalan, M. L. Dreyer, N. D. Theodore, and T. S. Cale, "Improving electromigration reliability in Al-alloy lines," Thin Solid Films **270**, 439 (1995).

[3.23] G. Lorimer, "Precipitation in aluminum alloys," in *Precipitation Process in Solids*, edited by K. C. Russel and H. I. Aaronson, The Metallurgical Society of AIME, 87 (1978).

CHAPTER 4

EFFECT OF POST-PATTERN ANNEALING ON THE RELIABILITY OF Al-BASED INTERCONNECTS

4.1 INTRODUCTION

The purpose of the present Chapter is to address the possibility of improving the electromigration resistance of Al and Al-Cu thin-film conductors with quasi-bamboo structures by post-pattern anneals that decrease the maximum polygranular segment length. Pure Al, Al-2Cu, and Al-2Cu-1Si lines were patterned and annealed at temperatures high enough to stimulate grain growth.

Prior work suggests that Al-Cu lines with quasi-bamboo structures fail by the mechanism illustrated in Fig. 4.1.[4.1] Al and Cu atoms are pushed downstream by the electron current, causing a counterflow of vacancies. The relatively rapid diffusion through the polygranular segment leads to an accumulation of Al and Cu at the downstream end, with a corresponding concentration of vacancies at the upstream end. The buildup of material at the downstream end produces an Al_2Cu precipitate. The accretion of vacancies at the upstream end produces a void, which usually appears in the bamboo grain just beyond the polygranular segment and grows across that grain to cause failure.

The void-precipitate pair, which is easily identified using scanning electron microscopy (SEM), delineates the polygranular segment. An ex-

ample of this is shown in Fig. 4.2. Using this technique, it has been found that the usual failure site in a quasi-bamboo Al-Cu line is the longest polygranular segment that it contains. To a good approximation, in as-patterned Al-2Cu-1Si lines, [4.1] the time to failure is determined by the longest polygranular segment length according to the simple relation

$$t_f = t_0 \, exp \, (-l/l_0) \tag{4.1}$$

where l is the polygranular segment length, and t_0 and l_0 are constants.

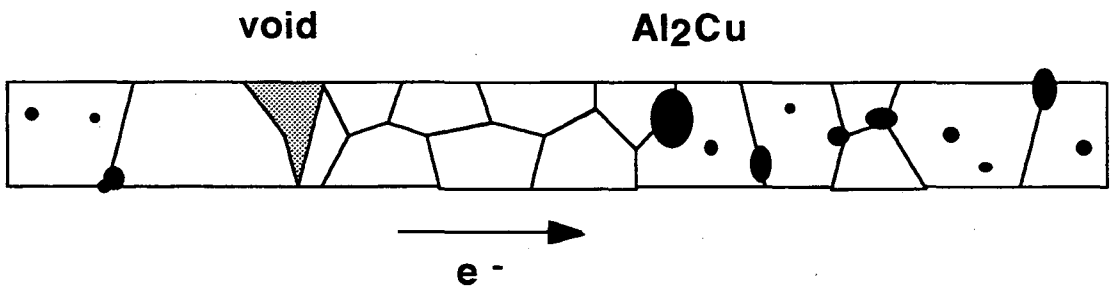

Fig. 4.1 Schematic illustration of the mechanism of electromigration failure in an Al-Cu line with a quasi-bamboo structure. The spacing between the void and the Al_2Cu precipitate is approximately equal to the length of the polygranular segment (Ref. 4.1).

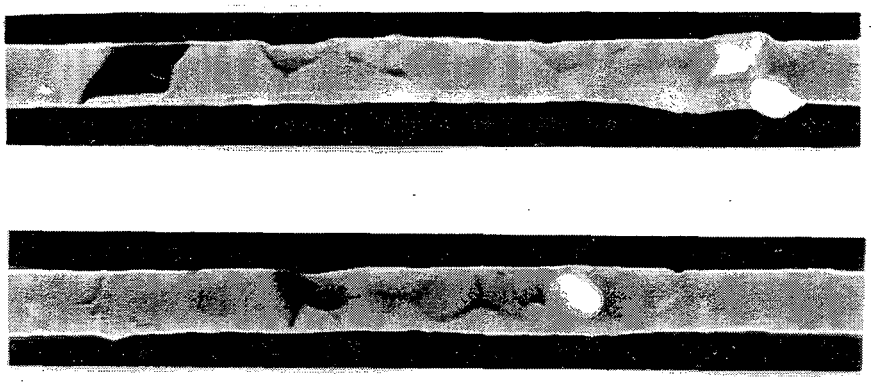

Fig. 4.2 SEM micrographs showing the typical morphology of the failure site. The void-precipitate separation is a reasonable measure of the polygranular segment length. (XBD 9511-05701)

The expected length of the longest polygranular segment in a line that is patterned from a given parent film decreases with the width of the line. It follows from Eq. (4.1) that the expected failure time should increase; and it does, roughly as illustrated in Fig. 1.5. However, the standard deviation of the failure time also increases. While no specific data is known, the likely reason for the increase in scatter in the failure times of narrow lines lies in the fact that they are patterned from polygranular films; the microstructure of the line is the microstructure of a path of

width, w, cut through a microstructure of mean grain size, G, as illustrated in Fig. 4.3. Even when w is very small, there remains a finite probability that its path through the microstructure will parallel a long grain boundary or adjacent grain boundary segments, with the consequence that it contains a long polygranular segment and will have a relatively short lifetime.

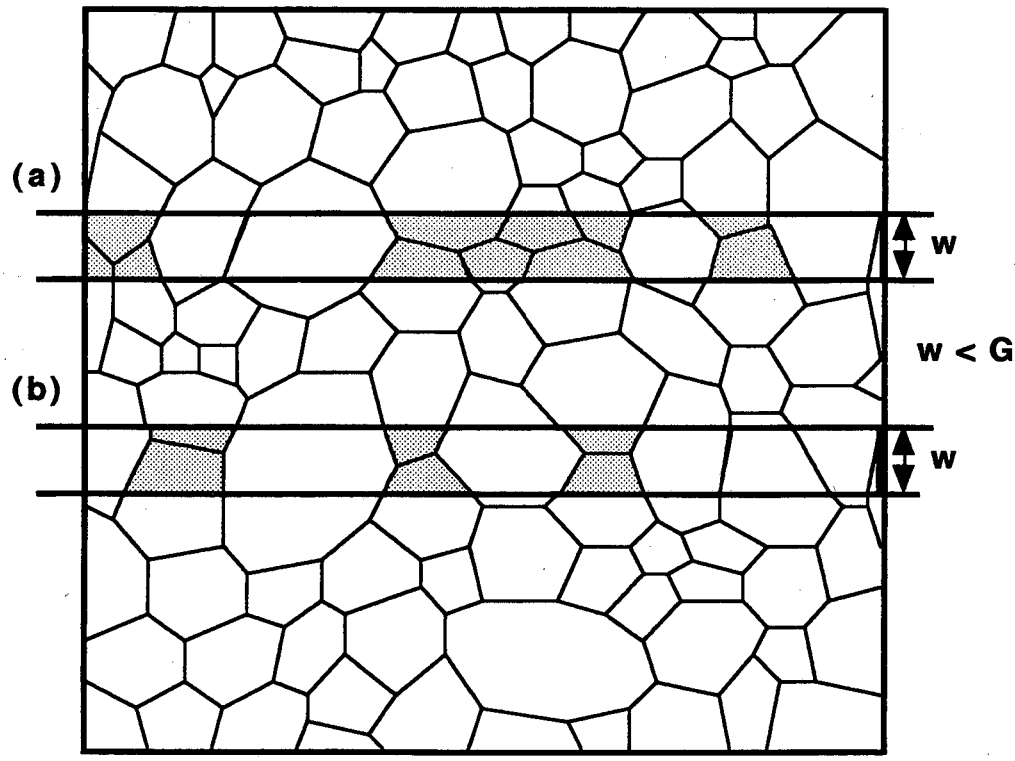

Fig. 4.3 Schematic illustration of patterning from a polygranular film. The microstructure of the line is derived from that of the film. Line (a) has a much longer polygranular segment length than line (b).

The simplest metallurgical method of avoiding long polygranular segments in narrow lines is to reduce or eliminate them by annealing at high temperature after the line has been patterned. The experimental evidence in Chapter 3 led to the conclusion that appropriate anneals are particularly effective in shortening relatively long polygranular segments. As demonstrated in the following, the result of the microstructural modification is a substantial improvement in the resistance to electromigration failure.

4.2 POST-PATTERN ANNEALING OF Al ALLOY LINES

4.2.1 Effect of Annealing Time

Figs. 4.4 and 4.5 show the results of electromigration tests on Al-2Cu-1Si lines annealed at 480 °C for various times. Fig. 4.5 is a plot of the median time to failure (MTF) and the deviation in the time to failure (DTF) as a function of the annealing time. As shown in the figure, the MTF increases by more than an order of magnitude when the annealing time is increased to 2 hrs. The DTF increases initially, but quickly asymptotes to a value that is retained for long annealing times. A similar phenomenon is observed for Al-2Cu lines, as shown in Fig. 4.6. It appears that the annealing treatment does provide a method for increasing the MTF without a concomitant increase in the DTF.

The microstructural effect of the annealing treatment, responsible for the reliability improvement, is illustrated in Fig. 4.7. The evolution of

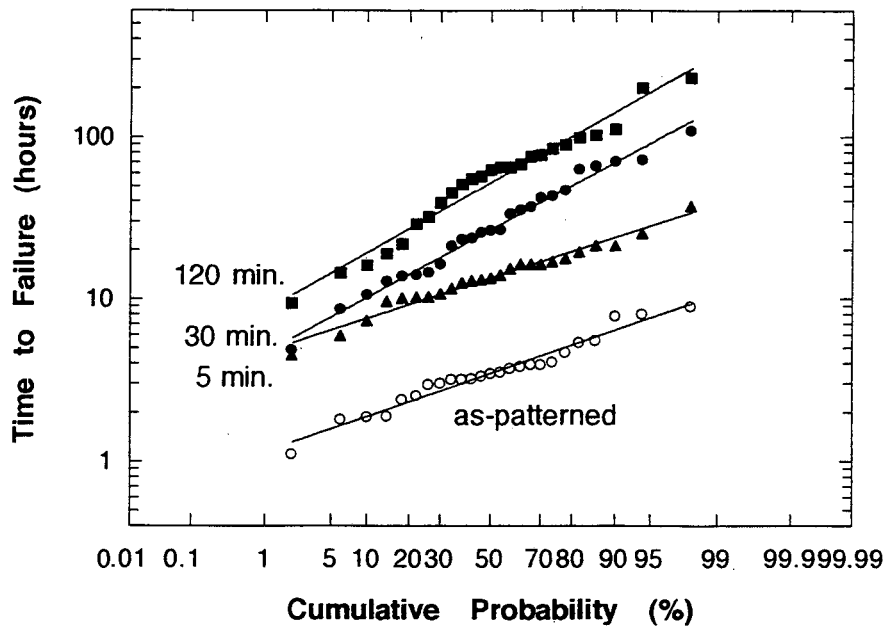

Fig. 4.4 Time-to-failure distributions with annealing times for Al-2Cu-1Si lines, annealed at T = 480 °C. The lines were tested at $j = 3 \times 10^6$ A/cm^2 and T = 225 °C.

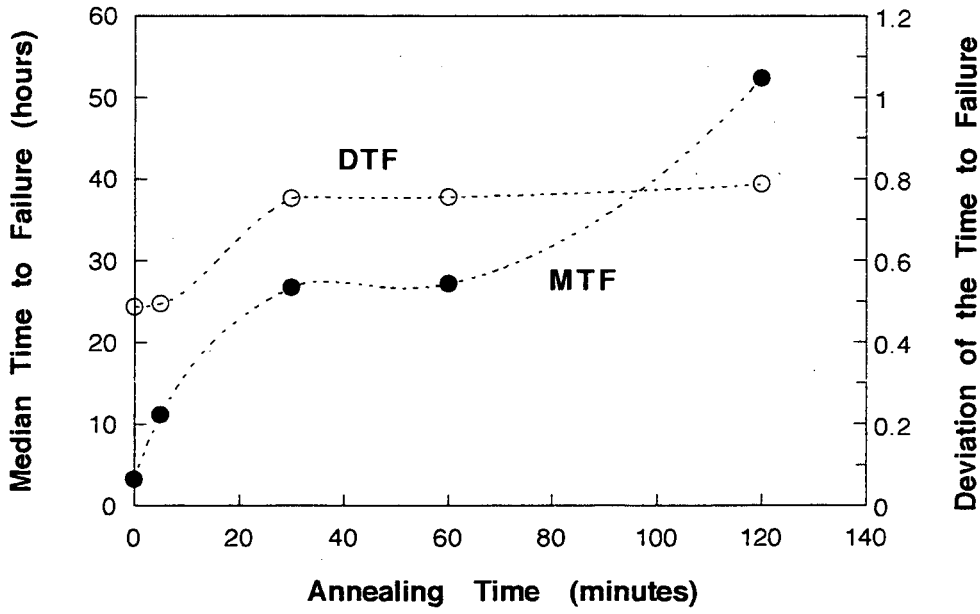

Fig. 4.5 Variations in MTF and DTF as a function of annealing time for Al-2Cu-1Si lines, annealed at T = 480 °C.

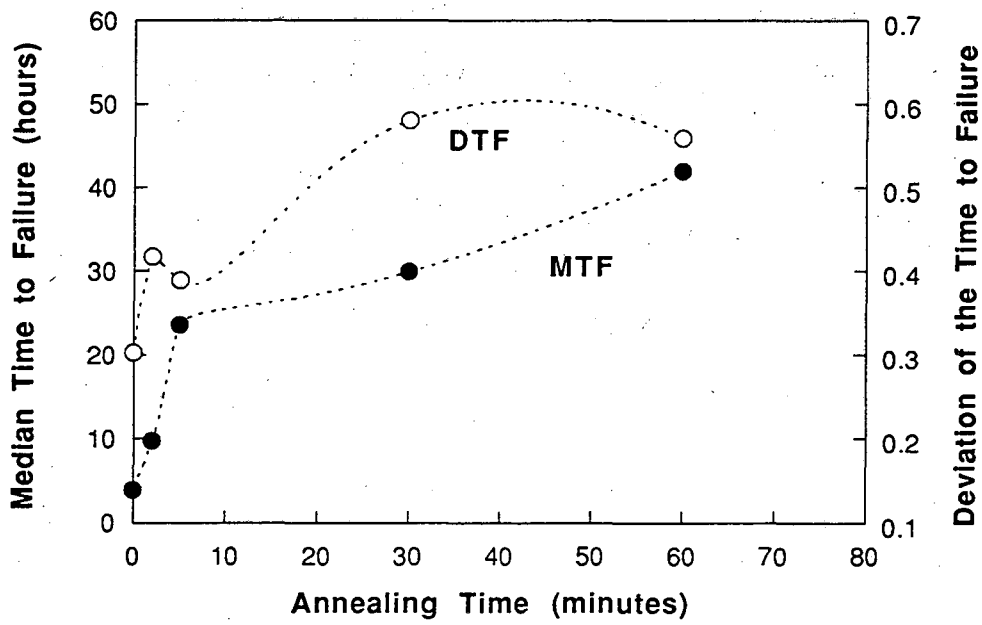

Fig. 4.6 Variations in MTF and DTF as a function of annealing time for Al-2Cu lines, annealed at 480 °C.

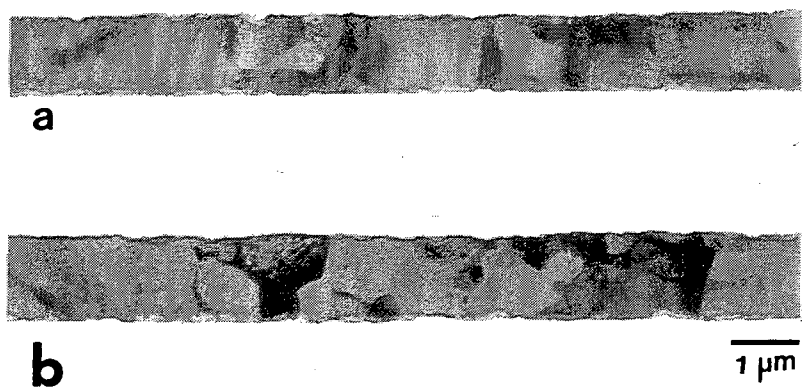

Fig. 4.7 TEM micrographs showing the grain structures of Al-2Cu-1Si lines: (a) as-patterned and (b) annealed at 480 °C for 2 hrs. Note the reduction in polygranular segment length after annealing. (XBD9511-05700)

the microstructure into a nearly bamboo structure with relatively short polygranular segments is apparent in the figure.

It has been common that the MTF and DTF are plotted as a function of the effective line width, w / G (the ratio of line width to mean grain size), which describes the evolution toward a bamboo microstructure. A typical example is shown schematically in Fig. 1.5. However, the trend in Figs. 4.5 and 4.6 is different from that shown in Fig. 1.5. In this work, post-pattern annealing leads to a similar (or greater) increase in the MTF during the evolution toward a bamboo structure, but the DTF quickly saturates. The net result is a significant increase in the time to first failure. The apparent reason for this benefit is that the longer polygranular segments are preferentially attacked and broken up during annealing, so that the probability of finding a very long polygranular segment becomes low. This argument was proven by the statistical analysis of polygranular segment lengths as a function of annealing parameters in Chapter 3.

4.2.2 Effect of Annealing Temperature

The influence of temperature for a given annealing time is illustrated in Fig. 4.8, which plots the statistics of failure for Al-2Cu lines annealed for 1 hr. at either 480, 520 or 540 °C. The mean lifetime increases with annealing temperature. This improvement is expected since increasing the annealing temperature increases the rate of grain growth and, hence, the rate at which a bamboo structure is developed in the line. The time to first failure is a particularly strong function of the annealing temperature (Fig. 4.8). Since the earliest failures are associated with the long-

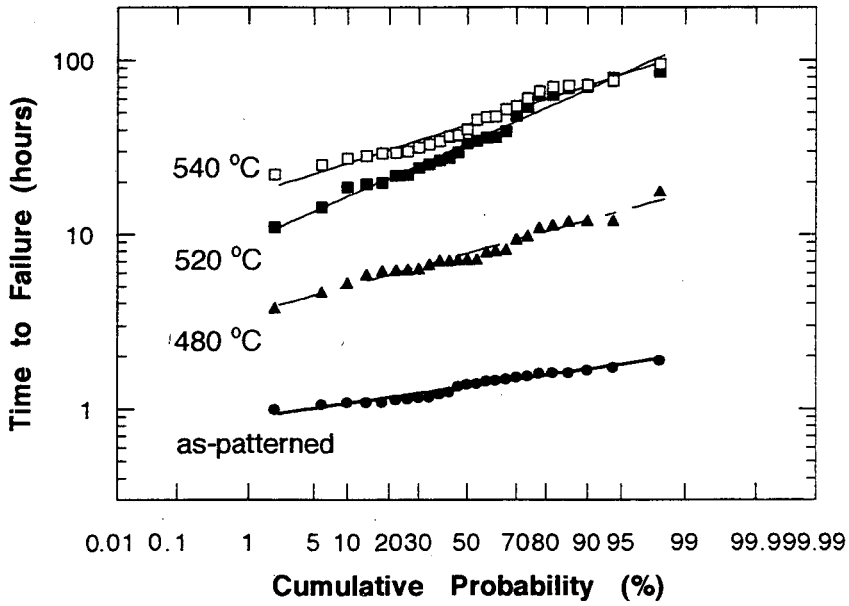

Fig. 4.8 Time-to-failure distributions as a function of annealing temperature for Al-2Cu lines, annealed for one hour at each T. The lines were tested at $j = 3 \times 10^6$ A/cm^2 and T = 225 °C.

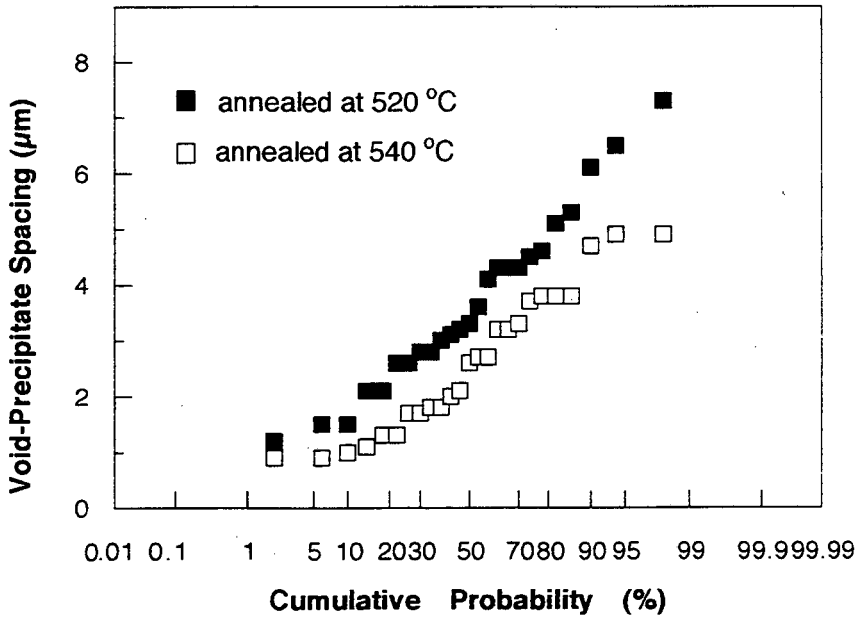

Fig. 4.9 The distributions of void-precipitate spacings at the failure sites of each group of the lines annealed at 520 °C and 540 °C for one hour.

est polygranular segments in the distribution of lines, this result suggests that high-temperature annealing is particularly effective in breaking up the longest polygranular segments.

The statistical analysis of polygranular segment lengths in Al-Cu lines is facilitated by the fact that the segment lengths at the failure site can be measured to a reasonable approximation from scanning electron micrographs. As shown in Figs. 4.1 and 4.2, the void-precipitate separation is a reasonable measure of the polygranular segment length at the failure site. Using this technique, the approximate polygranular segment lengths were measured at the failure sites of each of the lines annealed for 1 hr. at either 520 °C or 540 °C. The results are shown in Fig. 4.9. As expected, the 540 °C anneal produces shorter polygranular segments. In particular, there are no polygranular segments with lengths greater than 5 μm left after the 540 °C anneal, suggesting that the high temperature anneal does preferentially attack the longest segments. The preferential elimination of long segments at the higher annealing temperature is responsible for the fact that increasing the annealing temperature to 540 °C increased the time to first failure much more than it increased the MTF (Fig. 4.8).

4.2.3 Failure Time as a Function of Polygranular Segment Length

The failure times in these experiments were measured from the associated step-wise decreases in the total current of groups of parallel lines, and, hence, do not identify which particular line failed at which time.

However, prior work on as-patterned Al-2Cu-1Si lines has shown that there is a specific correspondence between the failure time and the polygranular segment length. [4.1] In order to obtain a valid empirical equation, that work proposed the following experimental steps. First, record an electromigration lifetime of each line from a set of parallel lines. Second, using SEM, measure the void-precipitate spacing, i.e., the polygranular segment length, at the failure site of an individual line. Third, assume that there is a one-to-one association between the sequence of decreasing failure times (t_f) and the sequence of increasing void-precipitate spacings (l), and plot the failure time as a function of the void-precipitate spacing. The validity of these experimental steps was examined by additional electromigration testing, in which a specific failure time was directly related to a specific void-precipitate spacing by interrupting the test after each failure. Prior work [4.1] reported these data, plotted in Fig. 4.10. The failure times in the figure are well fitted by a simple exponential equation

$$t_f = t_0 \exp(-l/l_0) \tag{4.1}$$

where the pre-exponential factor, t_0, is a characteristic time and l_0 is a characteristic length. Eq. (4.1) implies that the time to failure increases exponentially with decreasing length of the polygranular segment that leads to failure. In Fig. 4.10, both t_0 and l_0 depend on the width of the line.

The experiments mentioned above can also be applied to the data plotted in Figs. 4.8 and 4.9. The sequence of decreasing failure time in Fig. 4.8 can be associated with that of increasing polygranular segment length in Fig. 4.9 to plot failure time as a function of polygranular segment

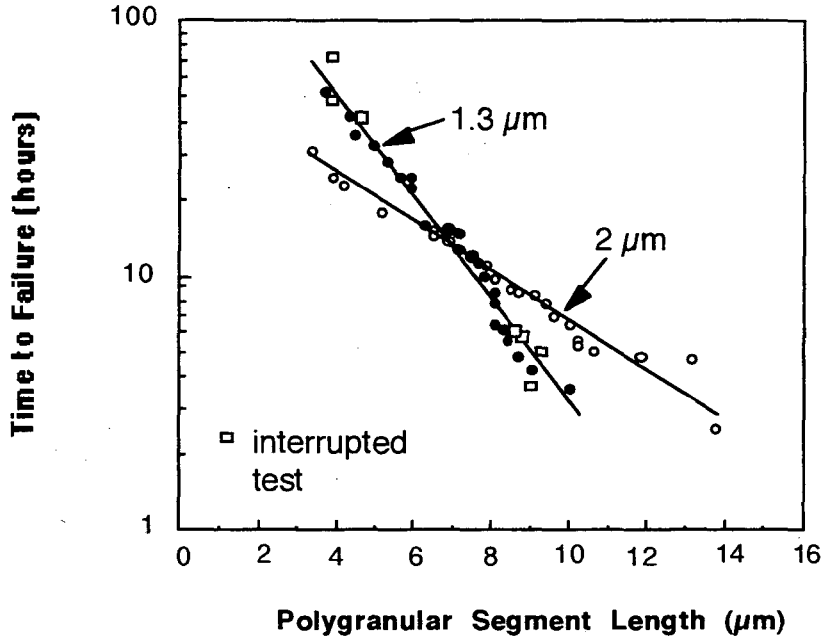

Fig. 4.10 Semi-log curves showing the relation between polygranular segment length and failure time for 1.3 μm and 2 μm lines. The open squares indicate data that were obtained by interrupting tests. Also see Ref. 4.1.

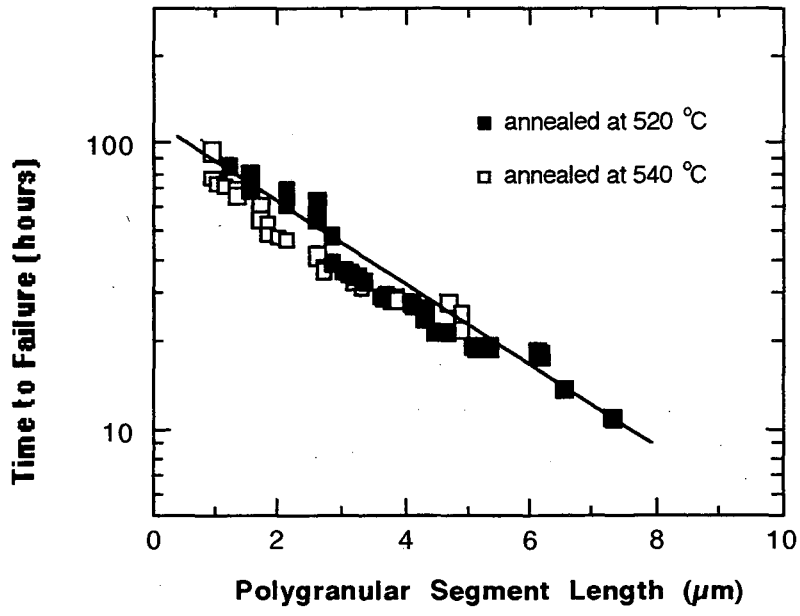

Fig. 4.11 A semi-log curve showing failure time as a function of polygranular segment length. The data for 520 °C and 540 °C anneals coalesce onto a single straight line.

length. The results are shown in Fig. 4.11. An exponential relation between the failure time and the polygranular segment length is clear in the figure. The 520 °C and 540 °C anneals do not significantly change the constants t_0 and l_0 in Eq. (4.1) as shown by the fact that the data in Fig. 4.11 essentially coalesce onto a single curve which obeys Eq. (4.1).

Table 4.1 The kinetic constants t_0 and l_0 values calculated from the curves in Figs. 4.10 and 4.11.

Composition	Characteristics	t_0 (hr.)	l_0 (μm)
Al-2Cu-1Si	as-patterned (w: 1.3 μm)	306	2.2
Al-2Cu-1Si	as-patterned (w: 2.0 μm)	64	4.4
Al-2Cu	520 °C, 1 hr. (w: 1 μm)	100	3.2
Al-2Cu	540 °C, 1 hr. (w: 1 μm)	100	3.2

Table 4.1 summarizes t_0 and l_0 values from Figs. 4.10 and 4.11. Regardless of the sample composition and the preparation method, a simple exponential relation is maintained for each set of lines. However, the specific values of the kinetic constants (t_0 and l_0) in Fig. 4.11 cannot directly be compared with those in Fig. 4.10 because of the differences in composition, geometry, and microstructure. In addition, it is difficult to discover which parameters determine those constants. While the discussion on the constants in Eq. (4.1) is postponed until Chapter 5, a brief explanation on t_0

and l_0 may be possible based on the data presented above. The characteristic time, t_0, can simply be defined as the lifetime when the segment length (l) becomes zero, i.e., the line becomes a perfect-bamboo structure. For a given set of test conditions (j and T) and line geometry, hence, it appears that the value of t_0 is a constant. On the other hand, it appears that the constant, l_0, determines the sensitivity of the lifetime to polygranular segment length. Hence, l_0 determines the slope of Eq. (4.1) on a semi-log plot. No simple physical argument is applied at this point, however, several variables may affect the value of l_0 . It is of interest that, in the case of the data in Fig. 4.11, l_0 is identical for the two sets of annealed lines.

4.3 POST-PATTERN ANNEALING OF PURE Al LINES

Fig. 4.12 presents the failure statistics for pure Al lines annealed for various times at 480 °C. Fig. 4.13 plots the MTF and DTF values computed from these curves as a function of annealing time. Fig. 4.14 shows typical microstructures for the three annealing times at sites where failures have initiated.

The data shown in Figs. 4.12 and 4.13 differ from those of aluminum alloy lines in three respects. First, since the pure Al lines do not contain Cu, their resistance to electromigration is uniformly less; the failure times are comparable to those of Al alloy lines even though the applied current is much smaller (1.2×10^6 A/cm^2 vs. 3.0×10^6 A/cm^2). Second, the MTF for pure Al lines decreases after a brief anneal before it begins the monotonic increase that was observed in the Al alloy lines. Third, the increase in the

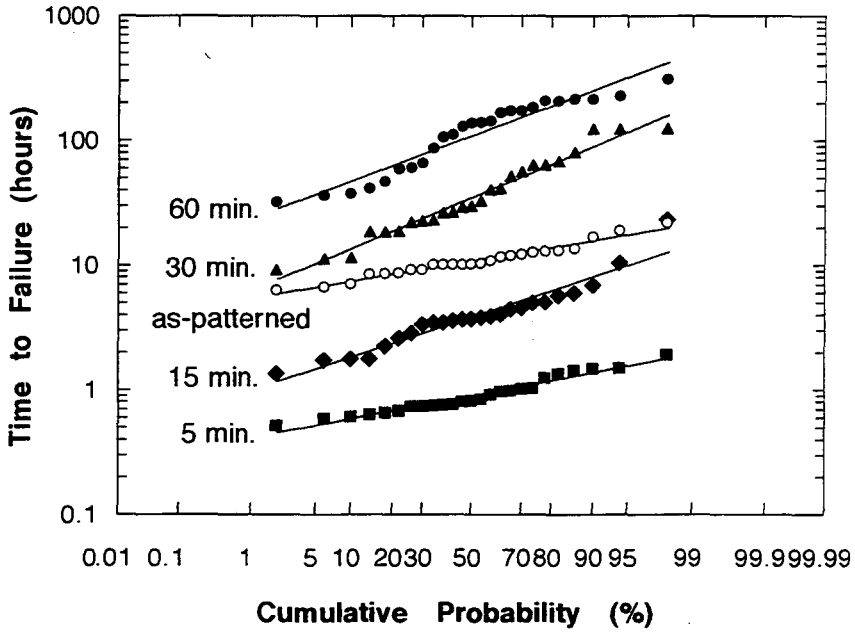

Fig. 4.12 Time-to-failure distributions with annealing times for pure Al lines, annealed at T = 480 °C. The lines were tested at $j = 1.2 \times 10^6$ A/cm^2 and T = 225 °C.

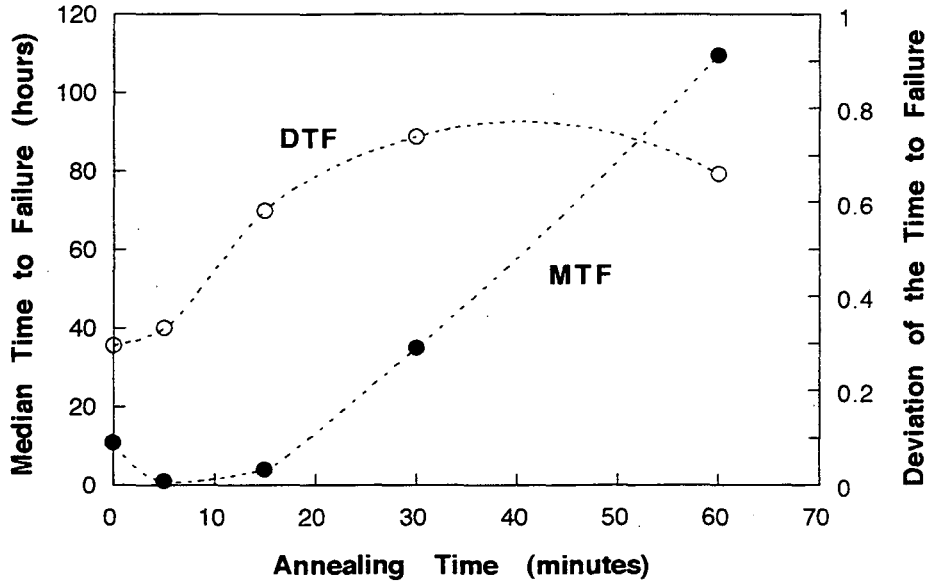

Fig. 4.13 Variations in MTF and DTF as a function of annealing time for pure Al lines, annealed at T = 480 °C.

MTF is more rapid for the pure Al lines.

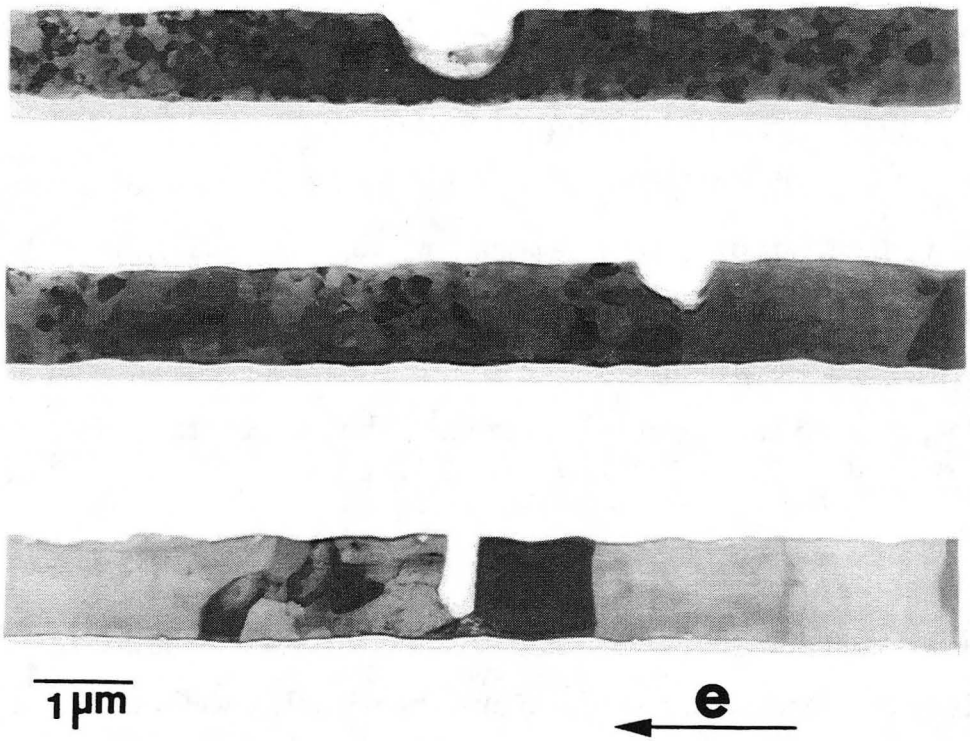

Fig. 4.14 TEM micrographs of Al lines showing the microstructure evolution into a nearly bamboo structure by post-pattern annealing: (a) as-patterned, (b) annealed for 5 min., and (c) annealed for 60 min. at 480 °C. The dramatic reduction in the polygranular segment length is apparent in (c) which shows the longest polygranular segment in the line with the void at its upstream end. (XBD 9504-01180)

The initial decrease in the MTF of the Al lines is a straightforward microstructural effect. The details of microstructure evolution as a function of annealing time were already presented in Chapter 3. Fig. 4.14 adds

further evidence. The microstructural change during the first 5 min. of annealing decreases the MTF, since the long polygranular segments have abrupt microstructural discontinuities at their terminal points that generate large flux divergences. The rapid initiation of a fatal void, after only 40 min. of testing, is clearly shown at the upstream end of a long polygranular segment in Fig. 4.14-(b).

Increasing the annealing time to 60 min. dramatically increases the MTF (Fig. 4.13), while the DTF stabilizes after an initial increase. The time to first failure increases substantially (Fig. 4.12), as with Al alloy lines. A typical microstructure of the failure site is shown in Fig. 4.14-(c). The line was examined using TEM over the whole length. The polygranular segment in the figure which created the void at its upstream end was the longest one.

Unfortunately, pure Al lines do not provide clear microstructural markers to delineate polygranular segments. Voids do mark the upstream ends of the segments, and there are, occasionally, well-defined hillocks to mark the downstream ends. Previously, Mockl et al. measured the void-hillock distance to address their argument on polygranular segment length. [4.2] In the present study, however, hillocks are frequently absent or invisible in SEM micrographs at those locations. It appears that the formation of a hillock is not necessarily related to polygranular segments in the line. The TEM micrographs in Fig. 4.14 support this argument; no hillock is observed at the downstream ends of the polygranular segments. For this reason, the simple SEM technique used for Al alloy lines cannot be applied to the pure Al lines. A different metallographic technique such as the one that was discussed in Chapter 3 (section 4) may be useful in order to test

the validity of Eq. (4.1) for pure Al lines.

4.4 EFFECT OF GRAIN STRUCTURE ON THE KINETICS AND MECHANISM OF ELECTROMIGRATION FAILURE

4.4.1 Effect of Post-Pattern Annealing on Reliability

Lines that have nearly uniform polygranular structures, e.g., the pure Al lines described in Figs. 4.12 - 4.14, have relatively low mean failure times because of the high fraction of grain boundaries. On the other hand, the DTF is also low because of the relative uniformity of the grain structures. Hence, in terms of the time to early failures, these structures are fairly reliable.

A short-time anneal that produces quasi-bamboo structures with long segment lengths, such as the 5 min. anneal of the pure Al lines (Fig. 4.14-(b)), causes an actual decrease in the MTF. Slightly longer anneals increase the MTF, but produce a relatively large scatter in failure times (DTF), with the consequence that the time to first failure remains relatively short. The reason for this is illustrated by the behavior of the alloy lines annealed at 520 °C (Figs. 4.8 and 4.9). The time to first failure in a set of lines is governed by the longest polygranular segment that is retained in any of the lines, and, hence, may remain relatively short even after almost all segments have been refined.

To achieve a high value of the time to first failure it is desirable to have perfect-bamboo structures. As demonstrated in the TEM analysis in

Chapter 3, however, it is not easy to obtain a fully bamboo configuration by post-pattern annealing. On the other hand, a sufficiently long anneal at a sufficiently high temperature ensures the absence of all long polygranular segments. This results in a substantial improvement in the time to first failure, as illustrated by the behavior of the Al-2Cu lines annealed at 540 °C (Figs. 4.8 and 4.9).

4.4.2. Failure Mechanism in "Near-Bamboo" Structures

Near-bamboo structures in the present work refer to predominantly bamboo structures with short polygranular segments. The failure mechanism in the lines with near-bamboo structures that are created by a high-temperature anneal after patterning is essentially identical to those observed in lines whose microstructures were achieved by annealing the parent film prior to patterning. [4.1] In both cases the failure occurs by void formation at the upstream end of the longest polygranular segment in the line. In both cases the failure kinetics of Al-Cu alloy lines are governed by the simple relation shown above in Eq. (4.1). Here l_0 is a characteristic length of the order of a few microns (3.2 μm in the case of 1 μm wide Al-2Cu lines studied in this work).

Both the failure mechanism and the kinetic law continue to be obeyed by lines whose maximum segment lengths are very short, less than 1 μm in the case of the Al-2Cu lines whose behavior is plotted in Fig. 4.11. This result is surprising in light of the prevalent view (originally traceable to Blech and Herring [4.3-4.5]) that there is a critical segment length below which microstructural features should be unimportant. [4.6-4.9] The "Blech

length", which is based on a balance between the diffusion gradient and the back-stress, is in the range of 5 to 10 μm for the experimental conditions used in this study, and is much longer than the lengths of the segments at which failure is observed. This result may not be surprising. The original "Blech length" arguments concerned the critical value of the total line length; they do not obviously apply to the lengths of internal polygranular segments, although they have been inferred to do so. The present work suggests that it is inappropriate to use the Blech length to judge the threat of internal polygranular segments. Further results supporting this argument will be discussed in the following sections.

4.4.3 Current Density Dependence

To examine whether the conclusions presented so far are independent of current density, electromigration tests were conducted over the current density range of 0.75×10^6 A/cm^2 to 2.5×10^6 A/cm^2. The results are plotted in Fig. 4.15. The MTF decreases sharply with increasing current density; it can be fit to a power law relation, MTF $\propto j^{-n}$ with $n \approx 3$, while the DTF remains nearly constant.

Nearly 30 years ago, Black proposed the following empirical relation to describe the MTF as a function of current density [4.10]

$$\text{MTF} = A\, j^{-n} \exp\left(E_f / kT\right) \tag{4.2}$$

where A is a material constant relating to structural, electrical and diffusional properties of thin-film conductors, and E_f is the activation energy for

electromigration-induced failure. A computer simulation has suggested that the current density exponent should be unity in an ideal case. [4.11] A theoretical model, in which the accumulation of vacancies is calculated in a grain boundary under electromigration, reports a n of 2, with a modification of eq (4.2) which incorporates a T^2 term. [4.12] On the other hand, experimental observations have indicated that the current density exponent, n, varies largely, and is usually greater than 2. [4.2, 4.13, 4.14] The occurrence of a higher order current density exponent is often attributed to the effect of Joule heating. However, it is difficult to distinguish the Joule heating effect from fundamental mechanisms, since Joule heating is extremely difficult to separate from the electromigration failure process. The value of the current density exponent is still subject to debate.

Over the current density range shown in Fig. 4.15, the failure sites do not appear to be affected. Fig. 4.16 shows the distributions of void-precipitate spacings at the failure sites along three sets of lines that were annealed at the same conditions (520 °C, 30 min.) and tested at three different current densities. The distributions of void-precipitate spacings are independent of the current density, reflecting the fact that the three sets of lines have statistically identical distributions of polygranular segment lengths. In keeping with this result, the DTF is independent of current density (Fig. 4.15). This proves the argument that the DTF (scatter in failure times) is governed by the scatter in the lengths of the polygranular segments that lead to failure (Fig. 4.16).

The results provide further documentation that the Blech length does not influence the failure mechanism of quasi-bamboo lines. If there was a current-dependent critical polygranular segment length for failure,

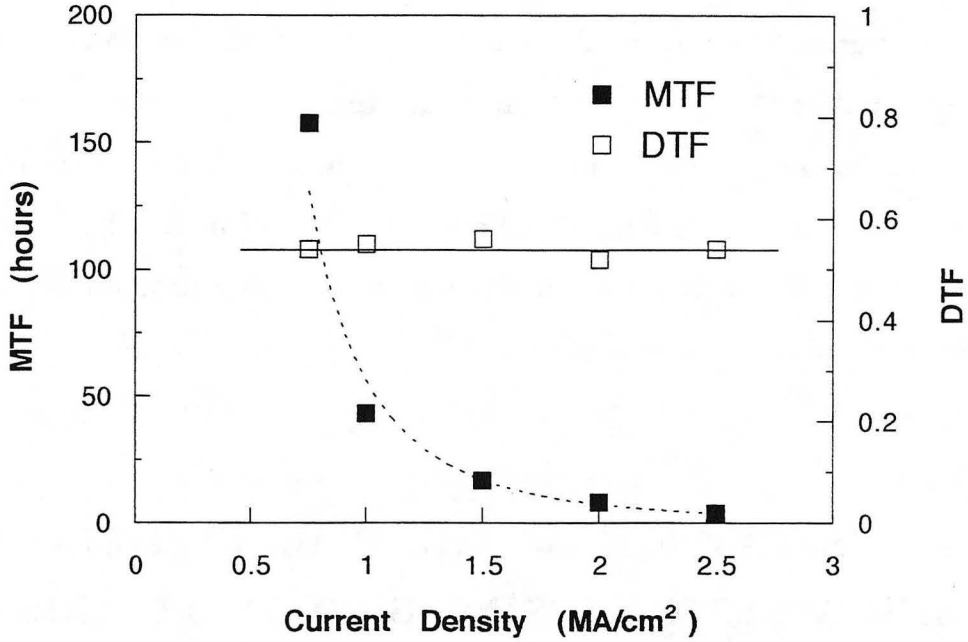

Fig. 4.15 Variations in MTF and DTF for Al-2Cu lines as a function of current density.

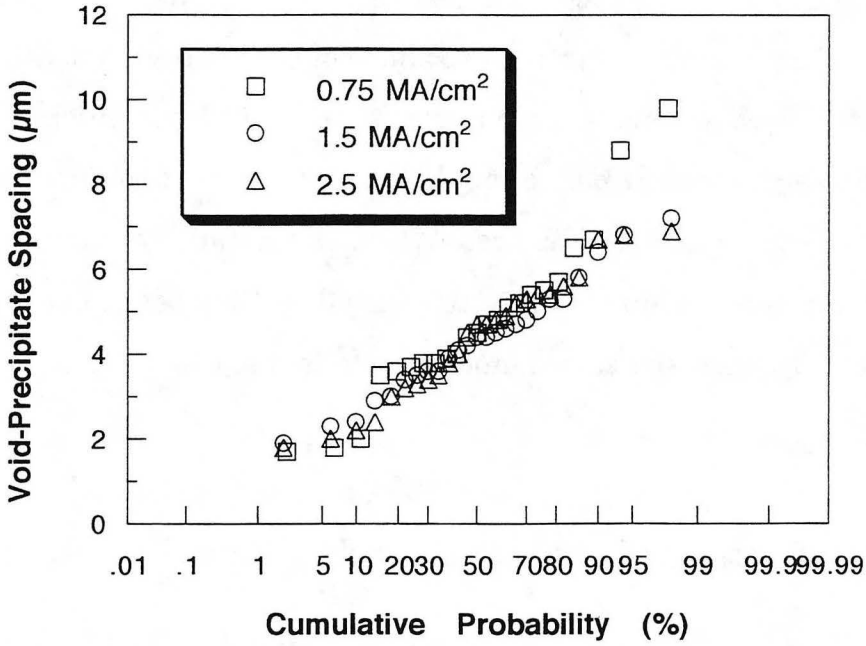

Fig. 4.16 Void-precipitate spacing distributions at the failure sites with the change in current density.

the distribution of polygranular segment lengths that cause failure would be truncated at this length, which would increase as the current density dropped. On the contrary, the distributions in Fig. 4.15 are essentially independent of current density. This supports the argument that microstructural features must be considered even in the lines that have only sub-Blech-length polygranular segments.

4.5 INVESTIGATION OF THE FAILURE MECHANISM AND KINETICS USING SILICON NITRIDE WINDOWS

The silicon nitride window technique was used for two purposes. First, this technique was used to observe failure sites directly, and to compare their microstructural features to those of other sites that did not produce failures. Second, this technique was used to study the microstructural effects of three groups of lines, annealed under different conditions, on the kinetics of electromigration failure. While the details of microstructural analysis using this technique were presented in Chapter 3, the reliability improvement by microstructural modification is discussed in this section.

4.5.1 Identification of the Weakest Polygranular Segment

Fig. 4.17 shows TEM micrographs of a line tested at $j = 0.8\text{x}10^6$ A/cm^2 and $T = 225$ °C. The line failed after about 150 hrs. The void is

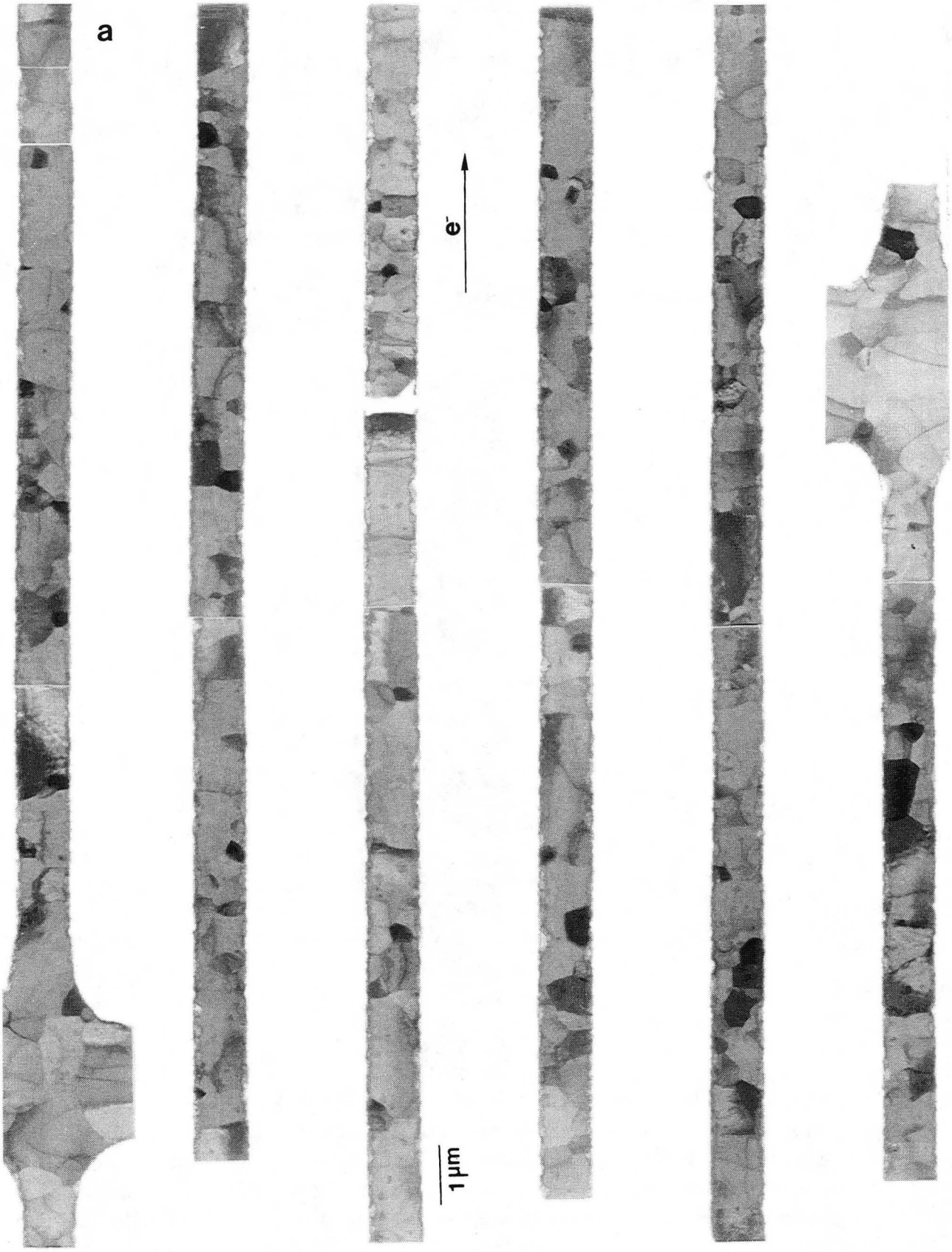
a
e⁻
1 µm

Fig. 4.17 TEM micrographs of an Al-2Cu line (100 μm in length) that was tested at j = 0.8x10^6 A/cm^2 and T = 225 °C. (a) Image along the whole line; the void is located at the upstream end (with respect to electron flow) of the longest polygranular segment in the line. (XBD 9604-01539) (b) Magnified image of the failure site. (XBD 9604-01538)

clearly located at the upstream end of the longest polygranular segment, whose length is approximately 3 μm. In addition, the Al_2Cu precipitate bounds the downstream end of the segment. Shorter polygranular segments did not produce voids in this test. The length of the failed segment is shorter than the "Blech length" for these testing conditions (~ 10 μm). Hence, this direct TEM observation confirms our previous conclusion, from void-precipitate pair spacings (Fig. 4.16), that the void failure occurs at the terminations of the longest polygranular segments, even when these segments have lengths below the Blech length. Coupling this observation with the fact that the relation between failure time and segment lengths shows no discontinuity or perturbation at the Blech length (Fig. 4.11), it can be concluded that the Blech length does not play a role in the electromigration failure of quasi-bamboo lines. This conclusion is in apparent agreement with Lloyd, [4.15] who considers the mass transport along multiple diffusion paths to explain the failure at the short polygranular segments.

4.5.2 Reliability Improvement by Microstructural Modification

In Chapter 3, the length of the longest polygranular segments in each member of three groups of lines was measured in order to map the statistics of the longest segment lengths. The results were plotted in Fig. 3.13. Each distribution was characteristic of each annealing condition. The distribution of the longest polygranular segments determines the distribution of failure times. Fig. 4.18 shows the typical failure-time distribu-

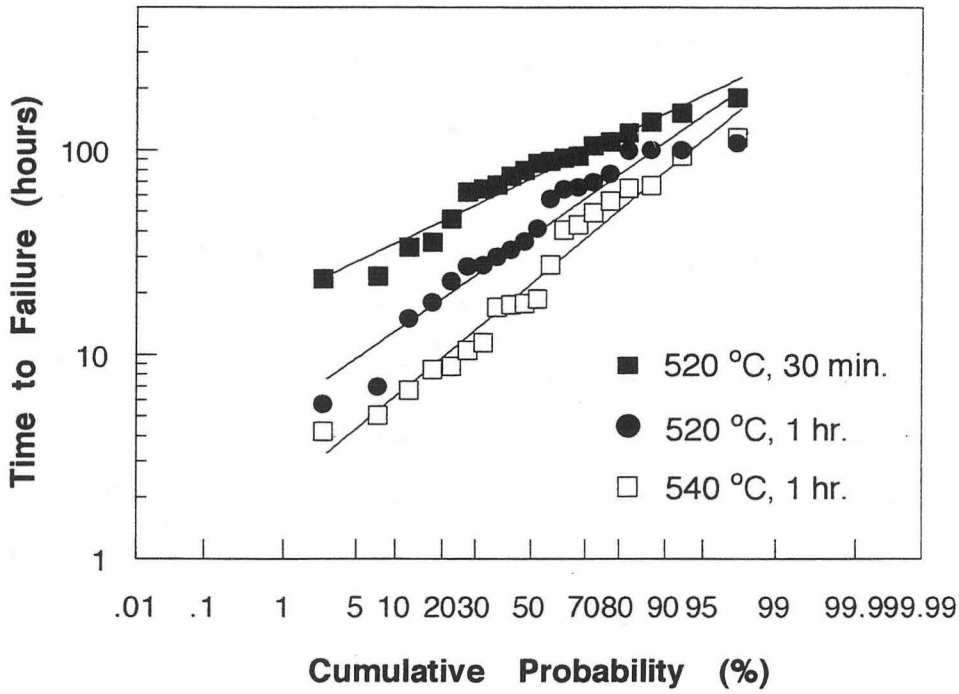

Fig. 4.18 Time-to-failure distributions for three annealing conditions. The three sets of Al-2Cu lines were tested at 225 °C under $j = 3x10^6$ A/cm^2.

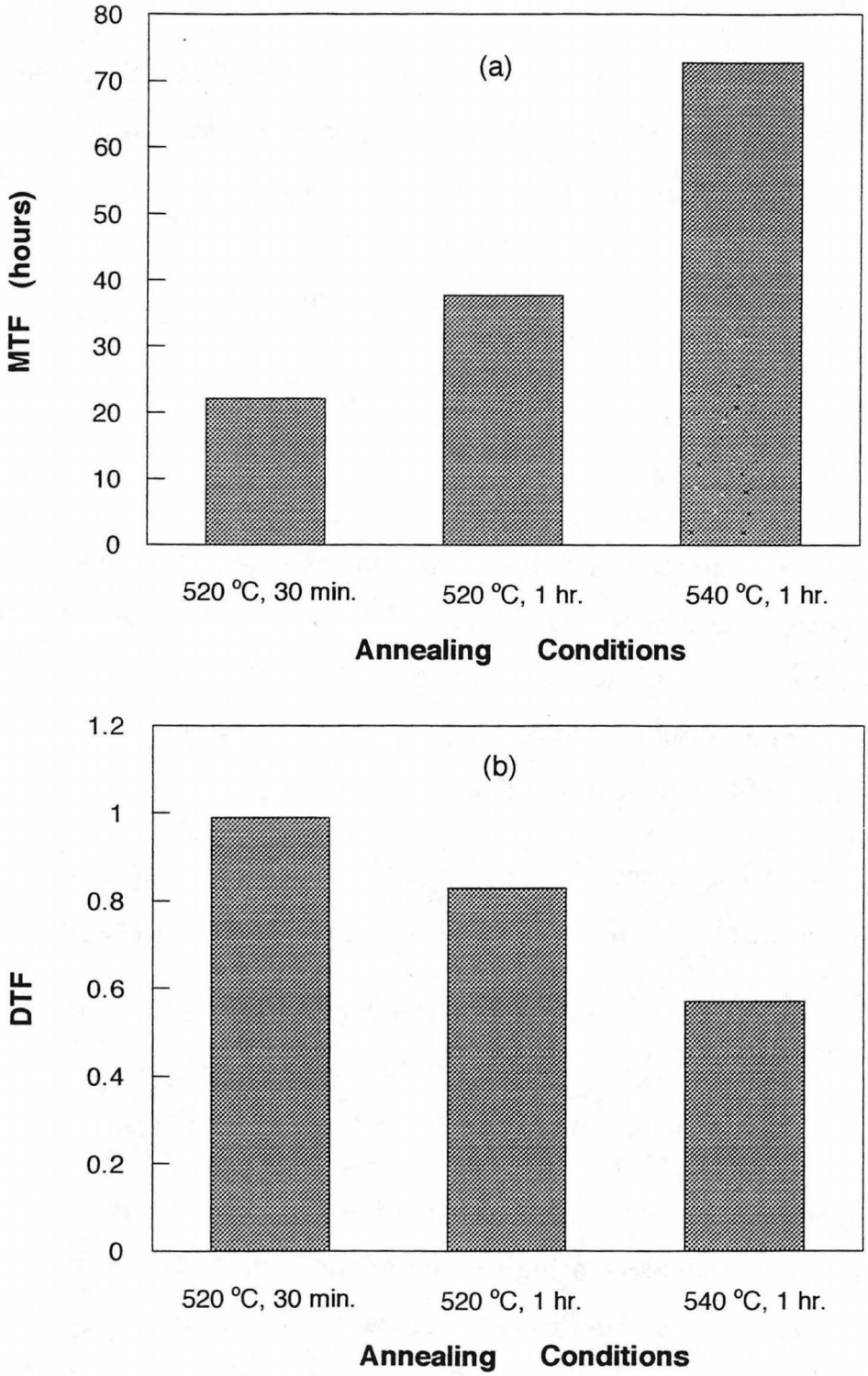

Fig. 4.19 Variations in (a) MTF and (b) DTF as a function of annealing conditions. These values were calculated from the distributions plotted in Fig. 4.18.

tions for the three groups of lines. The MTF and the DTF calculated from these distributions are plotted in Fig. 4.19. The distributions illustrated in Fig. 4.18 follow the segment length distributions shown in Fig. 3.13 where shorter segments lead to longer lifetimes, and a narrower distribution of segment lengths results in a smaller scatter in failure times.

4.6 CONCLUSION

The work reported in this Chapter shows that the reliability of Al-based interconnects can be dramatically improved by post-pattern annealing. The data shown in Figs. 4.4 - 4.6, 4.12, 4.13, and 4.18, in conjunction with the associated micrographs, lead to the following conclusions regarding the benefit of this heat treatment.

1) Post-pattern annealing is an effective metallurgical method that preferentially breaks up relatively long polygranular segments.

2) Post-pattern annealing refines the distribution of the lengths of the longest polygranular segments (failure unit), which govern the distribution of failure times in quasi-bamboo lines.

3) Appropriate annealing achieves a narrow failure-time distribution which ensures a high value of the time to first failure as well as a high median time to failure.

From the technological perspective, these conclusions demonstrate a straightforward metallurgical procedure that can be used to improve the electromigration resistance in narrow lines. The usefulness of this proce-

dure for a particular device depends, of course, on whether a high-temperature anneal is compatible with the processing requirements of that device. Some devices cannot tolerate exposure to high temperature after patterning. Others only accept a brief high-temperature anneal. While the annealing times used in the present work are relatively long, it is possible to shorten them significantly by modifying the deposition conditions to increase the grain size in the as-deposited conditions. Another option is to use multiple rapid thermal anneals to accelerate grain growth.

4.7 REFERENCES

[4.1] C. Kim and J. W. Morris, Jr., "The mechanism of electromigration failure of narrow Al-2Cu-1Si thin-film interconnects," J. Appl. Phys. **73**, 4885 (1993).

[4.2] U. E. Mockl, M. Bauer, O. Kraft, J. E. Sanchez, Jr., and E. Arzt, "Detailed study of electromigration induced damage in Al and AlCuSi interconnects," MRS Symp. Proc. **338**, 373 (1994).

[4.3] I. A. Blech, "Electromigration in thin aluminum films on titanium nitride," J. Appl. Phys. **47**, 1203 (1976).

[4.4] I. A. Blech and C. Herring, "Stress generation by electromigration", Appl. Phys. Lett. **29**, 131 (1976).

[4.5] E. Kinsbron, I. A. Blech, and Y. Komem, "The threshold current density and incubation time to electromigration in gold films," Thin Solid Films **46**, 139 (1977).

[4.6] E. Kinsbron, "A model for the width dependence of electromigration failure in aluminum thin-film stripes," Appl. Phys. Lett. **36**, 968 (1980).

[4.7] E. M. Atakov, J. J. Clement, and B. Miner, "Two electromigration failure modes in polycrystalline aluminum interconnects," IEEE Proceedings of the 32nd International Reliability Physics Symposium, 151 (1994).

[4.8] E. Arzt, O. Kraft, and U. E. Mockl, "Electromigration damage in conductor lines: recent progress in microscopic observation and mechanistic modeling," MRS Symp. Proc. **338**, 397 (1994).

[4.9] C. V. Thompson, Y.-C. Joo, and B. D. Knowlton, "Modelling of the structure and reliability of near-bamboo interconnects," MRS Symp. Proc. **391**, 163 (1995).

[4.10] J. R. Black, "Electromigration: a brief survey and some recent results," IEEE Trans. Electron Devices **ED-16**, 338 (1969).

[4.11] P. J. Marcoux, P. P. Merchant, V. Naroditsky, and W. D. Rehder, "A new 2D simulation model of electromigration," Hewlett-Packard J., June, 79 (1989).

[4.12] M. Shatzkes and J. R. Lloyd, "A model for conductor failure considering diffusion concurrently with electromigration resulting in a current exponent of 2," J. Appl. Phys. **59**, 3890 (1986).

[4.13] J. C. Blair, P. B. Ghate, C. T. Haywood, "Electromigration induced failure in aluminum film conductors," Appl. Phys. Lett. **17**, 281

(1970).

[4.14] H. A. Schafft, T. C. Grant, A. N. Saxena, and C. Kao, "Electromigration and the current dependence," IEEE Proceedings of the 23rd International Reliability Physics Symposium, 93 (1985).

[4.15] J. R. Lloyd, "Stress and electromigration," MRS Symp. Proc. **391**, 231 (1995).

CHAPTER 5

FAILURE KINETICS : THE KINETIC EQUATION

5.1 INTRODUCTION

In this Chapter, the generality of Eq. (4.1), $t_f = t_0 \; exp \; (-l/l_0)$, is explored based both on a previously reported simple model and on experimental results of the present work. The principal goal of this Chapter is to discuss the implications of the experimental results in the previous Chapters from a metallurgical perspective.

The present work substantiates the fact that the internal failures of lines with quasi-bamboo structures is controlled by the longest polygranular segments they contain, and can be retarded by decreasing the maximum segment length. Moreover, at least in the case of Al-Cu alloy lines, there is a simple relation (Eq. (4.1)) between the longest polygranular segment and the time to failure. It was previously reported [5.1] that an equation of the general form of Eq. (4.1) was obtained by assuming that the rate of failure is governed by the steady-state accumulation of vacancies at the end of a polygranular segment, along lines suggested by Nix and Arzt [5.2] and by Lloyd. [5.3] This Chapter briefly reviews their findings. The experimental results of the present work are then used to analyze Eq. (4.1) from a qualitative standpoint. Emphasis is on searching for the factors that govern the kinetic constants t_0 and l_0 in Eq. (4.1).

5.2 REVIEW OF THE DIFFUSION MODEL

The diffusion model, proposed by Nix and Arzt and developed by Lloyd, considers the electromigration of vacancies in a single grain boundary segment of length l that runs parallel to the line, as illustrated in Fig. 5.1. The boundary segment ends at blocking grain boundaries that extend across the entire cross section of the line. The grain boundary segment in the model simulates a polygranular segment that terminates at bamboo grains, based on the assumption that flux divergences within a polygranular segment (e.g. at grain boundary triple junctions) are negligible compared to those at the ends of the segment. Void formation and growth will occur at the upstream end of the grain boundary segment (i.e. at P indicated in Fig. 5.1) at which the local vacancy concentration is the maximum.

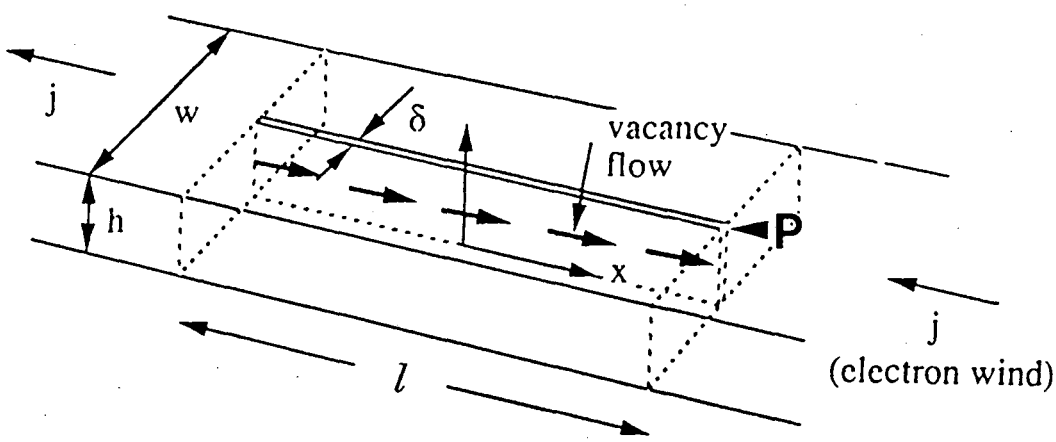

Fig. 5.1 A straight grain boundary segment of length l which represents a sequence of grain boundary segment that terminates at blocking grains (Ref. 5.2).

In the model the electromigration of vacancies is treated in a phenomenological way in order to calculate the local vacancy concentration at a particular point in the grain boundary segment. The phenomenological approach of electromigration, also used, for example, by Rosenberg and Ohring, [5.4] Shatzkes and Lloyd, [5.5] and Clement and Lloyd, [5.6] has been a common practice within a framework of irreversible thermodynamics by Huntington. [5.7] It is well-known that the drift velocity of vacancies, v, in the grain boundary can be expressed as

$$v = (D_{gb} \ / \ kT) \ Z^* \ e \ E \tag{5.1}$$

where D_{gb} (= $D_0 \ exp \ (-\Delta H \ / \ kT)$) is the grain boundary diffusivity of vacancies, Z^*e is the effective charge of the vacancy, and E is the electric field. The drift of vacancies induces a vacancy concentration gradient and, in turn, a diffusional flux that counterbalances the electromigration-induced drift. It follows that the one-dimensional diffusion equation is given in the following form, which is often called as the "electromigration equation":

$$\frac{\partial C_v}{\partial t} = D_{gb} \left(\frac{\partial^2 C_v}{\partial x^2}\right) - v \left(\frac{\partial C_v}{\partial x}\right) \tag{5.2}$$

where C_v is the vacancy concentration in the grain boundary and x is the coordinate position in the boundary.

Arzt and Nix solved Eq. (5.2) to find a steady-state profile of the vacancy concentration along the grain boundary segment. Their solution is simply expressed by

$$C_v = C_0 \ exp \ (v \ x \ / \ D_{gb}) \tag{5.3}$$

where C_0 is the initial vacancy concentration in the grain boundary of the stress-free line. In Eq. (5.3), the maximum vacancy concentration in the grain boundary segment is attained at the upstream end of the segment. The maximum concentration is then a function of the segment length, l, which is given by

$$C_{max} = C_0 \exp (v\, l \,/\, 2D_{gb}) \tag{5.4}$$

Consequently, the longer the grain boundary segment, the larger the resulting vacancy accumulation at the upstream end of the segment.

Kim and Morris explored Eq. (5.4) in order to derive a formula that is qualitatively similar to Eq. (4.1). They assumed that the failure time (t_f) is inversely proportional to the maximum vacancy concentration induced by the grain boundary segment shown in Fig. 5.1, that is,

$$t_f \propto \frac{1}{C_{max}} \tag{5.5}$$

This assumption leads to the following relation between the failure time and the length of the segment:

$$t_f = A \exp (-v\, l \,/\, 2D_{gb}) = A \exp (-l\, (Z^*eE \,/\, 2kT)) \tag{5.6}$$

where A is a constant. Given test conditions, Eq. (5.6) yields a function which is mathematically identical to Eq. (4.1). The characteristic time (t_0) is the constant A, while the characteristic length (l_0) is given by the following relation:

$$l_0 = 2kT \,/\, Z^*eE = 2kT \,/\, Z^*e\rho j \tag{5.7}$$

Eq. (5.7) suggests that l_0 depends on current density (j) and temperature (T). Fig. 5.2 roughly illustrates the change in l_0 that is described by Eq. (5.7).

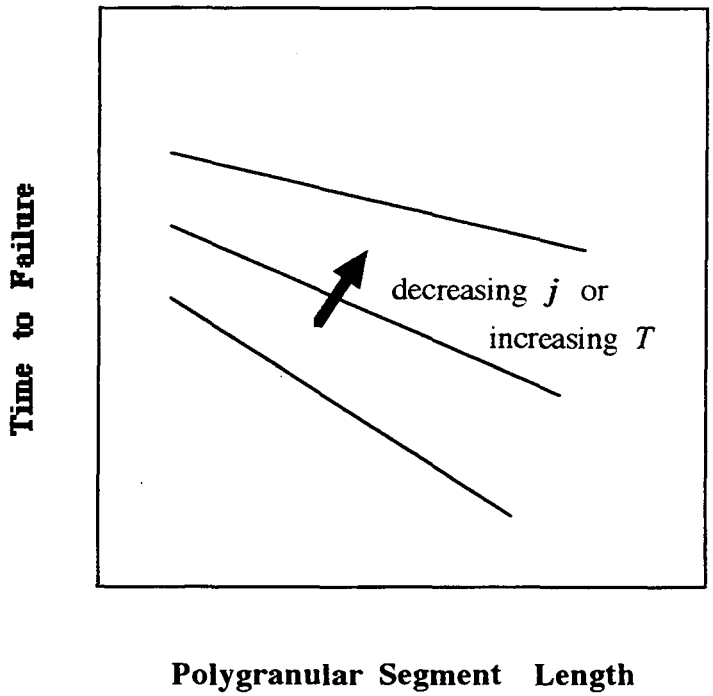

Fig. 5.2 Schematic curves that follow Eq. (4.1) based on the argument that l_0 is determined by Eq. (5.7). Suppose that the three sets of lines have identical geometry and microstructural configuration.

The most interesting results to emerge from the above analysis (Eqs. 5.6 and 5.7) are the predictions that failure occurs at the longest polygranular segment, and that the failure time increases exponentially with decreasing the length of the longest polygranular segment. These predic-

tions have been, at least qualitatively, proven by the experimental results of the prior work (Fig. 4.10). However, Eq. (5.7) cannot explain two different slopes (i.e. two different l_0 values) in Fig. 4.10. While the prior work reported that the value of l_0 calculated from Eq. (5.7) was about 4 μm for the both sets of lines, those from the experimental data in Fig. 4.10 were 2.2 μm and 4.4 μm for 1.3 μm and 2 μm wide lines, respectively. Presumably, the disagreement could result from the different line geometry or different microstructural configurations within the polygranular segments for the two sets of lines. Unfortunately, the diffusion model is too simple to consider these effects. It is difficult to argue about the validity of Eq. (5.7), without understanding the effects of line geometry and microstructural characteristics of polygranular segments.

5.3 EXPERIMENTAL ANALYSIS OF THE KINETIC EQUATION

In this work, the exponential dependence of failure time (t_f) on the polygranular segment length (l) that leads to failure was first demonstrated in Fig. 4.11. The data were obtained from two sets of lines annealed at different temperatures (520 °C and 540 °C). However, the lines had the same geometry, and were tested under the same conditions. Unlike those shown in Fig. 4.10, the data coalesce onto a single curve which obeys Eq. (4.1) in which $t_0 \approx 100$ hrs. and $l_0 \approx 3.2$ μm.

5.3.1 Characteristic Time

The reason for the same t_0 value in Fig. 4.11 appears to be simple. A characteristic time, t_0, is the time-to-failure in the absence of a polygranular segment, i.e., $l = 0$. It is expected that, if perfect bamboo lines with identical geometry were tested to failure under the same conditions, the lines would have almost the same lifetimes.

In contrast, the data shown in Fig. 4.10 were obtained from two sets of lines which had different line widths. Prior work suggests that there is a reason why t_0 for the narrow lines is larger than that for the wide lines. [5.1. 5.8. 5.9] The vacancy supersaturation that leads to void formation can be relieved by the vacancy diffusion to free surfaces. Under a given test condition, the vacancy diffusion is expected to increase with the surface-to-volume ratio of the line, as evidenced by previous studies on the effect of line thickness. [5.8. 5.9] The same argument can be applied to the effect of different line widths.

5.3.2 Characteristic Length

Fig. 4.11 shows that two sets of lines have essentially same l_0 value (3.2 μm) which were prepared by slightly different post-pattern anneals. For the two groups of lines, microstructural characteristics of the failure units were similar, except that there was a significant difference in the length of very long polygranular segments (Fig. 4.9).

The kinetic constant l_0 describes the sensitivity of lifetime depend-

ence on the polygranular segment length that leads to failure. For the sake of argument, let us suppose that there are two sets of geometrically identical lines, which are tested at the same conditions (T and j). If two different l_0 values exist for this case, the curves following Eq. (4.1) would look like those schematically drawn in Fig. 5.3. Note that both curves are expected to have the same t_0 value. The curve A has a smaller l_0 than the curve B, and the curve A becomes a stronger function of polygranular segment length. According to Fig. 5.3, although two lines have the same polygranular segment length, the line following the curve A should have a shorter lifetime.

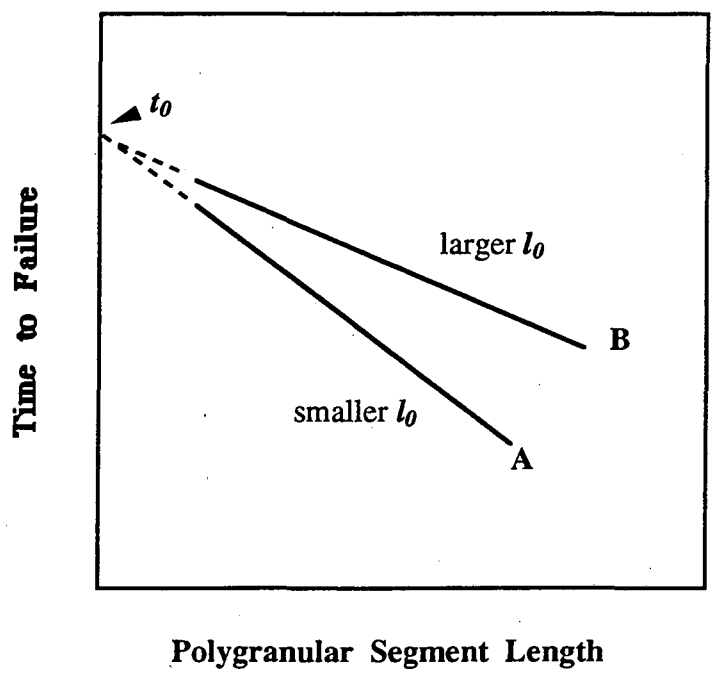

Fig. 5.3 Schematic curves following Eq. (4.1) while having different l_0 values. It is assumed that the two curves are obtained from the two sets of geometrically identical lines that are tested at the same condition.

If different l_0 values were observed like the case in Fig. 5.3, in addition to polygranular segment length, there necessarily would be more microstructural factors which influence the failure kinetics. Presumably, the following microstructural factors need to be considered for further investigation. First, the grain configuration within polygranular segments, including grain size and preferred crystallographic orientation, affects the atomic transport; highly textured, large grains substantially reduce electromigration flux within the segments. Second, the growth of fatal voids may depend on the nature of the bamboo grains next to polygranular segments; some specific grain orientations are more vulnerable to void formation. For example, Marieb et. al have suggested that, while void nucleation sites are fixed by polygranular segments, voids grow to failure faster in grains oriented with a {111} plane near perpendicular to the line. [5.10]

5.3.3 Effect of Current Density

For further discussion, the lines which were tested under different current densities were studied. Three groups of lines were annealed at the same condition (520 °C, 30 min.). As a consequence, these three groups had statistically identical distributions of polygranular segments (Fig. 4.16), except the two lines that have unusually long polygranular segments in the group tested under $j = 0.75\text{x}10^6$ A/cm^2.

The time-to-failure distributions for three different current densities are shown in Fig. 5.4. From Figs. 4.16 and 5.4, a semi-log plot showing failure time as a function polygranular segment length is constructed, as

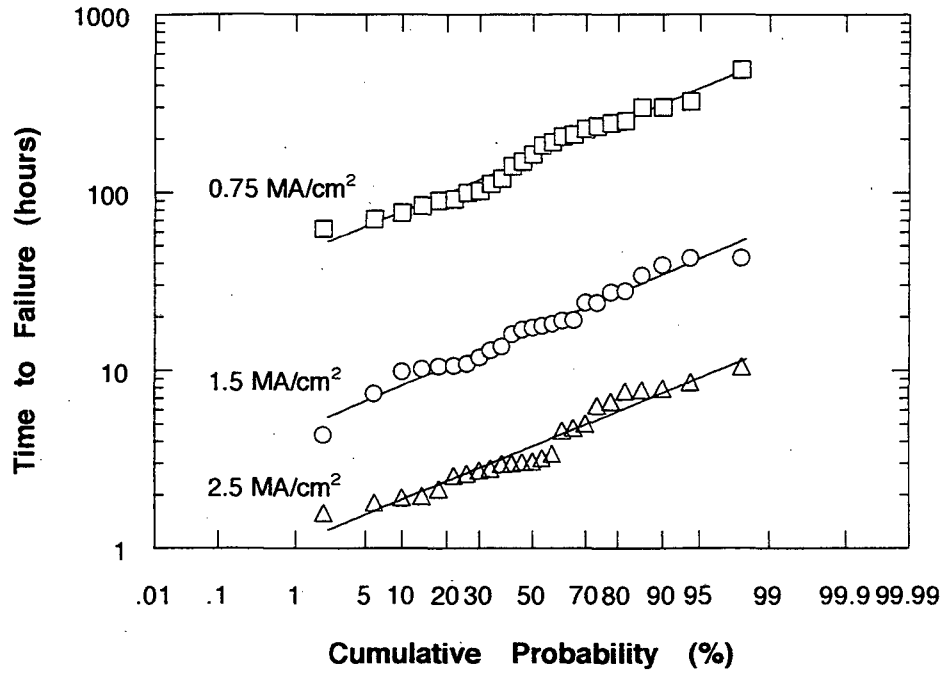

Fig. 5.4 Time-to-failure distributions for three different current densities. For the tests three sets of Al-2Cu lines were annealed at 520 °C for 30 min.

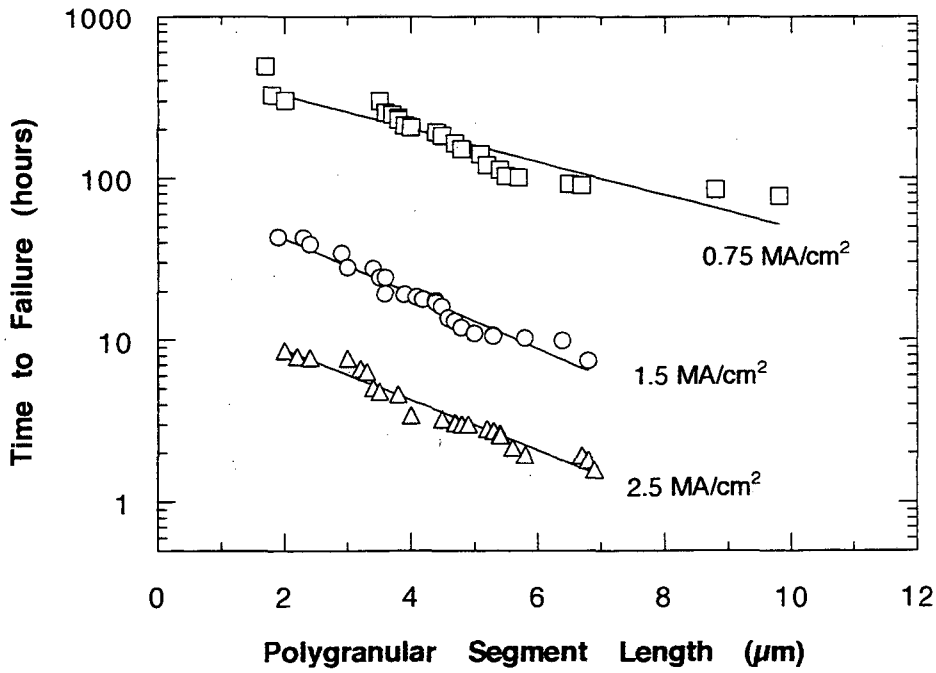

Fig. 5.5 Semi-log curves showing the relation between failure time and polygranular segment length with changing current density.

illustrated in Fig. 5.5. The data are fitted by Eq. (4.1). The constants t_0 and l_0 calculated from the three curves are summarized in Table 5.1. As expected, the characteristic length t_0 decreases rapidly with the current density. Unfortunately, however, it is difficult to draw a convincing argument on the effect of current density on l_0; no trend is observed when the current density varies.

While more experimental analysis is necessary, it seems that the current density plays only little role in determining the value of l_0. This argument applies well to the curves obtained from the lines tested under $j = 1.5\text{x}10^6$ A/cm^2 and $j = 2.5\text{x}10^6$ A/cm^2. Even for the data from $j = 0.75\text{x}10^6$ A/cm^2, except the two data points originated from unusually long polygranular segments, the slope of the curve almost matches those of other curves.

Table 5.1 The kinetic constants t_0 and l_0 values with the change in current density. These values were calculated from the curves plotted in Fig. 5.5.

Current Density (A/cm^2)	t_0 (hrs.)	l_0 (μm)
0.75 x 10^6	518.2	4.35
1.50 x 10^6	92.6	2.56
2.50 x 10^6	17.8	2.86

5.4 IMPLICATIONS

The mean grain size of the film does not reflect the reliability of quasi-bamboo lines. The mean length of polygranular segments does not predict the reliability, either. The microstructural parameter which predominantly determines the lifetime of each line is the longest polygranular segment within it, and the distribution of the longest segment lengths over a group of lines reflects the reliability of the group. The experimental results of this work strongly suggest that Eq. (4.1) provides a simple phenomenological basis for predicting the lifetimes of quasi-bamboo lines. Eq. (4.1) was previously proposed to govern the failures of as-patterned Al-2Cu-1Si lines. [5.1] The present work shows that it governs the failures of annealed Al-2Cu lines as well. Furthermore, the present work has demonstrated that the exponential relation between the longest segment length and the time to failure is maintained even for near-bamboo lines that had predominantly bamboo structures with extremely short polygranular segments.

Eq. (4.1) also proposes the need for, and a profitable direction for theoretical modeling. The results in Fig. 5.5 are in apparent disagreement with Eq. (5.7), since Eq. (5.7) expects that l_0 is inversely proportional to current density. As pointed out in the discussion of Figs. 4.10, 4.11, and 5.5, the flaw in Eq. (5.7) is the fact that this equation does not concern microstructural and geometrical features along a polygranular segment. Accordingly, Eq. (5.7) does not produce a correct value for the kinetic constant l_0. Furthermore, the model that leads to Eq. (5.7) is too simple to account for the two-stage failure sequence in Al-Cu lines. The theoretical

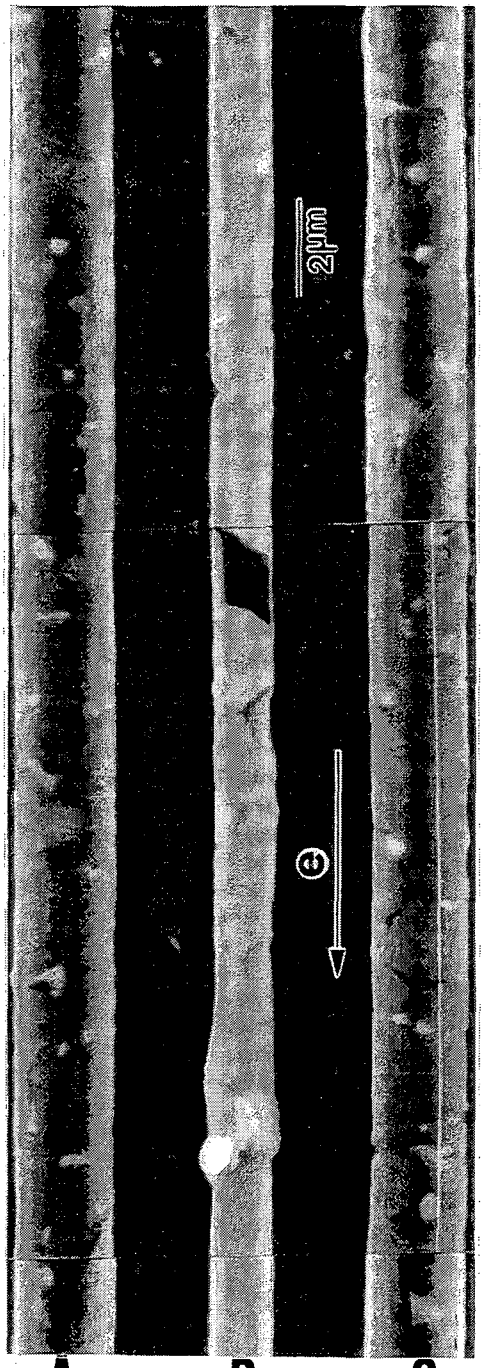

Fig. 5.6 SEM micrographs showing the reference lines (A and C) which were not stressed by current and the tested line (B) after the failure under $j = 3x10^6$ A/cm^2. Line B shows the depletion of Cu from the polygranular segment and the upstream bamboo grain. (XBD 9504-01175)

analysis of the failure is complex due to the presence of Cu solutes and Al_2Cu precipitates. It has been suggested that the failure is preceded by the depletion of Cu from the polygranular segment and a portion of the up-stream bamboo grain. [5.1] Fig. 5.6 supports this argument. Unfortunately, however, no theoretical model has been reported to explore the influence of Cu-sweeping kinetics on the overall failure kinetics. Further work is needed to develop an appropriate theoretical foundation.

5.5 CONCLUSION

Microstructural effects on electromigration failure kinetics are well described by a simple exponential relation between the failure time and the longest polygranular segment length within a line. This exponential relation is observed for different sets of lines prepared in a variety of ways. Furthermore, the relation is still valid even when the segment length is shorter than the critical polygranular segment length that is derived based on Blech's threshold-length argument. However, it is not yet clear which parameters govern the characteristic constants which are included in the exponential equation. Finding correct values for these constants at given test conditions (metallurgy, current density, temperature, geometry etc.) is necessary in order to provide a methodology for assessment of interconnect reliability.

5.6 REFERENCES

[5.1] C. Kim and J. W. Morris, Jr., "The mechanism of electromigration failure of narrow Al-2Cu-1Si thin-film interconnects," J. Appl. Phys. **73**, 4885 (1993).

[5.2] W. D. Nix and E. Arzt, "On void nucleation and growth in metal interconnect lines under electromigration conditions," Metall. Trans. **23A**, 2007 (1992).

[5.3] J. R. Lloyd, "The role of Cu in electromigration lifetimes of aluminum alloy conductors," Appl. Phys. Lett. **57**, 1167 (1990).

[5.4] R. Rosenberg and M. Ohring, "Void formation and growth during electromigration in thin films," J. Appl. Phys. **42**, 5671 (1971).

[5.5] M. Shatzkes and J. R. Lloyd, "A model for conductor failure considering diffusion concurrently with electromigration resulting in a current exponent of 2," J. Appl. Phys. **59**, 3890 (1986).

[5.6] J. J. Clement and J. R. Lloyd, J. Appl. Phys. **71**, 1729 (1991).

[5.7] H. B. Huntington, "Electromigration in metals," in *Diffusion in Solids: Recent Developments* (Academic Press, New York, 1974), edited by A. S. Nowick and J. J. Burton, p. 303.

[5.8] G. A. Scogan, B. N. Agarwala, P. P. Peressini, and A. Brouillard, "Width dependence of electromigration life in Al-Cu, Al-Cu-Si and Ag conductors," IEEE Proceedings of the 13th International Reliability Physics Symposium, 151 (1975).

[5.9] T. Kwok, "Effect of metal line geometry on electromigration lifetime in Al-Cu submicron interconnects," IEEE Proceedings of the 26th International Reliability Physics Symposium, 151 (1988).

[5.10] T. Marieb, P. Flinn, J. C. Bravman, D. Gardner, and M. Madden, "Observation of electromigration induced void nucleation and growth in polycrystalline and near-bamboo passivated lines," J. Appl. Phys. 78, 1026 (1995).

APPENDIX

BLECH LENGTH vs. CRITICAL POLYGRANULAR SEGMENT LENGTH

The Blech length has been one of the most controversial issues in the establishment of the failure mechanism in quasi-bamboo lines. The Blech-length arguments originated from the geometry effect on electromigration in a drift-velocity experiment, i.e., the critical value of the total line length, below which electromigration apparently stops. [A.1-A.3] These arguments have then been inferred to calculate a critical value of polygranular segment lengths below which the segments do not cause electromigration failure. [A.4-A.7] This Appendix discusses a few significant results reported previously, and points out some shortcomings in those investigations.

A.1 Blech Length: Effect of Line Length on Electromigration

The line length effect on electromigration was first demonstrated by Blech in 1976. [A.1] In his drift-velocity measurement of Al stripes, Blech found a threshold current density below which there was no drift of stripes by electromigration. This current density was inversely proportional to stripe length. Thus short lines ($\approx$ 30 μm) could withstand current densities up to 10^6 A/cm^2 without any signs of electromigration. Similar phenomena were also observed in the case of Au stripes studied by Kinsbron, Blech, and Komem in 1977. [A.3] Blech and Herring interpreted these behaviors as the fact that electromigration is suppressed by concomitant back-flux due

to stress or concentration gradients during passage of electrical currents. [A.2] This flux balance is given by

$$\frac{ND}{kT} eZ^* E = \frac{ND}{kT} \frac{\partial}{\partial X} (\mu_a - \mu_v) \tag{A.1}$$

where N is the atomic density, D is a diffusivity, Z^* is an effective charge, E is the electric field, μ_a and μ_v are the chemical potentials of the atoms and vacancies, respectively, and X is the distance along the film in the direction of electron flow. They further stated that, if grain boundaries could maintain a local equilibrium with respect to adding atoms or vacancies, either the atom pile-up or depletion at the stripe ends generates a stress gradient (not a concentration gradient). It follows that the net drift velocity v_d is given by

$$v_d = v_e - v_b = (eZ^* E - \Omega \frac{\partial \sigma_{nn}}{\partial X}) \frac{ND}{kT} \tag{A.2}$$

where Ω is the atomic volume, σ_{nn} is the stress normal to the grain boundaries, and μ_0 is a constant. From this equation it has been a common practice to refer to the critical stripe length (L_c) that can stop electromigration (i.e. $v_d = 0$) as a "Blech length".

The critical product of current density and line length, $(jL)_c$, reported by Blech was 1260 A/cm for Al films at 350 °C. [A.1] The threshold product increased gradually with the decrease in current density. The Blech length at service conditions is then on the order of 100 μm. [A.8] If this argument is accepted, the line shorter than the Blech length must be immortal. However, it is difficult to draw this conclusion from Blech's original data, since

the time frame for his drift-velocity measurement was too short (e.g. 15 hrs. at $j = 3.7\text{x}10^5$ A/cm^2, 45 hrs. at $j = 1.5\text{x}10^5$ A/cm^2).[A.1]

While there are many theoretical analyses that rely on Blech's arguments, no comprehensive experimental work has been presented until the recent report by Filippi et al. from IBM. [A.9] They investigated the length effect using a technologically realistic two-level structure with W studs. More interestingly, they tested the lines whose length was in the range 30 to 1000 μm for more than 2000 hrs. over the current density range, $0.5\text{x}10^6$ A/cm^2 - $2\text{x}10^6$ A/cm^2. In these test structures voids form preferentially at the cathode end, in the vicinity of the W stud, [A.10] due to large flux divergence at that location. During the test, resistance changes were monitored as a function of time. An increase in resistance with time was the evidence of continual electromigration-induced void growth. The critical current density j_c was then defined as the current density that resulted in resistance saturation. This work reported interesting experimental results including the following.

1) No evidence was found of a $(jL)_c$ below which electromigration does not cause damage. The resistance increase due to electromigration-induced damage was always observed.

2) For a given current density, shorter lines showed a slower rate of resistance increase.

3) While $(jL)_c$ increased as the line length decreased, j_c was independent of temperature in the range 175 - 250 °C.

This work also suggests that there is a short-length effect which leads to

the back-flux against electromigration. Unlike commonly known Blech-length concepts, however, the back-flux only retards overall electromigration kinetics, rather than completely halting electromigration.

A.2 Blech Length and Quasi-Bamboo Microstructures

Kinsbron first applied Blech's threshold-product ($(jL)_c$) concept for electromigration phenomenon in quasi-bamboo lines. [A.4] He proposed that there is a similar threshold product, $(jl)_c$, of current density (j) and internal polygranular segment length (l) below which no electromigration-induced voiding should occur. The critical polygranular segment length (l_c) has been referred to as the Blech length as well, since Kinsbron treated each polygranular segment like the conductor stripe for Blech's drift-velocity measurement. The central assumption of this reasoning was that the bamboo grains at the ends of polygranular segments act as perfectly blocking boundaries, so that these polygranular segments create stress-induced back-flux which can balance the forward electromigration-induced flux.

Since the work reported by Kinsbron, it has been popular to assume the existence of a critical polygranular segment length, especially, in relation to the modeling of electromigration failure in quasi-bamboo lines. [A.5-A.7] Furthermore, the statistics of polygranular segment lengths for both modeling and improvement of reliability have been a major driver of university and industry research. Recently, Thompson has suggested that the threshold product, $(jl)_c$, in quasi-bamboo structures is at least approximately 1000 A/cm. [A.11] Typical $(jl)_c$ values from others are listed in Table A.1.

Table A.1 The threshold product, $(jl)_c$, values reported from prior work.

Source	Composition	$(jl)_c$, A/cm	l_c at $j = 2\text{x}10^6$ A/cm^2
Kraft et al.	pure Al	244	1.2 μm
(Ref. A.13)	Al-2Cu	833	4.2 μm
Atakov et al	Al-1Cu	6350	32 μm
(Ref. A.5)	Al-1Cu	12060	603 μm

Experimentally, the existence of a critical polygranular segment length has not been proven acceptably, despite the efforts by Mockl et al. [A.12] and Kraft et al. [A.13] In order to demonstrate the short-length effect, they measured void-hillock distances as polygranular segment lengths. They reported, from lifetime testing over a current density range, that the higher MTF is associated with the longer segment. They further reported that, as long as the segments are longer than a critical length (l_c), failure sites are randomly distributed over those segments, that is, failure sites are not directly related to the segment lengths. However, these arguments need to be re-considered in light of the following points.

1) The concepts of stress-induced back-diffusion that they followed should lead to the result that longer segments produce smaller back-flux, and, hence, these segments are more vulnerable to failure. As one of the researchers pointed out elsewhere, [A.14]

the line is likely to fail at the longest of polygranular segments within it.

2) The void-hillock distances that were directly related to the MTF data were the average values of all the void-precipitate pairs (i.e. damage sites as well as failure sites) over 20 or 25 lines. However, in order to find a relevant relation between the lifetime and the segment length, only the void-hillock spacings at the failure sites should be related to the lifetimes of the lines.

3) It should be examined whether the void-hillock distance is a reasonable measure of the polygranular segment length, since the relative contribution of electromigration to hillocking and voiding is not known yet. For example, in the plots by Mockl et al. (Figs. 4 and 5 in Ref. A.12), it is not clear why the void-hillock distance rapidly increases as the ratio of line width to grain size falls below unity. Because of the following reasons, it is not a reliable way to estimate polygranular segment lengths from void-hillock pairs. Early work by Kinsbron et al. showed that hillocks can form even before the edge displacement (i.e. regardless of the void formation at the cathode). [A.3] Recent work has reported that hillock formation in thin films can result from a variety of other mechanisms in addition to the material buildup by electromigration. [A.15] The present study also demonstrated that the formation of hillocks is not necessarily related to the voiding due to polygranular segments.

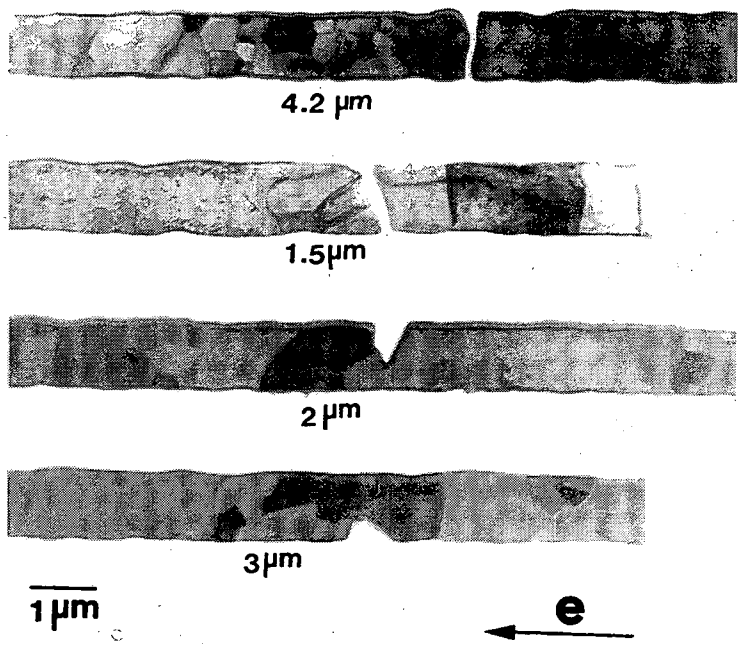

Fig. A.1 TEM micrographs showing the typical failure and damage sites in near-bamboo Al lines that are annealed for one hour at 480 °C. The polygranular segment lengths are indicated. (XBD 9504-01179)

The segment-length statistics of the present work do not agree with the statistics documented by Mockl et al. [A.12] and Kraft et al. [A.13] In the prior Chapters, this work demonstrated comprehensive experimental results from TEM and SEM combined with post-pattern anneals and lifetime tests. It was obvious that failures occur even at segments that are less

than a few microns, which are much shorter than the Blech lengths at given test conditions, as shown in Fig. A.1. Realistically, as also pointed out by Lloyd, [A.8] failure does occur at sub-Blech-length polygranular segments, although there is clearly an increase in lifetime when the segment length is shorter than the Blech length.

A.3 REFERENCES

[A.1] I. A. Blech, "Electromigration in thin aluminum films on titanium nitride," J. Appl. Phys. **47**, 1203 (1976).

[A.2] I. A. Blech and C. Herring, "Stress generation by electromigration," Appl. Phys. Lett. **29**, 131 (1976).

[A.3] E. Kinsbron, I. A. Blech, and Y. Komem, "The threshold current density and incubation time to electromigration in gold films," Thin Solid Films **46**, 139 (1977).

[A.4] E. Kinsbron, "A model for the width dependence of electromigration failure in aluminum thin-film stripes," Appl. Phys. Lett. **36**, 968 (1980).

[A.5] E. M. Atakov, J. J. Clement, and B. Miner, "Two electromigration failure modes in polycrystalline aluminum interconnects," IEEE Proceedings of the 32nd International Reliability Physics Symposium, 151 (1994).

[A.6] E. Arzt, O. Kraft, and U. E. Mockl, "Electromigration damage in conductor lines: recent progress in microscopic observation and mecha-

nistic modeling," MRS Symp. Proc. **338**, 397 (1994).

[A.7] M. A. Korhonen, P. Borgesen, D. D. Brown, and C.-Y. Li, "Microstructure based statistical model of electromigration damage in confined line metallizations in the presence of thermally induced stresses," J. Appl. Phys. **74**, 4995 (1993).

[A.8] J. R. Lloyd, "Stress and electromigration," MRS Symp. Proc. **391**, 231 (1995).

[A.9] R. G. Filippi, G. A. Biery, and R. A. Wachnik, "The electromigration short-length effect in Ti-AlCu-Ti metallization with W studs," J. Appl. Phys. **78**, 3756 (1995).

[A.10] C.-K. Hu, M. B. Small, and P. S. Ho, "Electromigration in Al(Cu) two-level structures: effect of Cu and kinetics of damage formation," J. Appl. Phys. **74**, 969 (1993).

[A.11] C. V. Thompson, Y.-C. Joo, and B. D. Knowlton, "Modeling of the structure and reliability of near-bamboo interconnects," MRS Symp. Proc. **391**, 163 (1995).

[A.12] U. E. Mockl, M. Bauer, O. Kraft, J. E. Sanchez, Jr., and E. Arzt, "Detailed study of electromigration induced damage in Al and Al-CuSi interconnects," MRS Symp. Proc. **338**, 373 (1994).

[A.13] O. Kraft, M. Bauer, and E. Arzt, "Electromigration-induced voiding mechanisms in metallizations," in *Stress-Induced Phenomena in Metallization*, AIP Conference Proceedings **373**, 131 (1996).

[A.14] E. Arzt and W. D. Nix, "A model for the effect of line width and mechanical strength on electromigration failure of interconnects with near-bamboo grain structures," J. Mater. Res. **6**, 731 (1991).

[A.15] K. E. Harris and A. H. King, "Hillock formation in tensile loaded films," MRS Symp. Proc. **391**, 73 (1995).

ERNEST ORLANDO LAWRENCE BERKELEY NATIONAL LABORATORY
ONE CYCLOTRON ROAD | BERKELEY, CALIFORNIA 94720

Prepared for the U.S. Department of Energy under Contract No. DE-AC03-76SF00098